ความสัมพันธ์ระหว่างปริมาณของแมกนีเซียมและเหล็กในแร่โอลิวีนบางชนิดกับรามานสเปกโทรสโกปี

นายทนง ลีลาวัฒนสุข

RELATIONSHIP BETWEEN MAGENSIUM AND IRON CONTENT IN SOME OLIVINE

AND  RAMAN SPECTROSCOPY

Mr. Thanong  Leelawatanasuk

Thesis Title          Relationship between magnesium and iron content in some

                      olivine and Raman spectroscopy

By                    Mr. Thanong Leelawatanasuk

Field of study        Geology

Thesis Advisor        Assistant Professor Chakkaphan Sutthirat, Ph.D.

Thesis Co-advisor     Mr. Sathon Vijarnwannaluk , Ph.D.

_____

        Accepted by the Faculty of Science, Chulalongkorn University in Partial

Fulfilment of the Requirements for the Master's Degree


        ........................................................Dean of the Faculty of Science

        (Professor Piamsak Menasveta, Ph.D.)

THESIS COMMITTEE


        ..............................................................Chairman

        (Assistant Professor  Virote Daorerk, M.Sc.)


        ............................................................Thesis Advisor

        (Assistant Professor Chakkaphan Sutthirat, Ph.D.)


        ..........................................................Thesis Co-advisor

        (Mr. Sathon Vijarnwannaluk, Ph.D.)


        ........................................................Member

        (Associate Professor Visut Pisutha-Arnond, Ph.D.)


        ........................................................Member

        (Mrs. Wilawan Atichat, M.Sc.)

ทนง ลีลาวัฒนสุข : ความสัมพันธ์ระหว่างปริมาณของแมกนีเซียมและเหล็กในแร่โอลิวีน
บางชนิดกับรามานสเปกโทรสโกปี    อ.ที่ปรึกษา : ผู้ช่วยศาสตราจารย์ ดร.จักรพันธ์
สุทธิรัตน์,  อ. ที่ปรึกษาร่วม: อ.ดร. สธน วิจารณ์วรรณลักษณ์    จำนวนหน้า 108 หน้า
ISBN: 974-17-7068-5


        ในอดีตเทคนิคการวิเคราะห์ด้วยเครื่อง    รามานสเปกโทรสโกปี    ไม่เป็นที่นิยมมากนักในหมู่
นักวิทยาศาสตร์   เนื่องจากเป็นเทคนิควิเคราะห์ที่ต้องใช้เวลาและค่าใช้จ่ายสูง   แต่ในปัจจุบันเทคนิคนี้กลับ
ได้รับความนิยมอย่างสูงในงานวิเคราะห์โดยไม่ทำลายตัวอย่างในวิทยาศาสตร์หลายแขนงอาทิเช่น
ธรณีวิทยา อัญมณีศาสตร์ และวัสดุศาสตร์ เป็นต้น ปรากฏการณ์รามาน เกิดจากโครงสร้างโมเลกุลของ
วัตถุถูกกระตุ้นด้วยแสงความยาวคลื่นเดี่ยว แล้วเกิดการกระเจิงแบบไม่ยืดหยุ่น กระเจิงรามานดังกล่าวจะมี
ความยาวคลื่นเปลี่ยนไปจากแสงต้นกำเนิด ซึ่งค่าการเปลี่ยนแปลงนี้จะเป็นรูปแบบเฉพาะในโครงสร้างของ
สารนั้นๆ     รามานสเปกตรัมของตัวอย่างในการศึกษาครั้งนี้ได้จากการวิเคราะห์โดยเครื่องเลเซอร์รามาน
สเปกโทรสโกป (Renishaw  model 1000)  ของสถาบันวิจัยและพัฒนาอัญมณีและเครื่องประดับแห่งชาติ
(องค์การมหาชน) โดยใช้หลอดอาร์กอนกำเนิดแสงเลเซอร์สีเขียวในช่วงความยาวคลื่น 514.5 นาโนเมตร

        โอลิวีนเป็นแร่ประกอบหินกลุ่มแร่ซิลิเกตที่เป็นองค์ประกอบสำคัญของชั้นเนื้อโลกด้านบน        มี
สมาชิกที่พบในธรรมชาติมากที่สุดสองประเภทคือ ฟอร์สเตอไรต์ $(Mg_2SiO_4)$ และ ฟายาไลต์ $(Fe_2SiO_4)$ ใน
รูปของโซลิดโซลูชั่น การศึกษาครั้งนี้ใช้ตัวอย่างทั้งสิ้น 27 ตัวอย่าง แบ่งเป็น 2 กลุ่มคือกลุ่มตัวอย่างขนาด
ใหญ่ 20 ตัวอย่าง  และ  กลุ่มตัวอย่างที่เป็นผงจำนวน 7 ตัวอย่าง   มีช่วงองค์ประกอบสมาชิกปลายอยู่
ระหว่าง $Fo_{91.5}$ ถึง  $Fo_{50.5}$  ซึ่งพบว่าค่าองค์ประกอบทางเคมีแสดงความสัมพันธ์อย่างเป็นแนวเส้นตรงกับ
การเลื่อนลงของตำแหน่งพีคอย่างเด่นชัด    ซึ่งปรากฏการณ์ดังกล่าวสามารถอธิบายได้โดยการเพิ่มขึ้นของ
ปริมาณธาตุเหล็กที่มีขนาดใหญ่กว่าในตำแหน่งแคทไอออน M1 และ M2 ของโครงสร้างโอลิวีน  ส่งผลให้
ความยาวพันธะหดสั้นลง  และแรงของพันธะเพิ่มสูงขึ้น  ส่งผลให้เกิดการเลื่อนลงทั้งอินเตอร์นัลโหมด  และ
แลตติสโหมดของตำแหน่งรามานในที่สุด  จากความสัมพันธ์ดังกล่าวทำให้สามารถประยุกต์เทคนิครามาน
ในการหาค่าองค์ประกอบเคมีเชิงคุณภาและกึ่งปริมาณของโอลิวีนในช่วง Fo ที่กว้างขวาง  ตำแหน่งพีคที่ใช้
ควรอยู่ในตำแหน่งของ $SiO_4$  อินเตอร์นัลโหมด (1000-800 ซม.$^{-1}$ ) เนื่องจากพีคทั้งหมดในบริเวณนี้มักจะ
ปรากฏ สำหรับขนาดตัวอย่างพบว่าไม่มีผลต่อการเลื่อนของรามาน แต่อาจจะทำให้รูปร่างของพีคกว้างขึ้น

ภาควิชา................ธรณีวิทยา.............ลายมือชื่อนิสิต.......................................................
สาขาวิชา...............ธรณีวิทยา............ลายมือชื่ออาจารย์ที่ปรึกษา.....................................
ปีการศึกษา............2547....................ลายมือชื่ออาจารย์ที่ปรึกษาร่วม...............................

In the past, Raman spectroscopy was considered to be inconvenient analytical method because of its high running cost and time consuming. Recently, this technique has become one of the most famous non-destructive analytical methods for materials in many scientific interests (e.g. gemology, geology and material sciences). Raman Effect is an inelastic scattering light wave activated by the monochromatic light within structure of material. The Raman scattering usually has wavelength that differs from the origin light; the different values of wavelength are specific pattern depending on structure of material.  All Raman spectra used under this study were obtained by Renishaw laser Raman spectroscope (Model 1000) at the Gem and Jewelry Institute of Thailand (Public organization). Green Ar/Ar laser source is used to generate the laser with wavelength of 514.5 nm.

Olivine is one of the most common rock-forming mineral in silicate group, originated particularly in the earth's upper mantle. Naturally, it consists mainly of 2 abundant solid-solution members; Forsterite ($Mg_2SiO_4$) and Fayalite ($Fe_2SiO_4$). Twenty single crystals and seven batches of very fine-grained natural olivine, which contain end-member contents ranging from $Fo_{91.5}$ to $Fo_{50.5}$, are available for this study. The relationship between the end-member contents of the studied olivine and their Raman spectra was observed. Raman peak positions significantly show linear downshift against increasing in Iron contents. This phenomenon can be explained by substitution of larger Fe cations along *M1* and *M2* sites in the olivine structure yielding the shorter bond length and stronger bond strength. These lead to the downshift of both internal and lattice vibration modes of waves in crystal. Consequently, the non-destructive Raman spectroscopic technique is possibly applied to both qualitative and semi-quantitative analyses for olivine within wide range of Fo content. The most suitable peaks for this purpose are assigned to the $SiO_4$ internal mode (1000- 800 $cm^{-1}$) because most of the spectrum peaks in this range are usually present. In addition, grain size of olivine does not effect positions of Raman peaks, but it would only broaden the peak shape.

Department............Geology............Student's signature......................................................

Field of study.........Geology.............Advisor's signature......................................................

Academic year.........2004................Co-advisor's signature................................................

# ACKNOWLEDGEMENTS

# CONTENTS

## LIST OF TABLES

LIST OF FIGURES

Figure                                                                                    page

CHAPTER I

INTRODUCTION

*1.1 General statement*

The Raman effect was initially discovered by an English physicist, named Professor Sir C. V. Raman and his colleague in 1928. They found that when a certain material has been shone by monochromatic light, two frequencies of light will scatter out. Most of the light is scattered elastically without changing in frequency (Reyleigh scattering) while very small portion of light is scattered inelastically and have different frequency. This inelastic scattering of light is now known as Raman scattering. The Raman scattering is caused by partially losing energy of incident light to molecular vibrations. Each of molecular vibrations results in different frequencies. As a results, Raman spectra of each material are unique and reflect crystal structure of that material.

In the first period after discovery of Raman spectroscopy, many scientists did not consider it as a useful instrument because it was very expensive and time-consuming analytical instrument. Therefore, most researches were restricted in small fields. Around 1990's, when many related technologies (e.g. computer processor, material technology, laser technology, etc.) have been developed, it is the begining of new age of Raman spectroscopy. Many weakness points in the past have been improved; that leads to increasing its performance to support various applications. However, databases for each application are still not enough. Recently, Raman spectroscopy is a crucial instrument among many non-destructive analytical instruments which are used in standard analytical laboratories, particularly in gemological works.

Olivine is one of the most common rock-forming silicate minerals; its general formula is $X_2SiO_4$ where X is divalent cation (e.g. Fe, Mg, Mn, Ca, Ni and Co). In nature, olivine is mainly composed of 2 end-members; i.e. Forsterite ($Mg_2SiO_4$) and Fayalite ($Fe_2SiO_4$), but pure phases of both forsterite and fayalite are rarely found. However, they

usually form as solid solution mineral ($(Fe, Mg)_2SiO_4$). In addition, the other types of olivine can be merely found in natural system or may be synthesized; some more information of olivine are reported in the next chapter. Chemical compositions of olivine can be analyzed using many destructive analytical methods, that are not suitable for gemological aspects. Based on the principle of Raman spectroscopy, positions of Raman peaks can be changed related to three major causes, i.e. chemical composition, temperature and pressure. Hence, it is possible to apply Raman spectroscopy to determine approximate end-member values of olivine; that may lead to new approach for gemological analysis.

## 1.2  Purpose of study

The purpose of this research is to study relationship between position changes of Raman spectrum and chemical compositions, especially magnesium (Mg) and iron (Fe), of some natural olivines.  This study aims at illustrating the shift of Raman peak position in relation to different chemical composition. This will help to estimate the end-member value of this mineral and also to be used as a guide line for further researches in related field.

## 1.3 Methodology

The method of study can be summarized as follows (see also Figure 1.1) :

1. Literature survey of previous works was taken place to understand olivine's nature and also theoretical background of Raman spectroscopy. In addition, work plan was consequently designed on the basis of their information.

2. Sample collection was carried out  from two main sources. Coarse-grained natural samples were bought from gem market, whereas fine-grained  samples with known end-member contents were provided by Professor Dr. C.M.B. Henderson of the Manchester University.

3. Twenty coarse-grained samples were selected based on their variety.

4. Selected samples were cut into 2 parts and then polished. One part was prepared for determining its general properties including Raman spectrum, whereas the other part was used for quantitative analysis.

5. Physical and optical properties (e.g. refractive index (RI), birefringence, specific gravity (SG), and luminescence under short wave (SW, 254 nm) and long wave (LW, 365 nm)) were examined by using basic gemological instruments at the Gem and Jewelry Institute of Thailand (GIT).

6. Quantitative analyses of the coarse-grained samples were completely done using Electron Probe Micro-Analyzer (EPMA) at Center of Gemstone Research, University of Meinz, Germany.

7. Raman spectra of all selected samples (both coarse-grained and fine-grained olivines) were subsequently collected to cover the whole range of end-members available for this project by using a Renishaw-1000 Raman Spectroscope at the GIT.

8. Discussion and summary of this study were finally constructed to clarify all aspect and objectives.

9. Thesis report has been consequently wrap up to fulfill the research project.

```
┌─────────────────────────────────────────┐
│     Literature survey of  previous works │
└─────────────────────────────────────────┘
                    │
                    ▼
┌─────────────────────────────────────────┐
│          Classification of samples       │
└─────────────────────────────────────────┘
                    │
                    ▼
┌─────────────────────────────────────────┐
│  Sample preparation (e.g. cut and polish)│
│              for analyses                │
└─────────────────────────────────────────┘
                    │
                    ▼
┌─────────────────────────────────────────┐
│ Determination of physical and optical    │
│              properties                  │
└─────────────────────────────────────────┘
                    │
                    ▼
┌─────────────────────────────────────────┐
│      Quantitative analysis using  EPMA   │
└─────────────────────────────────────────┘
                    │
                    ▼
┌─────────────────────────────────────────┐
│        Collection of Raman spectra       │
└─────────────────────────────────────────┘
                    │
                    ▼
┌─────────────────────────────────────────┐
│          Discussion and summary          │
└─────────────────────────────────────────┘
                    │
                    ▼
┌─────────────────────────────────────────┐
│         Reporting and presentation       │
└─────────────────────────────────────────┘
```
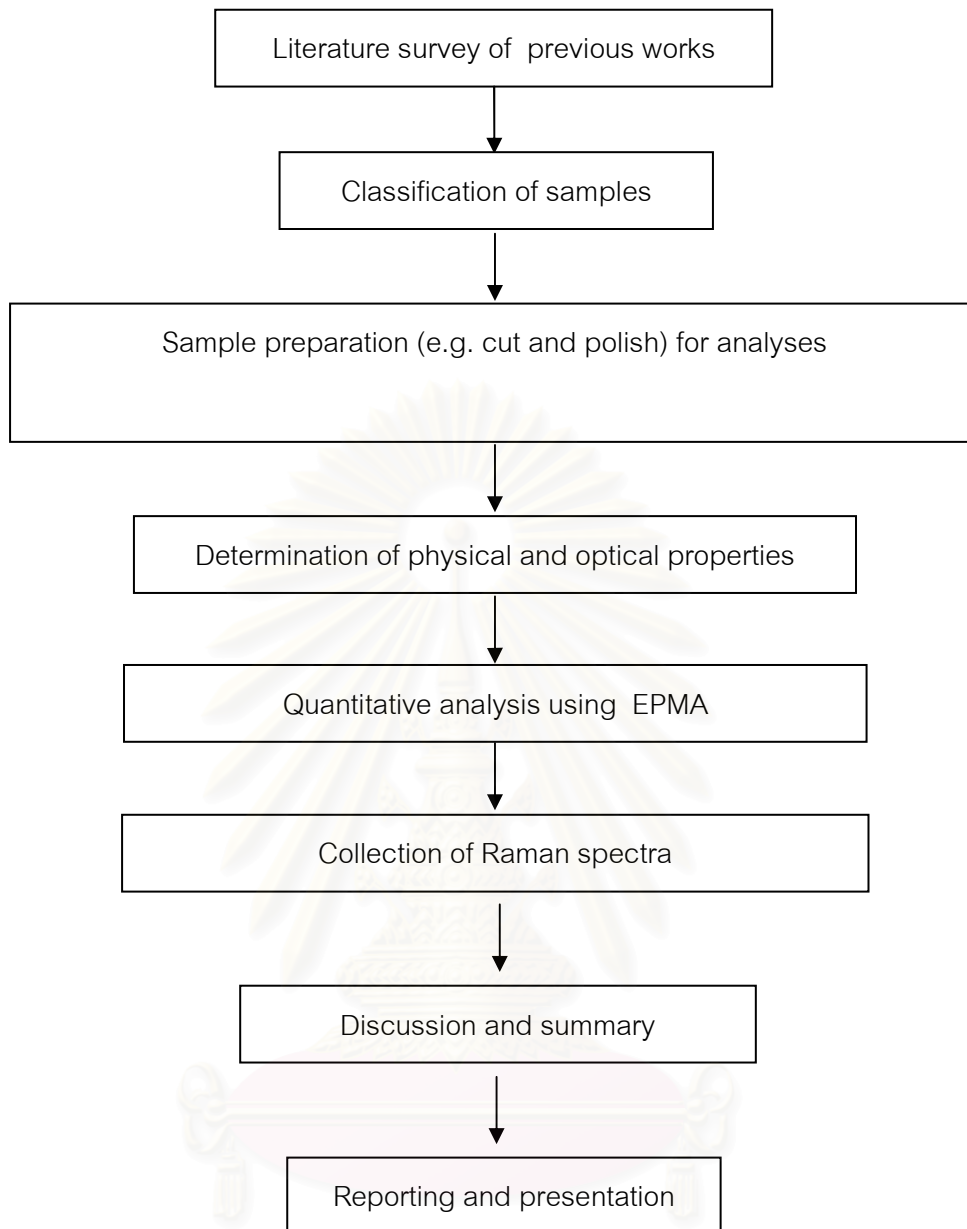
Figure 1.1  Schematic diagram showing methodology of this study

CHAPTER II

RAMAN SPECTROSCOPY AND OLIVINE

2.1    *Raman Spectroscopy*

Raman spectroscopy  is a   result of vibrational phenomena of molecular structure activated by light energy. The principal of vibrational spectroscopy is interaction between electrical field associated with  photon and changes induced by vibrational movements in electronic charges distribution within the substance. Generally, unit utilized to describe the frequency of these vibrational motions is wavenumber ($cm^{-1}$) which can be converted to wavelength(nm) by following equation  2.1:

$$\nu \,(cm^{-1}) = 10^7/\lambda \,(nm) \ldots\ldots\ldots\ldots\ldots\ldots\ldots\ldots(2.1)$$

where $\nu$ is  wavenumber  and $\lambda$ is wavelength.

The Raman effect was initially  discovered in 1928 (Raman and Krishnan, 1928). This effect has been studied using a light scattering experiment (Figure 2.1) in which the beam of incident light is usually in  visible region of electromagnetic spectrum. The light energy is slightly increased or decreased   by inelastic interaction with the vibration modes. The Raman spectra consist of the set of scattering peaks as a function of energy. Individual peaks of spectrum correspond to energies of the vibrational transitions within specimen's molecule; that was given simplified terminology as "the frequencies of vibrational modes".



Figure 2.1  Professor Dr. C.V.Raman  and his experimental equipment using to observe  Raman effect.

The most obvious application of Raman spectroscopy is qualitative and quantitative analyses   because it is a sensitive probe for microscopic structure and bonding  within material and it can determine crystalline solids, liquids or gases. Raman spectroscopy can provide very useful structural information, that earn from positions, symmetries and relative intensities of the observed peaks . In addition, changes in some variable conditions (e.g.  temperature, composition, and pressure) may effect molecular structure of substance, in turn, it leads to modification of Raman pattern.
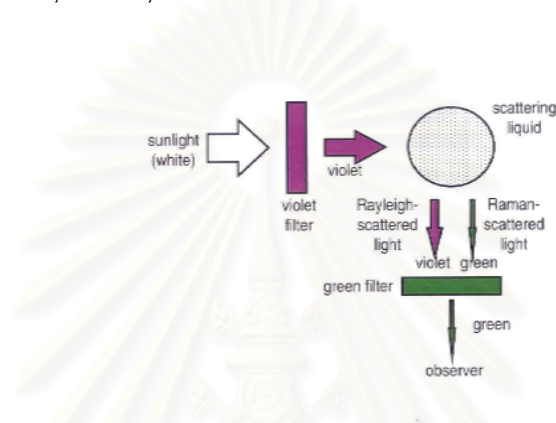
Figure 2.2.  Schematic diagram shows Prof. C.V. Raman's experiment.

Traditional Raman spectroscope has been introduced as an analytical tool for minerals for several decades but there were some problems  that make this analytical technique was not widely used. For examples, they have  the expensive running cost and time consuming process. However, technological developments, that have been modified recently, are making this analytical technique more available. The previous model can be completely replaced by the modern one that is more compact, higher sensitive, easy-to-use and more flexible instrument. Hence, the Raman spectroscopy is now an effective instrument for specimen identification, molecular structure analysis, interatomic force, thermodynamic researches and so on.

### 2.1.1 Raman scattering experiment

While the visible light (commonly a monochromatic beam from laser source) shone on the specimen, most of the photons scatter from the specimen without any change. However, there is a very small portion of the incident light (~ $10^{-3}$ of the incident intensity) is scattered by the atoms, and around $10^{-6}$ of this scattered light interacts with the atoms in such a way to induce a vibrational mode. During the vibration, the energy of scattered light is reduced by an amount corresponding to the vibrational transition. This inelastic scattering is known as Raman scattering, while elastic scattering without any change in energy is known as Reyleigh scattering (Figure 2.3).

**Raman**

$\nu_0$
(laser) → Sample

$\nu_0 \pm \nu_m$(Raman scattering)

$\nu_0$(Rayleigh scattering)
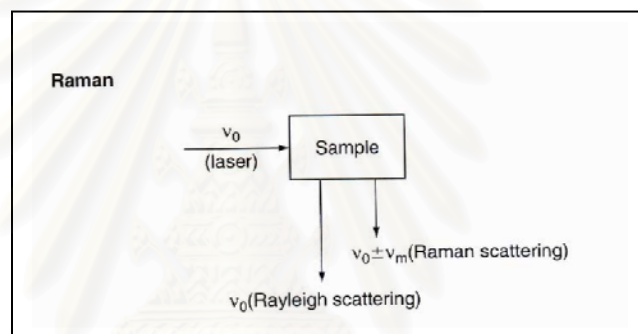
Figure 2.3   Schematic diagram showing Reyleigh scattering and   Raman scattering (Ferraro et al., 2003).

In Raman spectroscopy, the inelastic scattering light can also be analyzed using spectrometer. However, sets of Raman spectrum usually  appear as weak peaks that shift in energy from the Reyleigh scattering peak and the incident beam. These shifts of energy level were named as stoke's shift when the energy is less than the energy of incident ray and anti-stoke's shift when the energy is higher than the energy of incident ray. It should however notified that Reyleigh scattering is characterized by the same energy obtained from the incident light (Figure 2.4).   The positions of Raman peaks are related to the incident laser line and correspond to the frequencies of Raman-active vibration modes in the specimen.
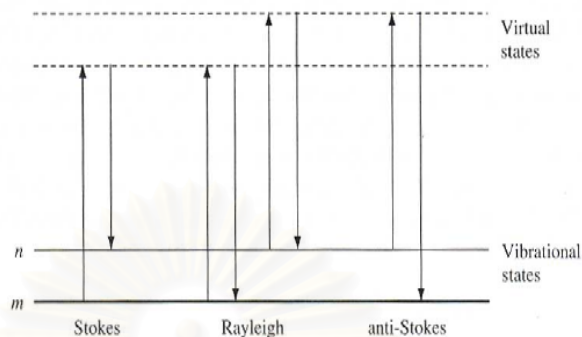
Figure 2.4.   The origin and character of stoke and anti-stoke (Smith and Dent, 2005).

The  Raman-active vibration mode will be caused when  the incident light beam induces an instantaneous dipole moment in the molecule by deforming its electronic wave function. This dipole moment is corresponding to the certain set of molecular vibration. Consequently, particular mode of molecular vibration can be set up or destroyed with this incident lights. The Raman shift can be expressed by following equation 2.2:

$$\nu\varDelta_{Raman\ shift} = \nu_{laser} - \nu_{light\ scattered} \ldots\ldots\ldots\ldots\ldots 2.2$$

where $\nu$  is  wavelength (cm$^{-1}$)

### 2.1.2  Instrumentation for Raman experiments
*Monochromatic light sources*:

Raman spectroscopic experiment requires actually particular light source. Usually, laser is the best choice for this purpose because it can give high intensity of monochromatic light.  Most Raman spectroscopic studies  use  laser  in the visible range of spectrum. The most famous excitation source is Argon ion gas laser which can generate high power  laser with extreme stability. The wavelength of this laser is in blue-green region usually at   488 nm and 514.5 nm and generally provides the power of about 1-2 W output for  4-5 W laser. The other continuous gas lasers used for Raman

spectroscopy include the Krypton and Helium-Neon lasers. He-Ne laser is produced by a lasing transition of $Ne^+$ in red region which is occasionally used for Raman work. The Krypton laser has a number of lasing lines in yellow to ultraviolet region and it is suitable for studies in samples that have fluorescence or absorption in blue-green region of the light spectrum. Other light sources, such as dyed laser, are rarely used for Raman experiment.

*Spectrometer:*

In general, grating monochromater, which dispersion takes place by selective reflection of the grating surface due to constructive and destructive interference caused by the regularly ruled surface, is considered to be the most suitable spectrometer for Raman spectroscope.

*Detectors:*

In the early development of Raman spectrometry, the standard detector was photomultiplier. The photosensitive element is a semiconductor material (commonly GaAs). But the recent Raman spectrometers contain commonly charge couple device (CCD) as a detector because of its obviously higher sensitivity.

## 2.2. Olivine

Olivine is one of the most significant rock-forming minerals occurred in the earth crust. Its general formula is $X_2SiO_4$ where X is cations that mostly occupy octahedral coordination within 2 distinct crystallographic sites, *M2* and *M1*, respectively. Olivine group mineral is systematically subdivided into 9 end-members as shown in Table 2.1. Some of them are generally occurred in the natural system, on the other hand, several members are more common in synthetic system.

Table 2.1.    End-Members of olivine group and their chemical compositions.

| Mineral | Formula |
|---------|---------|
| Fayalite | $Fe_2SiO_4$ |
| Forsterite | $Mg_2SiO_4$ |
| Liebenbergite | $Ni_2SiO_4$ |
| Tephroite | $Mn_2SiO_4$ |
| Laihunite | $Fe^{3+}_2SiO_4$ |
| Monticellite | $CaMgSiO_4$ |
| Kirschsteinite | $Ca(Fe,Mg,Mn)SiO_4$ |
| Glaucochroite | $MnCaSiO_4$ |
| Calcio-olivine | $Ca_2SiO_4$ |

Nomenclature of olivine in the past was complicated because of the persistence of various names, such as *picrotephroite* ($MnMgSiO_4$) and *knebelite* ($MnFeSiO_4$), besides simplified nomenclature for intermediate members of solid solution series were generally taken addition of prefix, such as manganoan, ferroan and magnesian into account . The other alternative way to name series of chemical composition is utilization of atomic  end-member percentage,  e.g.    Fo $_{90.5}$. The most abundant mineral olivine found in common rock is usually in Forsterite – Fayalite series; in addition, this olivine series are typically used for gem material. Therefore, this report would be more appropriate to review properties of forsterite and fayalite only; that will directly provide information for this research project.

2.2.1  Optical and Physical properties

The refractive indices of olivine vary linearly with their chemical compositions, both $\alpha$ and $\gamma$ will increas by about 0.002 per atomic percent of $Fe_2SiO_4$ (Figure 2.5). The optic axial angle ($2V_\gamma$)  varies systematically from $82^\circ$  of forsterite to   $134^\circ$ of fayalite(Figures 2.5 and 2.6). The other optical and physical properties are summarized in Table 2.2. These properties are conclusively related to Mg:Fe ratio directly.
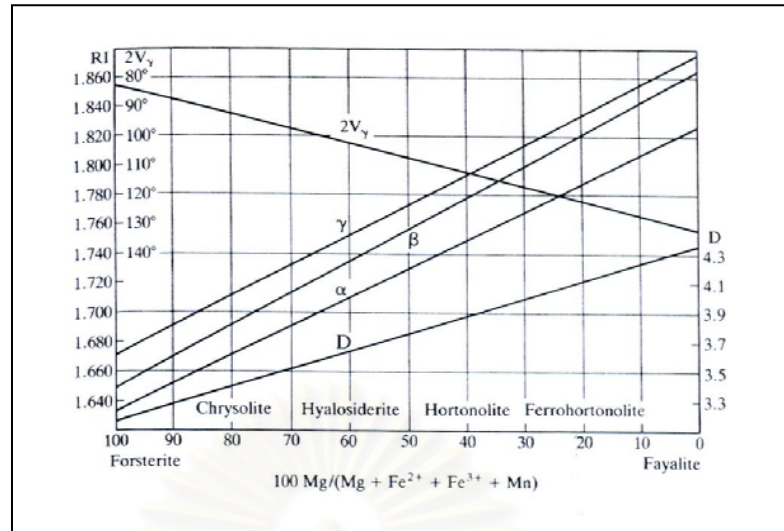
Figure 2.5    Relationship between refractive index (RI), density and

optical axis   (Klein  and Hurlbut, 1999).

Table 2.2.    Physical  properties of forsterite and fayalite.

|  | Forsterite ($Mg_2SiO_4$) | Fayalite($Fe_2SiO_4$) |
|---|---|---|
| Crystal system | Orthorhombic | Orthorhombic |
| $\alpha$ | 1.635 | 1.827 |
| $\beta$ | 1.651 | 1.869 |
| $\gamma$ | 1.670 | 1.879 |
| Bire | 0.035 | 0.052 |
| $2V_\gamma$ | $82°$ | $134°$ |
| SG | 3.222 | 4.392 |
| H | 7 | 6.5 |
| Unit cell | *a* 4.75 Å, *b* 10.20 Å, *c* 5.98 Å | *a* 4.82 Å, *b* 10.48 Å, *c* 6.09 Å |
| Pleochroism | None | $\alpha = \gamma$  pale yellow, $\beta$ orange yellow, reddish brown |
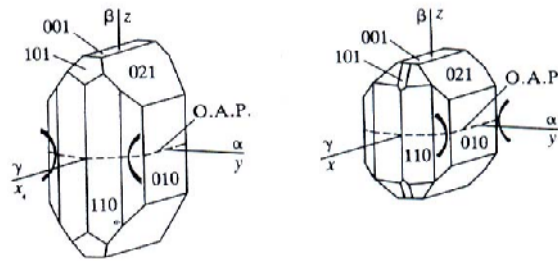
Figure 2.6.    Crystal morphology of forsterite (left) and fayalite(right)  (Deer et al., 1992).

2.2.2  Structure

The  structure  of  olivine  generally    consists  of  individual  silica-oxygen  ($SiO_4$) tetrahedra linked by cation atoms (e.g. Mg,Fe, etc.). Consequently each cation atom has 6  nearest  oxygen  neighbours  forming  octrahedral  coordination  (Figure  2.7).  The oxygens  lie  in  sheet  parallel  to  the  (100)  plane  and  form  approximately  in  hexagonal arrangement.  Octahedral  voids  occupied  by  metal  cations  are  defined  systemically  as *M* sites. Half of *M* sites are located in centres of symmetry (Cs), so called *M 1* site*;*  the other  half  of  them  are  on  reflection  plane,  called  *M2*  site  (Figure  2.7).  Besides*,*  one- eighth  of  the  available  tetrahedral  voids  are  occupied  by  Si  atoms.    Each  oxygen  is therefore bonded to one silicon and three octahedrally coordinated atoms.

Olivines  are  classified  as  orthosilicate  minerals  or  island  silicates;  however,   their major structural feature is not the silicate tetrahedral. Chain of  edge-sharing octahedral coordinations contain cation atoms and these chains lie parallel to the direction of C-axis (see Figure 2.7).
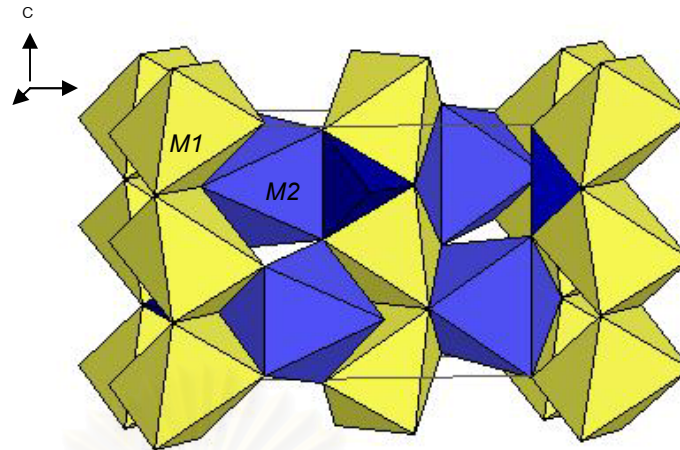
Figure 2.7   Structure of olivine showing yellow octahedral coordination represent *M1*

sites and blue octahedral coordination  represent  *M2*  sites.

### 2.2.3 Chemistry

Chemical compositions of natural olivines commonly vary from $Mg_2SiO_4$ (forsterite) to $Fe_2SiO_4$(fayalite). Names of both end-members are related to the compositions of $Fo_{90-100}$ and $Fo_{0-10}$ respectively. The other intermediate members between both forsterite and fayalite are listed below.

|  |  |
|---|---|
| Forsterite | $Fo_{90-100}$ |
| Chrysolite | $Fo_{70-90}$ |
| Hyalosiderite | $Fo_{50-70}$ |
| Hortonolite | $Fo_{30-50}$ |
| Ferrohortonolite | $Fo_{10-30}$ |
| Fayalite | $Fo_{0-10}$ |

In the natural system, partial replacements of cation appear to have been  taken place in forsterite – fayalite series. Fe-rich olivines tend to be replaced by Mn and Ca cations, whereas Mg-rich olivines are frequently substituted by  Ni and Cr. Besides, chromium may also occur in form  of minute exsolved plate of chromite. Ca contents are usually   ranging between   0.0 and 1.0 %weight   in common olivine. In addition, phosphorous with  trace amount would be found  in some olivine.

2.2.4 Paragenesis

Olivine is a major constituent in many ultramafic rocks. Mg-rich olivines, which have compositions ranging between $Fo_{96}$ –$Fo_{87}$ are commonly found in dunite and peridotite. Ultramafic nodules in basalt and kimberlite usually have olivines with composition in range between $Fo_{91}$ and $Fo_{86}$. Olivine with compositional range of $Fo_{80}$-$Fo_{50}$ can be found in gabbroic rocks (Deer et al., 1992).

Iron-rich olivine occurs in both alkaline and acid hypabyssal to plutonic rocks. Fayalite is also present with small amount in many acid and alkaline volcanic rocks, such as obsidians, rhyolite, trachytes and phonolites, in some specific locality (Deer et al., 1992).

The other types of olivines are mostly metamorphic origin. These metamorphic olivines appear to occur principally in ultramafic compositions, impure carbonates and iron-rich sediments. Metamorphism could deviate these compositions and produce olivines with either high magnesium- or iron-rich phases. Development of Mg-rich olivine is found in various mineral assemblages formed during progressive metamorphism of serpentinites as revealed by reactions below.

$$5Mg_3Si_2O_5(OH)_4 + 2CaMgSi_2O_6 \leftrightarrow 6Mg_2SiO_4 + Ca_2Mg_5Si_8O_{22}(OH)_2 + 9H_2O$$
serpentine       diopside       *forsterite*       tremolite

$$5Mg_3Si_2O_5(OH)_4 \leftrightarrow 6Mg_2SiO_4 + Mg_3Si_4O_{10}(OH)_2 + 9H_2O$$
serpentine       *forsterite*       talc

$$5Mg_3Si_2O_5(OH)_4 + Mg(OH)_2 \leftrightarrow 2Mg_2SiO_4 + 3H_2O$$
serpentine       brucite       *forsterite*
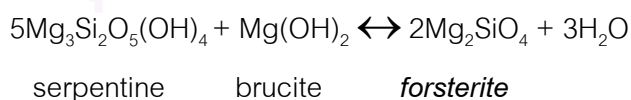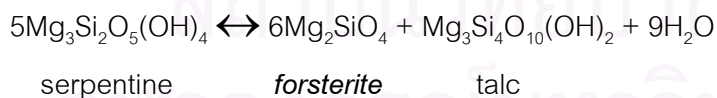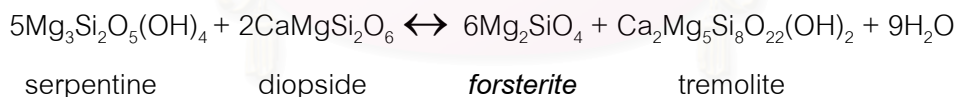
The formation of Mg-rich olivines in metamorphosed impure carbonate rocksunder anhydrous and hydrous conditions can be illustrated using the following reactions.

Anhydrous condition:

$$2CaMg(CO_3)_2 + SiO_2 \rightarrow Mg_2SiO_4 + 2\ CaCO_3 + 2CO_2$$

    dolomite    quartz    *forsterite*    calcite

Hydrous condition:

$$Ca_2Mg_5Si_8O_{22}(OH) + 11CaMg(CO_3)_2 \leftrightarrow 8Mg_2SiO_4 + 13CaCO_3 + 9CO_2 + H_2O$$

    Tremolite             dolomite        *forsterite*    calcite
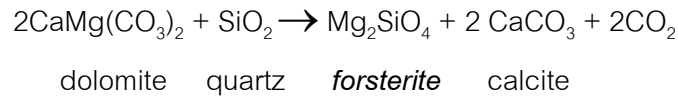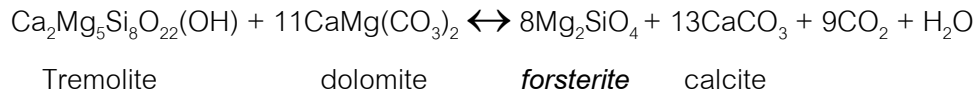
On the other hand, fayalite is often associated with iron-rich augite $((Ca,Na)(Mg,Fe,Al)(Si,Al)_2O_6)$ and grunerite $(Fe_7Si_8O_{22}(OH)_2)$, and typically occurs in medium-grade thermal metamorphism within compositions of iron-rich sediment and cherty rock. Reaction of these iron-containing silicate compositions is described below.

$$2FeCO_3 + SiO_2 \rightarrow \quad Fe_2SiO_4 + 2CO_2$$

    siderite    quartz      *fayalite*
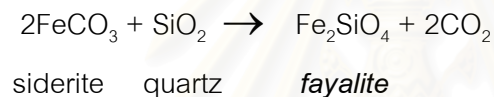
In addition, thermodynamic data of equilibration between forsterite - fayalite composition and temperature have been carried out by many researchers. As shown in Figure 2.8, forsterite is crystallized at higher temperature (1,890 $^\circ$C for pure phase) and reductions of liquidus and solidus are significantly related to increasing of Fe (fayalite) content.
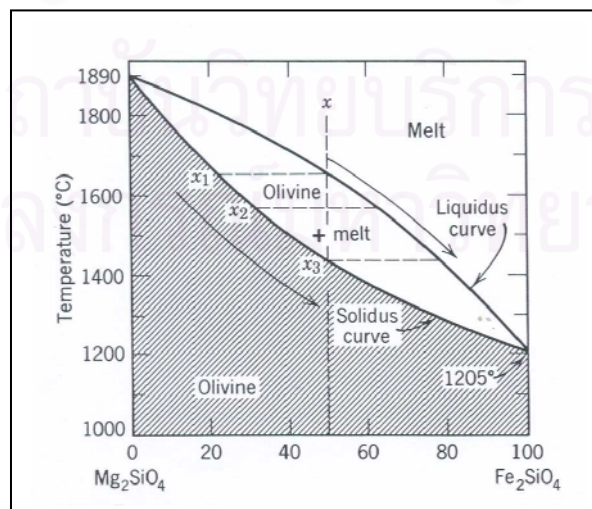


Figure 2.8   Temperature-composition diagram for the system $Mg_2SiO_4$-$Fe_2SiO_4$ at

atmospheric pressure (Klein  and Hurlbut, 1999)..

*2.3 Vibrational Spectra of Olivine*

Olivine is an orthorhombic mineral group belonging to the space group *Pbnm* which has 4 $M_2SiO_4$ formula units per unit cell. The current data of olivine crystal optic vibration modes can be predicted into 81 modes that are shown in the irreducible presentation below (Chopelas, 1991):

$$11A_g + 11B_{1g} + 7B_{2g} + 7B_{3g} + 10A_u + 9B_{1u} + 13B_{2u} + 13B_{3u}$$

where $A_g$ refers to the modes belonging to symmetrical vibration of a
molecule with respect to the center of symmetry.

$A_u$ refers to the modes belonging to symmetrical vibration of a
molecule with not respect to the center of symmetry.

$B_g$ refers the modes belonging to asymmetrical vibration of a
molecule with respect to the center of symmetry.

$B_u$ refers the modes belonging to asymmetrical vibration of a
molecule with not respect to the center of symmetry.

The subscript numeric (i.e.1,2 or 3) refer to the off-axis configurations.

Among 81 normal modes of the lattice, 36 modes are Raman active (i.e. $11A_g$, $11B_{1g}$, $7B_{2g}$ and $7B_{3g}$ ), whereas 35 modes are infrared active (i.e. $9B_{1u}$, $13B_{2u}$ and $13B_{3u}$), besides $10A_u$ modes are able to be both Raman and infrared inactive. In addition, 36 raman active modes can be assigned into 2 major modes of vibration. The high-wavenumber modes between 800– 1000 $cm^{-1}$ fall in the region expected for $SiO_4$ internal mode. However, observed bands may be due to combinations of the $V_1$ (symmetric) and $V_3$ (asymmetric) stretching modes of the $SiO_4$ groups in the structure. This internal mode assignment appears to be an useful approximation. The $SiO_4$ groups in the structure are distorted ($C_s$ site symmetry) and raman spectra tend to show systematic change according to degree of distortion. The lower-wavenumber modes are described as lattice modes consisting of mixed vibrations of *M2* cation translations and external vibration of $SiO_4$ tetrahedra.

Table 2.3 . Classification of 81 vibration modes of olivine (modified from Chopelas,1991).

| Mode | $11A_g$ | $11B_{1g}$ | $7B_{2g}$ | $7B_{3g}$ | $10A_u$ | $9B_{1u}$ | $13B_{2u}$ | $13B_{3u}$ |
|---|---|---|---|---|---|---|---|---|
| *SiO$_4$ internal* | 6 | 6 | 3 | 3 | 3 | 3 | 6 | 6 |
| $V_1$ | 1 | 1 | 0 | 0 | 0 | 0 | 1 | 1 |
| $V_2$ | 1 | 1 | 1 | 1 | 1 | 1 | 1 | 1 |
| $V_3$ | 2 | 2 | 1 | 1 | 1 | 1 | 2 | 2 |
| $V_4$ | 2 | 2 | 1 | 1 | 1 | 1 | 2 | 2 |
| *Lattice* | 5 | 5 | 4 | 4 | 7 | 6 | 7 | 7 |
| SiO$_4$ rot | 1 | 1 | 2 | 2 | 2 | 2 | 1 | 1 |
| SiO$_4$ trans | 2 | 2 | 1 | 1 | 1 | 0 | 1 | 1 |
| M1 trans | 0 | 0 | 0 | 0 | 3 | 3 | 3 | 3 |
| M2 trans | 2 | 2 | 1 | 1 | 1 | 1 | 2 | 2 |
| *Activity* | *R* | *R* | *R* | *R* | *0* | *IR* | *IR* | *IR* |

R: Raman Active,  IR: Infrared Active,  O: Raman and infrared Inactive

CHAPTER  III

EXPERIMENTS AND RESULTS

*3.1 Sample Preparation*

The  natural  olivine  samples  available  for  this  study  were  collected  from  2 sources. The gem quality  coarse-grained  samples were   bought  from the gem market (Figure 3.1). However, their end-member percentages and origins are not known.  In addition, seven batches of fine-grained samples with grain size of about 100  microns  were  provided   by Prof.  Dr.  C.M.B.  Henderson,  University  of Manchester. They were mostly natural gabbroic olivine from Zimbabwe (Figure 3.2); their end-member  percentages  have  been  published  and  accepted.   The  first sample group was initially characterized on the basis of colors that vary slightly from yellowish  green  to  dark  yellowish  green  (Figure  3.1);   consequently,  20  samples were selected as representatives for this study.



Figure 3.1  Coarse-grained  olivine samples with  gem quality  from gem trade are
separated  into 5 groups  based on colors (i.e. yellowish green to
dark yellowish green).
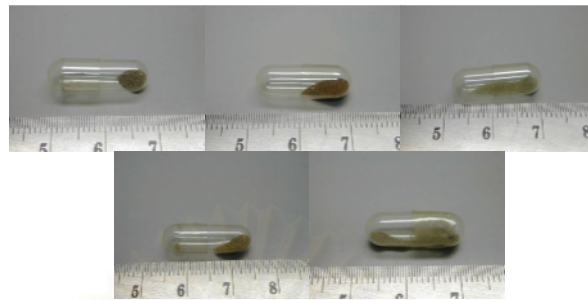
Figure 3.2.  Some fine-grained gabbroic olivine samples with average grain size of
about 100 microns from Zimbabwe.

The chosen samples were cut into 2 parts; the first parts were prepared for
Electron Probe Micro-Analysis (EPMA) at Center of Gemstone Research, University
of Mainz, Germany. Four olivine grains were placed together in a mold and then
filled by resin. Subsequently, 5 wafer samples (Figure 3.3) with 4 olivine grains each
were polished until their surfaces are appropriate to be analyzed. The second parts
were brought to gemstone lapidary shop for surface polishing (Figure 3.3)  then their
physical and  optical  properties were carried out as well as collection of Raman
spectra.
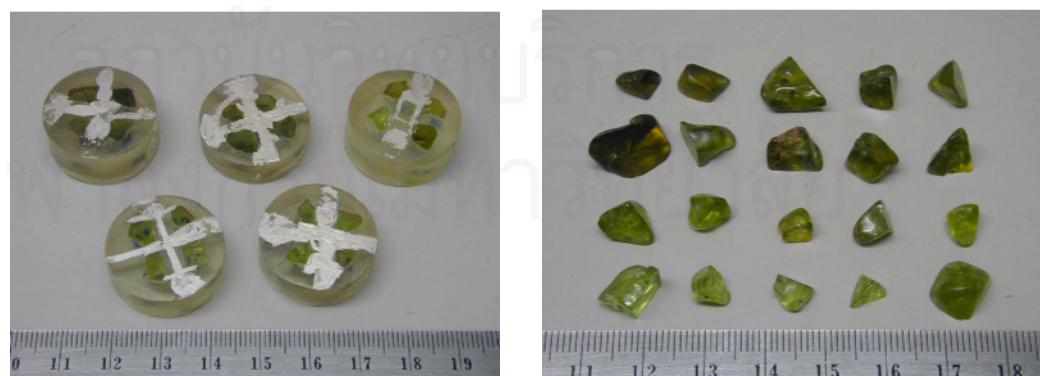


Figure 3.3  Selected coarse-grained olivine samples were cut and separated into 2
parts; the first group was prepared for EPMA analysis (left), the other
group was used   for determination of physical and optical  properties
and raman spectroscopy (right).

*3.2 General Properties*

The 20 samples of coarse-grained natural olivines were determined for their physical and optical properties, such as size, color, refractive indices , specific gravity and ultraviolet fluorescence.

In general, samples have size ranging between 0.80 and 7.59 carat. Their colors shade slightly from greenish yellow to yellowish green within light to dark tones. They are mostly transparent to semi-transparent, partly effected by abundance of inclusions.

All of samples were well polished on one side to be used for measurement of refractive indices (R.I.) using refractometer. Monochromatic, sodium equivalent light source was combined with A-Kruss refractometer (Figure 3.4) and used for this research. Refractive indices of all samples are slightly ranging between 1.650-1.668 for $n_\alpha$ and 1.690-1705 for $n_\gamma$; however, they fall conclusively in range of normal olivine. In addition, dark samples are likely present higher R.I. than the others; that is suspected to have higher Fe content.



Figure 3.4.   A-Kruss refractometer with sodium light source used in this research project.

These samples were weighed in air and in water at room temperature using Mettler Toledo (model   AG204) electronic balance (Figure 3.5). Consequently, specific gravity (S.G.) of each sample was automatically determined. They yield S.G. within a narrow range of about  3.3 -3.4. These values are  actually accepted for olivine range.



Figure 3.5    Mettler Toledo (model  AG204) electronic balance used to weigh and determine specific gravity of coarse-grained samples.

Although olivines are not expected to be activated by ultraviolet wave, additional sample testing on fluorescence under ultraviolet light was also concerned in this research project.  Under dark box condition, all samples were placed into Mineralight lamp (UVGL 25) that can produce both long-wave (365 nm) and short-wave(254 nm) ultraviolet radiations (Figure 3.6). Result of this investigation confirms that all olivine are inert and do not reveal phosphorescence. The  properties of most coarse-grained olivine samples are present in Table 3.1.

Figure 3.6.    Mineralight lamp (UVGL 25) generating both long-wave (365 nm) and short-wave(254 nm) of ultraviolet engaged to observe fluorescence phenomena of the studied olivines.

Table 3.1  Show the RI and SG of 20 coarse-grained samples

| Sample No. | Color | Weight (ct) | Refractive Index $(n_\alpha - n_\gamma)$ | Specific Gravity | Fluorescence under UV light |
|---|---|---|---|---|---|
| PD 01 | Dark gY | 1.43 | 1.668-1.705 | 3.43 | Inert |
| PD 02 | Dark gY | 6.48 | 1.660-1.692 | 3.35 | Inert |
| PD 03 | Dark gY | 4.83 | 1.660-1.690 | 3.35 | Inert |
| PD 04 | Dark gY | 3.04 | 1.660-1.690 | 3.35 | Inert |
| PD 05 | Dark gY | 2.26 | 1.655-1.690 | 3.34 | Inert |
| PD 06 | Dark gY | 7.59 | 1.665-1.700 | 3.41 | Inert |
| PD 07 | Dark gY | 3.44 | 1.660-1.695 | 3.37 | Inert |
| PD 08 | Dark gY | 4.07 | 1.658-1.690 | 3.34 | Inert |
| PD 09 | Dark gY | 3.43 | 1.660-1.690 | 3.33 | Inert |
| PD 10 | Dark gY | 2.42 | 1.650-1.690 | 3.35 | Inert |
| PD 11 | gY | 2.42 | 1.651-1.690 | 3.32 | Inert |
| PD 12 | gY | 1.94 | 1.650-1.690 | 3.31 | Inert |
| PD 13 | gY | 1.17 | 1.658-1.690 | 3.37 | Inert |

| | | | | | |
|---|---|---|---|---|---|
| PD 14 | gY | 2.03 | 1.651-1.690 | 3.33 | Inert |
| PD 15 | yG | 1.22 | 1.650-1.690 | 3.33 | Inert |
| PD 16 | yG | 3.43 | 1.652-1.690 | 3.32 | Inert |
| PD 17 | Light yG | 1.41 | 1.650-1.690 | 3.32 | Inert |
| PD 18 | Light yG | 1.17 | 1.652-1.690 | 3.30 | Inert |
| PD 19 | Light yG | 0.80 | 1.652-1.690 | 3.35 | Inert |
| PD 20 | Light yG | 4.06 | 1.655-1.690 | 3.33 | Inert |

gY = greenish yellow   yG = yellowish green

## 3.3   Chemical Composition

All 20 samples of coarse-grained natural olivines have been analyzed using  the JEOL Electron Probe Micro-Analyzer (EPMA) model JXA 8900 equiped with EDXRF system at  Center of Gemstone Research, Institute of Geosciences, University of Mainz, Germany. Analytical condition of sample analysis was set as focused beam at 20 kV and 20 nA with  different counting times for each element. The TAP crystal in spectrometer 1 was selected to analyze Al, Si and Mg with counting times of 40, 40 and 100 seconds, respectively. The PET crystal in spectrometer 2 was used for Ti, Cr and Ca with equal counting times of 100 seconds. The LiFH in spectrometer 5 was used for Fe and Mn  with identical counting times of 100 seconds. Standards used for calibration were wollastonite for Si and Ca, synthetic corundum for Al,  pure metal MgO for Mg, pure metal $Fe_2O_3$ for Fe, metallic chromium for Cr, pure metal $MnTiO_3$ for Mn and Ti. All analyses were automatically undertaken ZAF collection before reporting in form of % oxide, in which detection limit of each element is about 0.01 weight %. Each sample was set to analyze  5 spots, this is designed to check  homogeneity of composition of each sample. All analyses were then recalculated based on 4 oxygens to atomic formula and end-member (Appendix1). Mean analyses, averaged from 5 spots, were also calculated statistically; these analyses and their end-member proportions are present in Table 3.2.

In conclusion, end-member compositions of all analyzed samples fall in range of $Fo_{91.5}$ - $Fo_{83.9}$. In addition, seven fine-grained samples are characterized by Fe-richer olivines ($Fo_{73.5}$ – $Fo_{50.5}$). Thus, the whole range of Fo content available for this study is $Fo_{91.5}$ - $Fo_{50.5}$.

Table 3.2    Average of 5 EPMA analyses for each coarse-grained olivine sample.

| | PD01 | PD02 | PD03 | PD04 | PD05 | PD06 | PD07 | PD08 | PD09 | PD10 |
|---|---|---|---|---|---|---|---|---|---|---|
| MgO | 45.52 | 48.63 | 49.47 | 48.95 | 45.74 | 48.92 | 48.84 | 48.86 | 49.35 | 50.43 |
| $Al_2O_3$ | 0.02 | 0.02 | 0.02 | 0.02 | 0.02 | 0.02 | 0.02 | 0.02 | 0.02 | 0.02 |
| $SiO_2$ | 40.39 | 39.82 | 40.49 | 41.10 | 39.32 | 39.12 | 39.56 | 40.00 | 39.40 | 38.85 |
| CaO | 0.13 | 0.13 | 0.11 | 0.13 | 0.10 | 0.13 | 0.13 | 0.13 | 0.07 | 0.10 |
| MnO | 0.17 | 0.15 | 0.15 | 0.15 | 0.18 | 0.15 | 0.14 | 0.16 | 0.15 | 0.10 |
| FeO | 15.40 | 10.65 | 10.32 | 10.96 | 14.43 | 10.30 | 10.86 | 10.81 | 10.23 | 9.24 |
| NiO | 0.29 | 0.35 | 0.34 | 0.36 | 0.31 | 0.33 | 0.35 | 0.35 | 0.38 | 0.39 |
| $Cr_2O_3$ | 0.02 | 0.03 | 0.03 | 0.03 | 0.03 | 0.03 | 0.03 | 0.03 | 0.05 | 0.06 |
| Total | 101.93 | 99.78 | 100.92 | 101.71 | 100.12 | 99.01 | 99.93 | 100.37 | 99.64 | 99.18 |
| Formula 4(O) | | | | | | | | | | |
| Mg | 1.675 | 1.794 | 1.800 | 1.770 | 1.710 | 1.819 | 1.802 | 1.793 | 1.822 | 1.865 |
| Al | 0.001 | 0.000 | 0.001 | 0.001 | 0.001 | 0.001 | 0.000 | 0.001 | 0.000 | 0.001 |
| Si | 0.997 | 0.985 | 0.988 | 0.996 | 0.986 | 0.976 | 0.979 | 0.984 | 0.976 | 0.964 |
| Ca | 0.003 | 0.003 | 0.003 | 0.003 | 0.003 | 0.003 | 0.004 | 0.003 | 0.002 | 0.003 |
| Mn | 0.003 | 0.003 | 0.003 | 0.003 | 0.004 | 0.003 | 0.003 | 0.003 | 0.003 | 0.002 |
| Fe | 0.318 | 0.220 | 0.211 | 0.222 | 0.303 | 0.215 | 0.225 | 0.223 | 0.212 | 0.192 |
| Ni | 0.006 | 0.007 | 0.007 | 0.007 | 0.006 | 0.007 | 0.007 | 0.007 | 0.008 | 0.008 |
| Cr | 0.000 | 0.001 | 0.001 | 0.001 | 0.001 | 0.001 | 0.001 | 0.001 | 0.001 | 0.001 |
| Total | 3.003 | 3.014 | 3.012 | 3.003 | 3.013 | 3.024 | 3.020 | 3.015 | 3.024 | 3.035 |
| %Fo | 83.9 | 88.9 | 89.4 | 88.7 | 84.8 | 89.3 | 88.8 | 88.8 | 89.4 | 90.6 |
| %Fa | 16.1 | 11.1 | 10.6 | 11.3 | 15.2 | 10.7 | 11.2 | 11.2 | 10.6 | 9.4 |

Table 3.2. (continued)

|  | PD11 | PD12 | PD13 | PD14 | PD15 | PD16 | PD17 | PD18 | PD19 | PD20 |
|---|---|---|---|---|---|---|---|---|---|---|
| MgO | 50.82 | 50.77 | 50.26 | 51.24 | 51.58 | 51.51 | 52.36 | 51.65 | 50.56 | 51.62 |
| $Al_2O_3$ | 0.04 | 0.04 | 0.02 | 0.03 | 0.03 | 0.02 | 0.02 | 0.02 | 0.02 | 0.03 |
| $SiO_2$ | 38.49 | 37.85 | 38.16 | 38.19 | 37.94 | 38.24 | 38.71 | 38.21 | 37.58 | 38.81 |
| CaO | 0.09 | 0.10 | 0.08 | 0.10 | 0.10 | 0.07 | 0.07 | 0.07 | 0.09 | 0.11 |
| MnO | 0.09 | 0.13 | 0.15 | 0.11 | 0.13 | 0.14 | 0.12 | 0.13 | 0.12 | 0.11 |
| FeO | 8.47 | 8.86 | 9.77 | 8.69 | 8.55 | 8.37 | 8.50 | 8.55 | 9.24 | 8.87 |
| NiO | 0.39 | 0.39 | 0.32 | 0.38 | 0.38 | 0.38 | 0.37 | 0.36 | 0.36 | 0.38 |
| $Cr_2O_3$ | 0.06 | 0.05 | 0.06 | 0.05 | 0.04 | 0.05 | 0.04 | 0.04 | 0.04 | 0.05 |
| Total | 98.45 | 98.19 | 98.81 | 98.80 | 98.76 | 98.77 | 100.18 | 99.00 | 98.00 | 99.96 |
| Formula 4(O) | | | | | | | | | | |
| Mg | 1.889 | 1.899 | 1.873 | 1.902 | 1.916 | 1.910 | 1.914 | 1.912 | 1.899 | 1.893 |
| Al | 0.001 | 0.001 | 0.001 | 0.001 | 0.001 | 0.001 | 0.001 | 0.000 | 0.000 | 0.001 |
| Si | 0.960 | 0.950 | 0.954 | 0.951 | 0.945 | 0.951 | 0.949 | 0.949 | 0.946 | 0.955 |
| Ca | 0.002 | 0.003 | 0.002 | 0.003 | 0.003 | 0.002 | 0.002 | 0.002 | 0.002 | 0.003 |
| Mn | 0.002 | 0.003 | 0.003 | 0.002 | 0.003 | 0.003 | 0.003 | 0.003 | 0.003 | 0.002 |
| Fe | 0.177 | 0.186 | 0.204 | 0.181 | 0.178 | 0.174 | 0.174 | 0.177 | 0.195 | 0.182 |
| Ni | 0.008 | 0.008 | 0.006 | 0.008 | 0.008 | 0.008 | 0.007 | 0.007 | 0.007 | 0.007 |
| Cr | 0.001 | 0.001 | 0.001 | 0.001 | 0.001 | 0.001 | 0.001 | 0.001 | 0.001 | 0.001 |
| Total | 3.039 | 3.049 | 3.045 | 3.048 | 3.054 | 3.048 | 3.050 | 3.051 | 3.053 | 3.044 |
| %Fo | 91.4 | 91.0 | 90.0 | 91.2 | 91.4 | 91.5 | 91.5 | 91.4 | 90.6 | 91.1 |
| %Fa | 8.6 | 9.0 | 10.0 | 8.8 | 8.6 | 8.5 | 8.5 | 8.6 | 9.4 | 8.9 |

## 3.4 Raman Experiment

The ambient Raman spectra were collected using  Renishaw–1000 Raman microprobe at the Gem and Jewelry Institute of Thailand (Public Organization) (Figure 3.7). All measurements were carried out without polarization analyzer. The monochromatic light source for this experiment is Argon ion laser which produces green laser line with wavelength of 514.5 nm. All spectra were recorded with a Leica 50 microscope objectives.
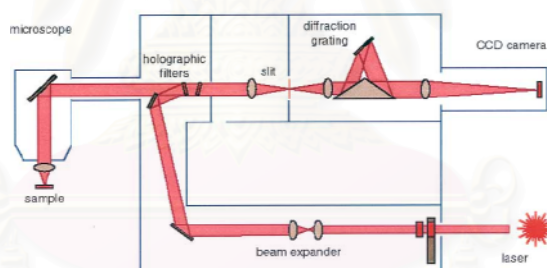


Figure 3.7   Renishaw – 1000 Raman  microprobe used in this study (top) and the schematic of its configuration (bottom).

Beam size of laser on surface was set as  approximately 5 micron. Calibration of wavenumber   was carried on until accuracy was close to $\pm$ 1 cm$^{-1}$ that was determined using plasma emission lines at 520 cm$^{-1}$ of silicon standard. The  non polarized Raman spectra of each sample were obtained at room temperature within the wavenumber range of 250 – 2000 cm$^{-1}$(Figure 3.8). For coarse-grained sample,

three analytical points have been performed on the polished surface. On the other hand, fine-grained samples (with average grain size of about 100 microns) have been selected three grains to represent each sample and to obtain good spectrum; each selected grain must have smooth surface. It seems to have no change on Raman peak positions which can be observed from all spectra analyzed in the same sample. However, presence or absence of some minor peaks can be distinguished. Spectra and frequency reported in this work are the average from those spectra.
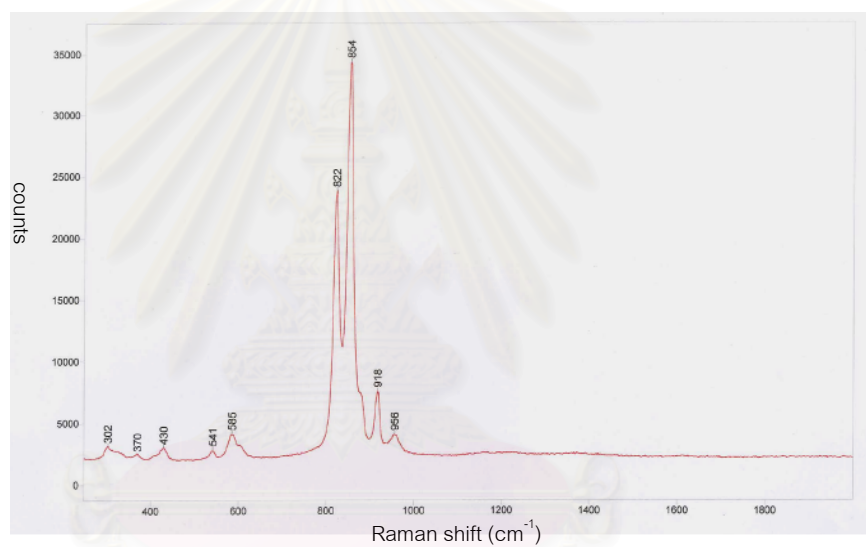


Figure 3.8. Non polarized Raman spectrum of olivine in range 250-2000 cm$^{-1}$

## 3.5   Raman spectroscopy result

The Raman spectra can be observed mostly in the range below 1000 cm$^{-1}$ only; in addition, they  can be subdivided  into 2 main regions: high-wavenumber region consisting of 4 main peaks in range of 800-1000 cm$^{-1}$ and low-wavenumber region consisting of several small peaks in the range below 600 cm$^{-1}$(Figure 3.9). The spectra belong to coarse-grained samples show very well sharp peaks. In contrast, the raman spectra obtained from fine-grained samples are broadening, especially in the low-wavenumber region.
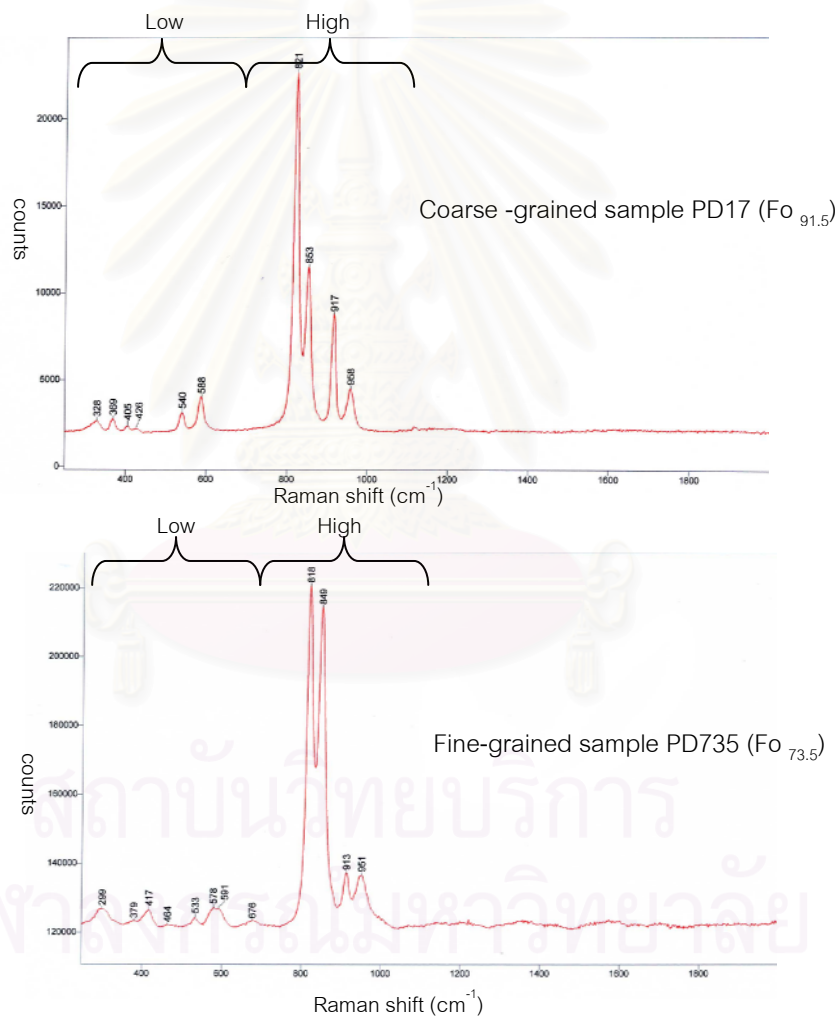


Figure 3.9   Raman spectra of studied samples;   coarse-grained

sample PD17 with Fo content of 91.5 (top) and fine-grained sample

PD735 with Fo content of 73.5 (bottom).

Thirteen peak positions of Raman spectra were observed and recorded in Table 3.3 from high Fo content to low Fo content.

Table 3.3  Peak positions of Raman spectra observed from all studied samples.

| %Fo | sample no. | p1 | p2 | p3 | p4 | P5 | p6 | p7 | p8 | p9 | p10 | p11 | p12 | p13 |
|---|---|---|---|---|---|---|---|---|---|---|---|---|---|---|
| 91.5 | PD16 | 958 | 917 | np | 853 | 821 | np | 588 | 540 | 426 | 405 | 369 | 328 | np |
| 91.5 | PD17 | 960 | 917 | 878 | 854 | 822 | 603 | 584 | 541 | 429 | np | 370 | np | 301 |
| 91.5 | PD18 | 960 | 915 | 878 | 853 | 821 | 603 | 582 | np | 433 | np | np | 323 | 300 |
| 91.4 | PD11 | 958 | 917 | 878 | 853 | 822 | 604 | 586 | 542 | 428 | np | 369 | np | 301 |
| 91.4 | PD15 | 959 | 917 | 878 | 853 | 821 | 603 | 583 | 542 | 431 | np | 370 | np | 300 |
| 91.2 | PD14 | 960 | 918 | np | 854 | 822 | np | 588 | 541 | 429 | 406 | 370 | 327 | np |
| 91.1 | PD20 | 957 | 916 | np | 853 | 821 | np | 587 | 539 | 429 | 406 | 369 | 331 | 301 |
| 91.0 | PD12 | 959 | 916 | 877 | 853 | 821 | 602 | 583 | 540 | 428 | np | 368 | np | 301 |
| 90.6 | PD10 | 957 | 916 | np | 852 | 821 | np | 586 | 538 | np | 404 | 367 | 329 | 303 |
| 90.5 | PD19 | 957 | 916 | 878 | 853 | 821 | 602 | 584 | 540 | 428 | np | 369 | np | 300 |
| 90.0 | PD13 | 959 | 917 | np | 853 | 822 | np | 588 | 541 | 426 | 405 | 369 | 327 | np |
| 89.5 | PD3 | 958 | 919 | np | 856 | 824 | 606 | 588 | 543 | 431 | 408 | 371 | np | 304 |
| 89.5 | PD9 | 960 | 918 | np | 854 | 823 | np | 589 | 541 | 428 | 405 | 369 | 327 | 302 |
| 89.4 | PD6 | 958 | 918 | 880 | 855 | 823 | 603 | 585 | 540 | 430 | np | np | np | 302 |
| 89.0 | PD2 | 960 | 919 | np | 855 | 824 | np | 589 | 543 | 433 | 408 | 372 | 330 | 304 |
| 88.8 | PD8 | 961 | 919 | np | 856 | 824 | np | 589 | 543 | 431 | 408 | 371 | 328 | 304 |
| 88.7 | PD4 | 961 | 918 | np | 854 | 822 | np | 588 | 541 | 428 | 406 | 371 | np | np |
| 88.7 | PD7 | 959 | 919 | np | 856 | 825 | np | 590 | 543 | np | 408 | 370 | np | 302 |
| 84.8 | PD5 | 960 | 919 | np | 855 | 823 | 606 | 587 | 541 | 433 | np | 372 | np | 302 |
| 83.9 | PD1 | 957 | 919 | np | 854 | 823 | 606 | 588 | 541 | 428 | 407 | 369 | 325 | 301 |
| 73.5 | PD735* | 951 | 913 | np | 849 | 818 | 591 | 578 | 533 | 417 | np | np | np | 299 |
| 70.6 | PD706* | 951 | 912 | np | 848 | 818 | 592 | 578 | 534 | 415 | np | np | 338 | 302 |
| 67.8 | PD678* | 950 | 913 | np | 850 | 819 | np | 578 | 533 | 415 | np | np | np | 306 |
| 61.7 | PD617* | 944 | 912 | np | 848 | 819 | 591 | np | 531 | 416 | np | np | 337 | 304 |
| 60.5 | PD605* | 940 | 912 | np | 847 | 817 | np | 575 | 529 | np | 408 | np | 334 | 304 |
| 58.8 | PD588* | 941 | 910 | np | 847 | 817 | 591 | np | 529 | 420 | 400 | np | 335 | 304 |
| 50.5 | PD505* | 938 | 910 | np | 846 | 817 | np | 578 | 526 | 419 | 405 | np | 329 | 301 |

Remark:  *  : fine-grained sample,   np:  not present

*3.6 Relationship between composition of olivine and Raman spectra*

Comparison of equivalent peak positions clearly illustrates downshift of Raman spectra in higher iron (Fe) olivines. This downshift occurs clearly in high-wavenumber region of spectra which contains 4 main peaks at about 960-938, 919-910, 854-846 and

824-817 cm$^{-1}$(Figure 3.10). Meanwhile, low-wavenumber region (below 600 cm$^{-1}$) shows very little variation of peak position.
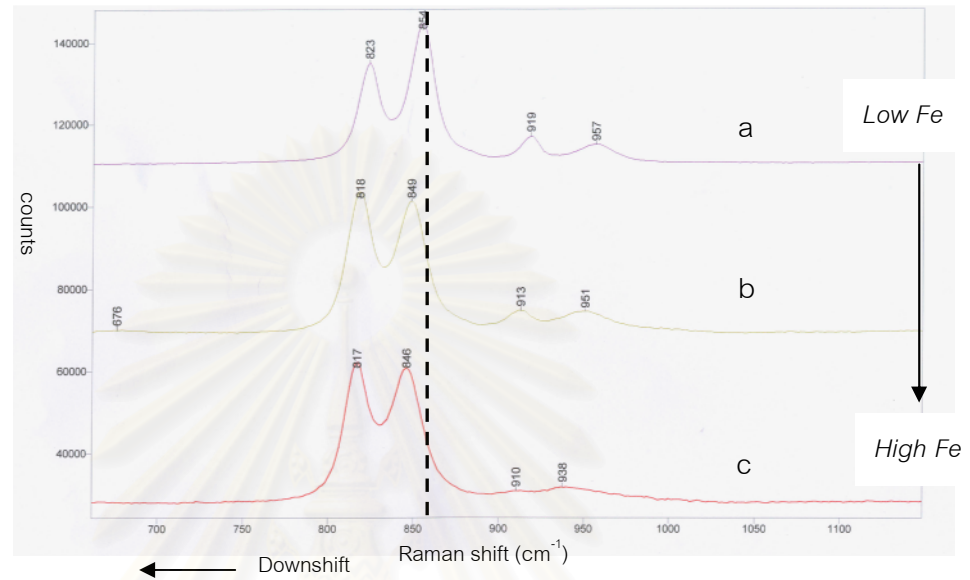


Figure 3.10  Three sets of spectra from (a) lower Fe to (c) higher Fe show the down shift of Raman peak position in high-wavenumber (700 – 1000 cm$^{-1}$) region  (a: Fo $_{91.5}$, b: Fo $_{70.6}$, c: Fo $_{50.5}$) and dash line is reference line revealing downshift to the left (lower wavenumber) of higher Fe content.

The correlation plot between the Fo content  and peak position of all ambient spectra was subdivided into 3 regions of spectra from high-wavenumber to low-wavenumber; region 1 ranges from1000 to 800 cm$^{-1}$; region 2 ranges from 650 to 500 cm$^{-1}$; region 3 ranges from  500 to 250 cm$^{-1}$ (Figure 3.11).
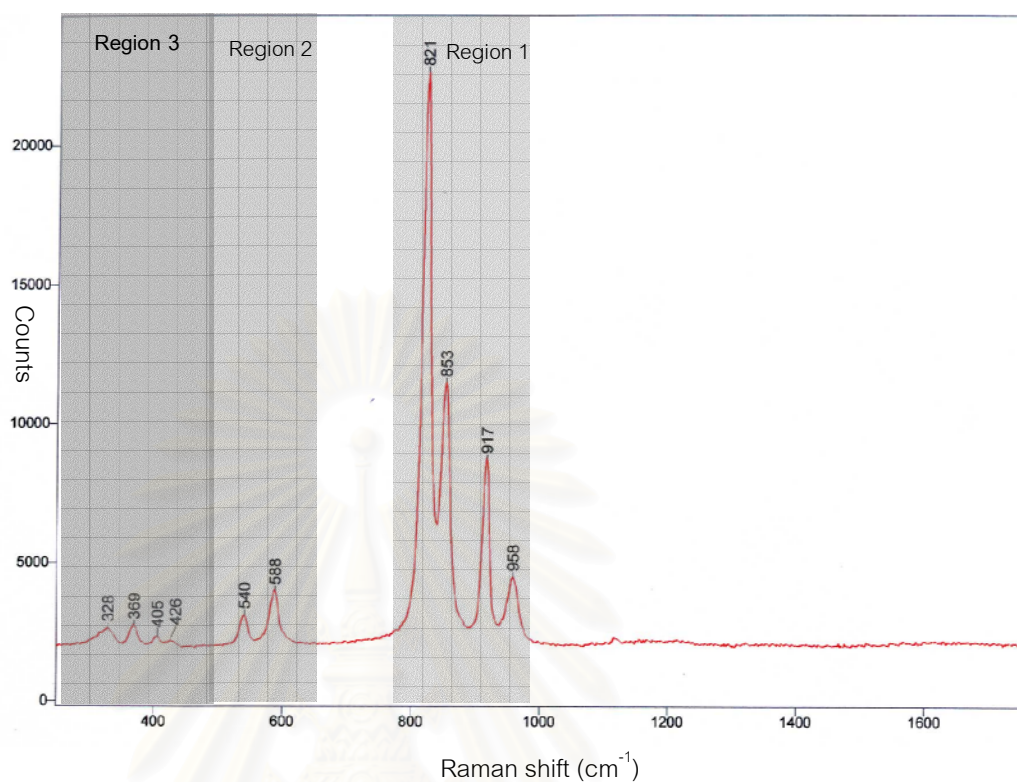
Figure 3.11  Three regions of spectra  divided for correlation plot; region 1 ranges
from1000 -800 cm$^{-1}$;  region 2 ranges from 650 – 500 cm$^{-1}$; region 3
ranges from  500 -  250 cm$^{-1}$.
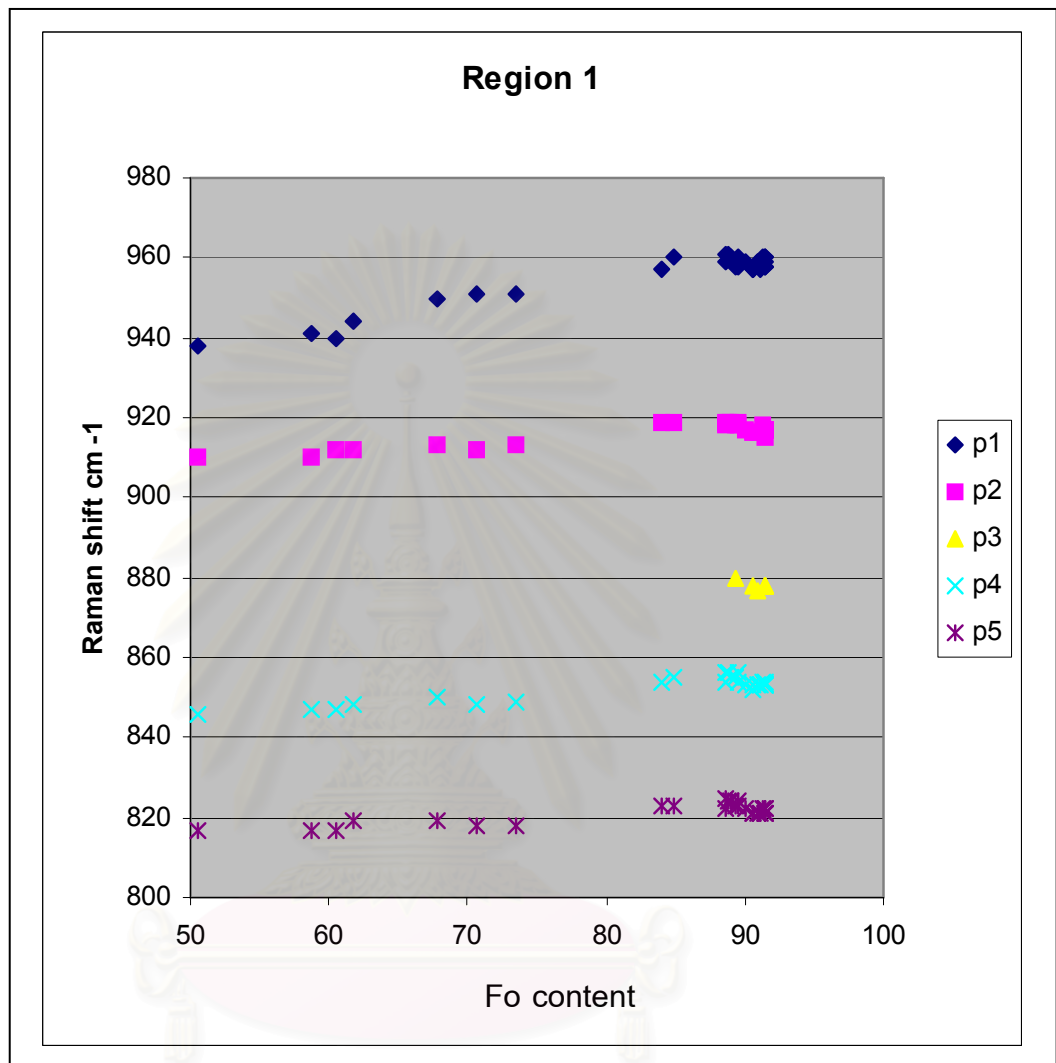
Figure 3.12. Correlation between Fo contents and Raman spectra peak positions of region 1 (1000 – 800 cm$^{-1}$).
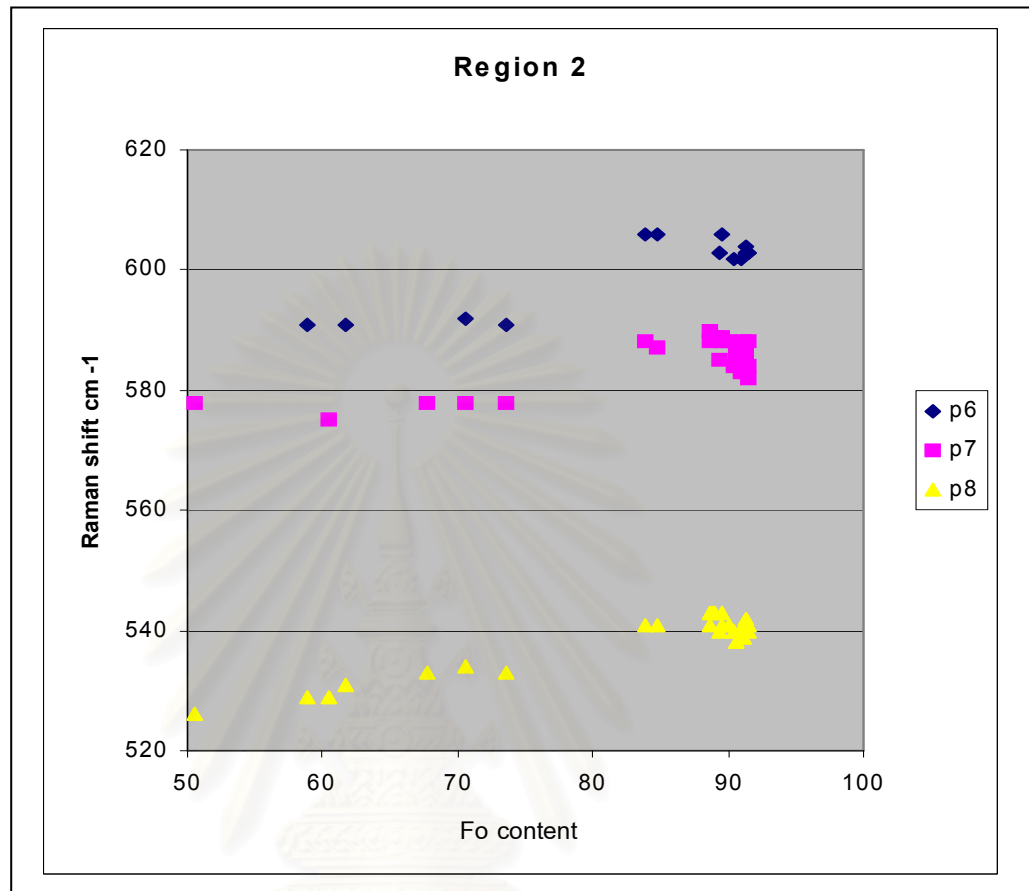
Figure 3.13  Correlation between Fo contents and Raman spectra peak positions of
region 2 (650 – 500 cm$^{-1}$).
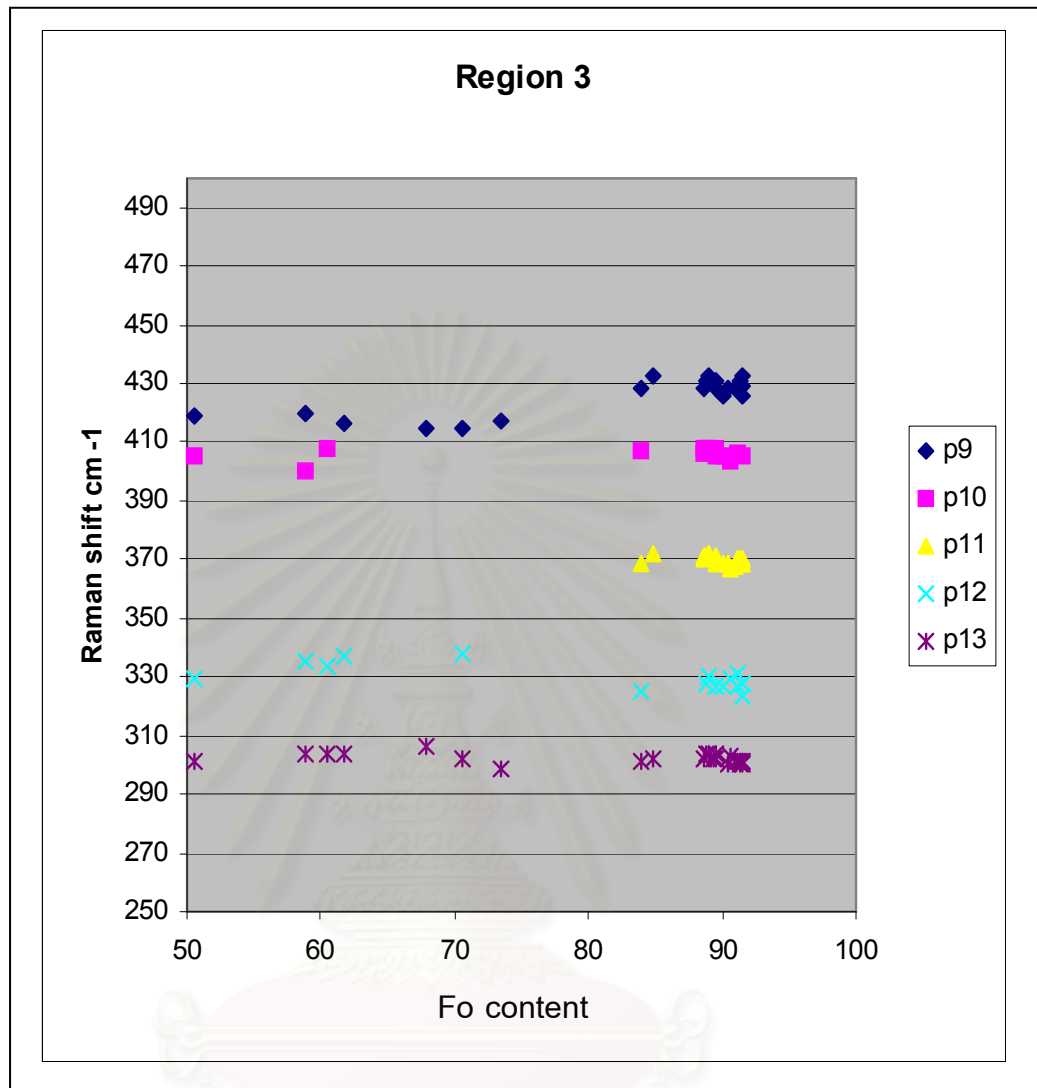
Figure 3.14  Correlation between Fo contents and Raman spectra peak positions of
region 3 (500 – 250 cm$^{-1}$).

From the correlation plot above, region 1 consists of 5 peaks at about 960-940, 920-910, 880-877, 855-846 and 825-817 cm$^{-1}$, respectively; every observe peak position reveals obviously down shift of iron-richer samples (less Fo content) in this region except the peak at about 880-877 cm$^{-1}$ which is present in some samples only. Region 2 contains 3 peaks at about 606-591, 589-578 and 540-526 cm$^{-1}$, respectively, and also reveal downshift of peak positions of lower Fo contents. Region 3 comprises 5 peaks at about 430-415, 408-400, 370-369, 325-335 and 300-304 cm$^{-1}$, respectively, but the peak positions in this region show very slightly variation.

Linear regression equations were carried out from plots between Fo contents and peak positions. Most abundance peaks expected in region 1 (i.e. p1(960-940 cm$^{-1}$), p2 (920-910 cm$^{-1}$) ,p4(855-846 cm$^{-1}$) ,p5(825-817cm$^{-1}$)) were considered for this investigation because these 4 peaks always present in every samples and peaks p4 and p5 have highest intensity. Peaks in the other regions are not suitable to find out the relationship, even though some positions tend to show high downshift value. However, these peaks are weak and broaden especially in fine-grained samples. Consequently, some peak positions of these regions are not clearly marked and might not be represent the exact value of their modes. The linear regression equations and their chi-square values are present in (Figures 3.15 to 3.18).
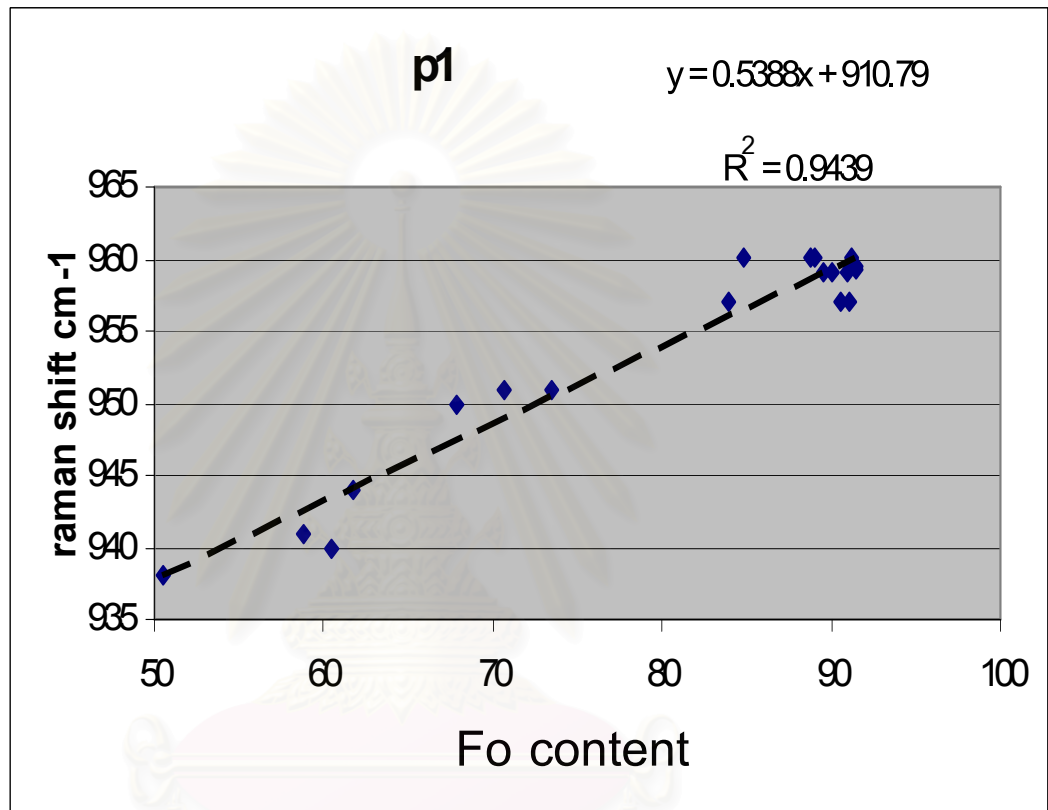
Figure 3.15 Plots between Raman peak position (960-940 cm$^{-1}$; p1) and Fo
content and linear regression equation with chi-square value.
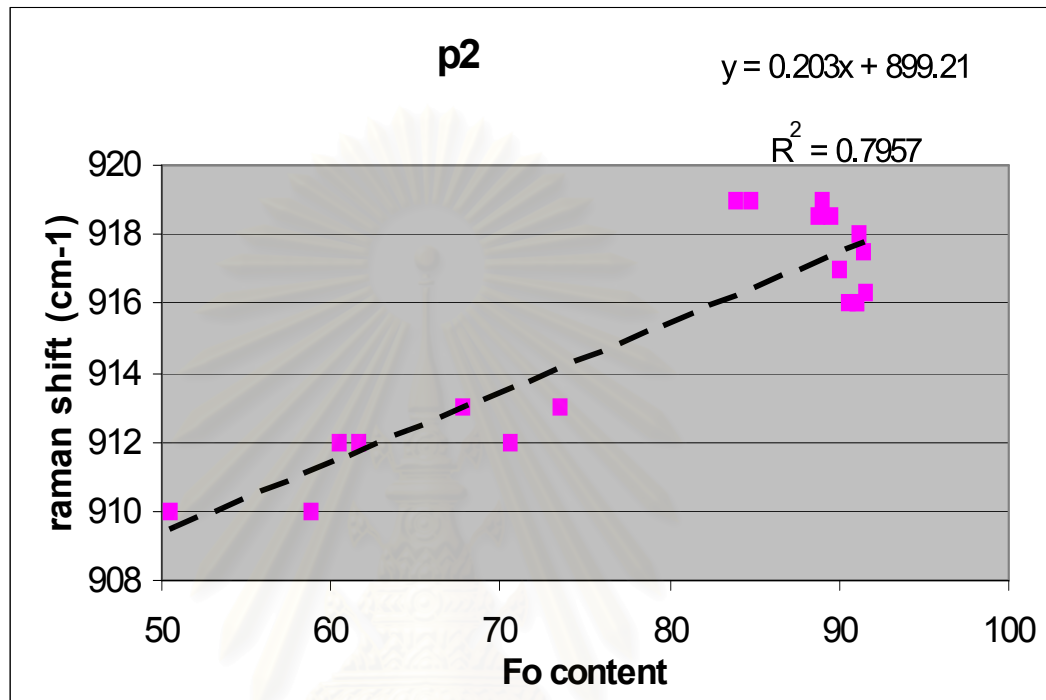
Figure 3.16  Plots between Raman peak position (920-910 cm$^{-1}$; p2) and Fo

content and linear regression equation with chi-square value.
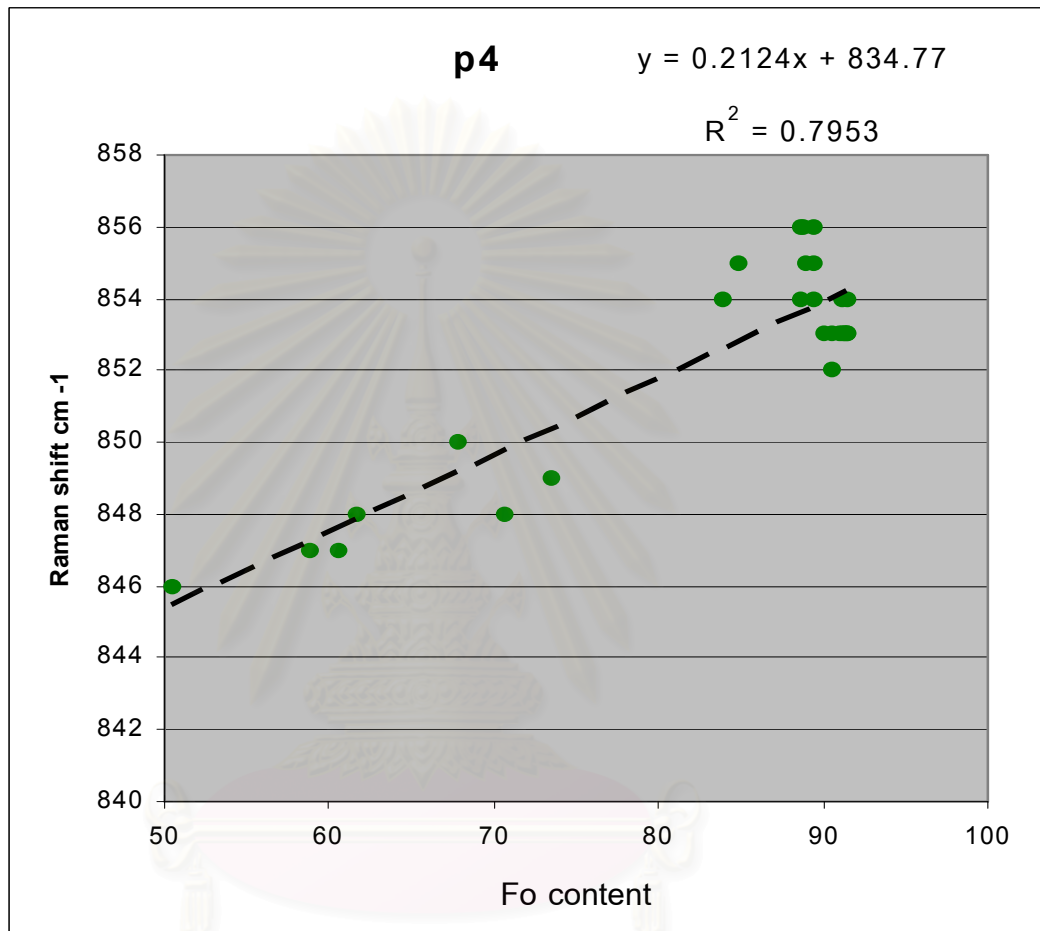
Figure 3.17  Plots between Raman peak position (855-846 cm$^{-1}$; p4) and
Fo content and linear regression equation with chi-square value.
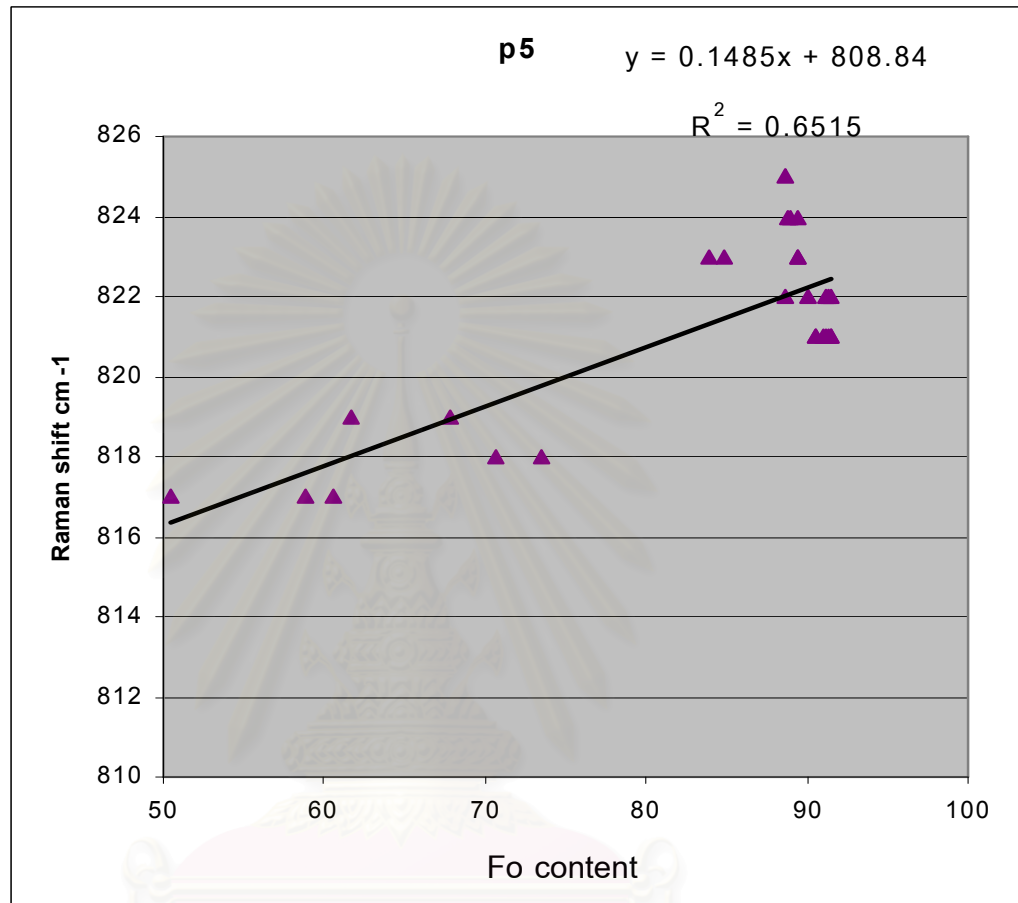
Figure 3.18  Plots between Raman peak position (825-817cm$^{-1}$; p5) and

Fo content and linear regression equation with chi-square value.

CHAPTER IV

DISCUSSION AND CONCLUSIONS

## 4.1 Assignment on Raman active modes of olivines

The assignment of Raman modes of olivines have been studied by many researchers (e.g. Bonilla,1982; McMillan and Hofmeister, 1988; Chopelas, 1991; Kolesov et al.,1995; Lin, 2000; Kolesov and Geiger, 2004). Among 81 vibration modes of olivine, 36 modes are Raman active including $11A_g$, $11B_{1g}$, $7B_{2g}$ and $7B_{3g}$ where $A_g$ modes mean the symmetrical vibration modes and $B_{xg}$ modes are asymmetrical vibration modes. All 36 vibration modes can be grouped into 2 main modes; i.e. internal modes and lattice modes. Internal modes are the vibration modes that are related to $SiO_4$ tetrahedra, whereas lattice modes are assigned to the translational and rotational vibration of $SiO_4$ tetrahedra associated with $M2$ site.

Internal modes of olivine are assigned to the internal molecular vibration of $SiO_4$ tetrahedra and the intensity of these modes usually fall within the high-wavenumber region that is significantly higher than those the lattice modes. Vibration of $SiO_4$ tetrahedra can be divided into 4 types; containing 2 symmetrical vibration modes $(V_1$ and $V_2)$ and 2 asymmetrical vibration modes $(V_3$ and $V_4)$ as shown in Figure 4.1.



| $v_1$-symmetric stretch | $v_2$-symmetric bend | $v_3$-asymmetric stretch | $v_4$-asymmetric bend |
| 800-950 cm$^{-1}$ | 300-500 cm$^{-1}$ | 850-1200 cm$^{-1}$ | 400-600 cm$^{-1}$ |
| Raman (often strong) | Present in Raman | Infrared (strong), Raman | Infrared, Raman |
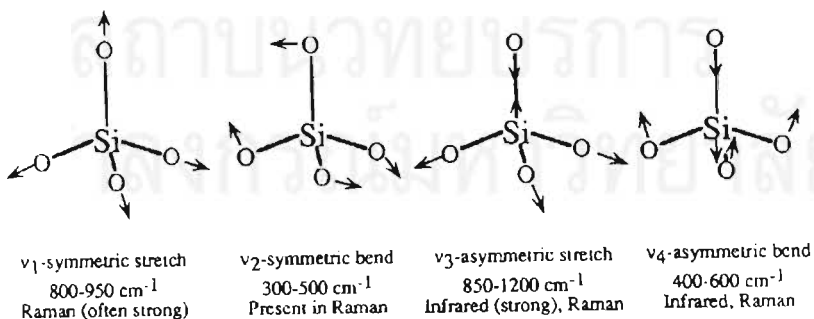
Figure 4.1 Characters of four internal modes of $SiO_4$ tetrahedra ( after Williams,1995).

On the other hand, lattice modes show large variation consisting of $SiO_4$ rotation which is expected to have highest frequency. The $SiO_4$ translation yields the lowest frequency. The $SiO_4$ and *M2* translations are actually mixed, whereas *M1* translations are Raman inactive. Table 4.1 shows classification of raman active modes of olivine. In addition, mode frequencies in wavenumber ($cm^{-1}$) of end-member forsterite and fayalite and their assignments are summarized in Table 4.2.

Table 4.1. Classification of 36 Raman active modes of olivine.

(modified from Chopelas 1991)

|  | $11A_g$ | $11B_{1g}$ | $7B_{2g}$ | $7B_{3g}$ |
|---|---|---|---|---|
| *$SiO_4$ internal modes* |  |  |  |  |
| $V_1$ (symmetrical stretching) | 1 | 1 | 0 | 0 |
| $V_2$(symmetrical bending) | 1 | 1 | 1 | 1 |
| $V_3$(asymmetrical stretching) | 2 | 2 | 1 | 1 |
| $V_4$(asymmetrical bending) | 2 | 2 | 1 | 1 |
| *Lattice modes* |  |  |  |  |
| $SiO_4$ rotation | 1 | 1 | 2 | 2 |
| $SiO_4$ translation | 2 | 2 | 1 | 1 |
| *M1* translation | 0 | 0 | 0 | 0 |
| *M2* translation | 2 | 2 | 1 | 1 |

Table 4.2.   Mode frequencies in cm$^{-1}$ and their assignments of forsterite (Fo)
and fayalite (Fa)  (modified from Chopelas 1991)

| Forsterite | Fayalite | Assignment |
|---|---|---|
| $A_g$ | | |
| 965 | 932 | V3 |
| 856 | 840 | V1+V3 |
| 824 | 814 | V1+V3 |
| 608 | 562 | V4 |
| 545 | 505 | V4 |
| 422 | 369 | V2 |
| 339 | 237 | M2 translation |
| 329 | 289 | SiO$_4$ rotation |
| 304 | 259 | M2 translation |
| 226 | 171 | SiO$_4$ translation |
| 183 | 119 | SiO$_4$ translation |
| $B_{1g}$ (xy) | | |
| 975 | 947 | V3 |
| 866 | 851 | V3(+V3) |
| 838 | 822 | V1(+V3) |
| 632 | 577 | V4 |
| 582 | 524 | V4 |
| 434 | 384 | V2 |
| 383 | 312 | M2 translation |
| 351 | 277 | M2 translation |
| 318 | 260 | SiO$_4$ rotation |
| 274 | 193 | SiO$_4$ translation |
| 220 | 154 | SiO$_4$ translation |
| $B_{2g}$ (xz) | | |
| 881 | 860 | V3 |
| 586 | 553 | V4 |
| 439 | 405 | V2 |
| 365 | 309 | mix(SiO$_4$ rotation) |
| 323 | 290 | mix(M2 translation) |
| 242 | 189 | mix(SiO$_4$ rotation) |
| 175 | 102 | mix(SiO$_4$ translation) |
| $B_{3g}$ (yz) | | |
| 920 | 900 | V3 |
| 592 | 549 | V4 |
| 435 | - | mix(SiO$_4$ rotation) |
| 410 | 376 | V2 |
| 374 | 281 | mix(M2 translation) |
| 315 | 186 | mix(SiO$_4$ rotation) |
| 286 | 113 | mix(SiO$_4$ translation) |

According to Chopelas (1991), study of polarized Raman spectra shows that axis vibration ($A_g$) modes of olivine are easily obtained by low power (20 – 200 mW) laser but the off-axis ($B_{xg}$) modes require more power up to 1 W to bring signal above the noise level of spectra, especially in the lattice mode. In comparison with this study, all non-polarized spectra were obtained using approximately 20 mW laser power. Thus, the spectra obtained in this study are expected to comprise dominant $A_g$ modes together with weaker $B_{xg}$ modes. Because $B_{xg}$ modes prefered higher power for activation. In coarse-grained samples, the well shape peaks in spectra show combination of dominant $A_g$ mode together with some $B_{xg}$ modes (Figure 4.2) in both internal and lattice modes. However, many peaks belonging to $B_{xg}$ lattice modes show weaker intensity but still have well shapes. In contrast, the Raman spectra of fine-grained samples (Figure 4.3) still contain dominant internal $A_g$ modes together with internal and lattice $B_{xg}$ modes but all lattice modes usually present boarded peak especially in $B_{xg}$ modes are broaded with very low intensity.
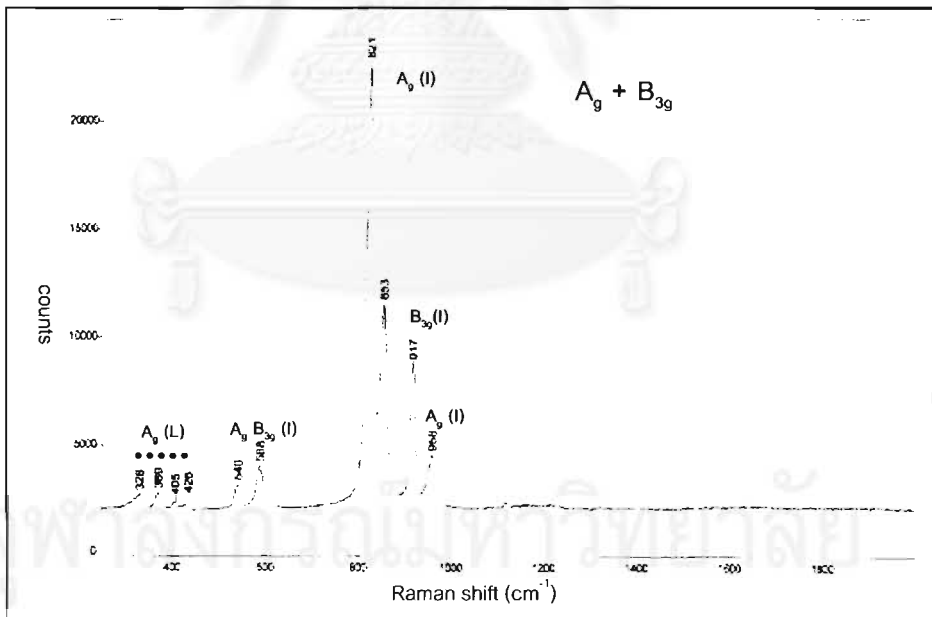


Figure 4.2  Raman spectrum of coarse-grained olivine (PD10) showing axis vibration ($A_g$) and off-axis vibration ($B_{3g}$) modes, which I and L stand for internal mode and lattice mode, respectively.
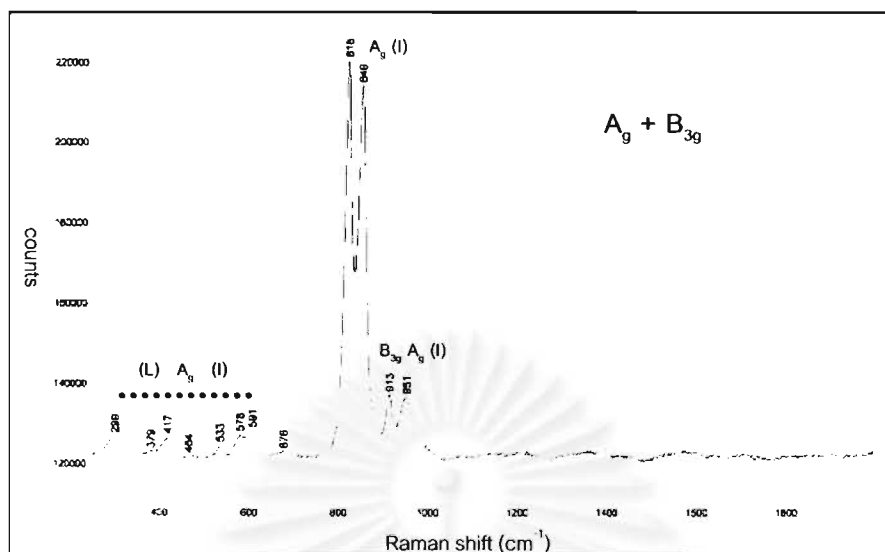
Figure 4.3 Raman spectrum of fine-grained olivine (PD735) showing axis vibration ($A_g$) and off-axis vibration ($B_{3g}$) modes, which I and L stand for internal mode and lattice mode, respectively. Most peaks in lattice mode region show broaden peaks with low intensity.

In this study, 13 modes can be observed and the interpretation of each assignment is given in Table 4.3.

Table 4.3. Thirteen mode frequencies (in cm$^{-1}$) and their assignments of olivine sample observed in this study.

| Peak no. | Freq. (cm$^{-1}$) Fo$_{-90}$ | Freq. (cm$^{-1}$) Fo$_{-50}$ | Relative strength | Mode | Assignment |
|---|---|---|---|---|---|
| P1 | 960 | 940 | Moderate | A$_g$ internal | V3 |
| P2 | 917 | 910 | Moderate | B$_{3g}$ internal | V3 |
| P3 | 878 | - | Moderate | B$_{2g}$ internal | V3 |
| P4 | 853 | 846 | Strong | A$_g$ internal | V1+V3 |
| P5 | 822 | 817 | Strong | A$_g$ internal | V1+V3 |
| P6 | 603 | 591 | Weak | A$_g$ internal | V4 |
| P7 | 585 | 578 | Weak | B$_{2g}$ internal | V4 |
| P8 | 542 | 529 | Weak | A$_g$ internal | V4 |
| P9 | 430 | 420 | Weak | B$_{3g}$ lattice | Mix (SiO$_4$ rotation) |
| P10 | 405 | 405 | Weak | B$_{3g}$ internal | V2 |
| P11 | 370 | - | Weak | B$_{3g}$ lattice | Mix(M2 translation) |
| P12 | 327 | 329 | Weak | A$_g$ lattice | SiO$_4$ rotation |
| P13 | 301 | 301 | Weak | A$_g$ lattice | M2 translation |

## 4.2 Grain Size Effect

From this study, one obvious phenomenon from fine-grained samples is the low intensity and broadening of the peaks, particularly in low frequencies region. The most possible explanation for this phenomenon is the grain size effect.

Wang (1999) suggested 2 main groups of factors that can affect Raman signal intensity (Table 4.4). The first group effects on the strength of Raman photon production, whereas the second group involves collection of Raman photon. Regarding all effects on strength of Raman photon production, they would not be crucial causes of the phenomenon (grain size effect) mentioned above. Because all these causes are conclusively based on composition of materials; which they are olivine composition even their chemical compositions are somehow different. In addition, coarse-grained samples vary from Fo$_{91.5}$ – Fo$_{83.5}$ while fine-grained samples contain Fo$_{73.5}$ – Fo$_{50.5}$ ; in this case,

both groups of sample have variation in composition but the such phenomenon does not appear in all cases of coarse-grained sample. Concerning heterogeneity of mineral sample, all sample grains selected for this study are quite homogenous in term of colors and chemical composition. Therefore these reasons would support that affection on strength of Raman photon production is not related to the grain size effect observed in this study.

Table 4.4. Main factors may affect signal intensity of Raman spectra (Wang,1999)

| Factors affecting the strength of Raman photon production | Factors affecting the collection of Raman photon |
|---|---|
| a. Raman cross section – intrinsic strength of the oscillating dipole of the target mineral<br>b. The number of molecules within the volume irradiated by laser beam<br>c. Internal heterogeneity within mineral | a. Multiple reflections of the excitation laser beam<br>b. Multiple internal reflections of the scattered raman signal |

Multiple reflection of the excitation beam and multiple internal reflections of the scattered raman would be more appropiate causes of low intensity of Raman signal in fine-grained samples. As reported by Wang(1999), both reasons directly affect on collection of Raman photon. Regarding all coarse-grained samples, their surfaces were well polished; consequently, they may reduce reflections of either incident beam or scattered raman. Thus it leads to higher intensity of recorded Raman spectra and perhaps yields well shape of these peaks. On the other hand, all fine-grained samples have tiny grain size of about 100 microns in diameter, besides their surface are not completely smooth. These characteristics directly increase multiple reflections that subsequently yield low intensity of Raman spectra.

To confirm the hypothesis, experiment on grain size effect has been performed using sample (no. PD02) with size of about 10 mm and contains 88.9% Fo content. The

sample was analyzed using Raman spectroscope with original size then it was ground into various sizes. Subsequently, some grains with size of about 200 and 40 microns in diameter were selected to obtain Raman spectra. The same collecting condition was set during the experiment. The result confirms the hypothesis, the bigger grain gives well shape and high intensity of spectra. Intensity is decreased and some peaks are broadened while size of sample is reduced (Figure 4.4).
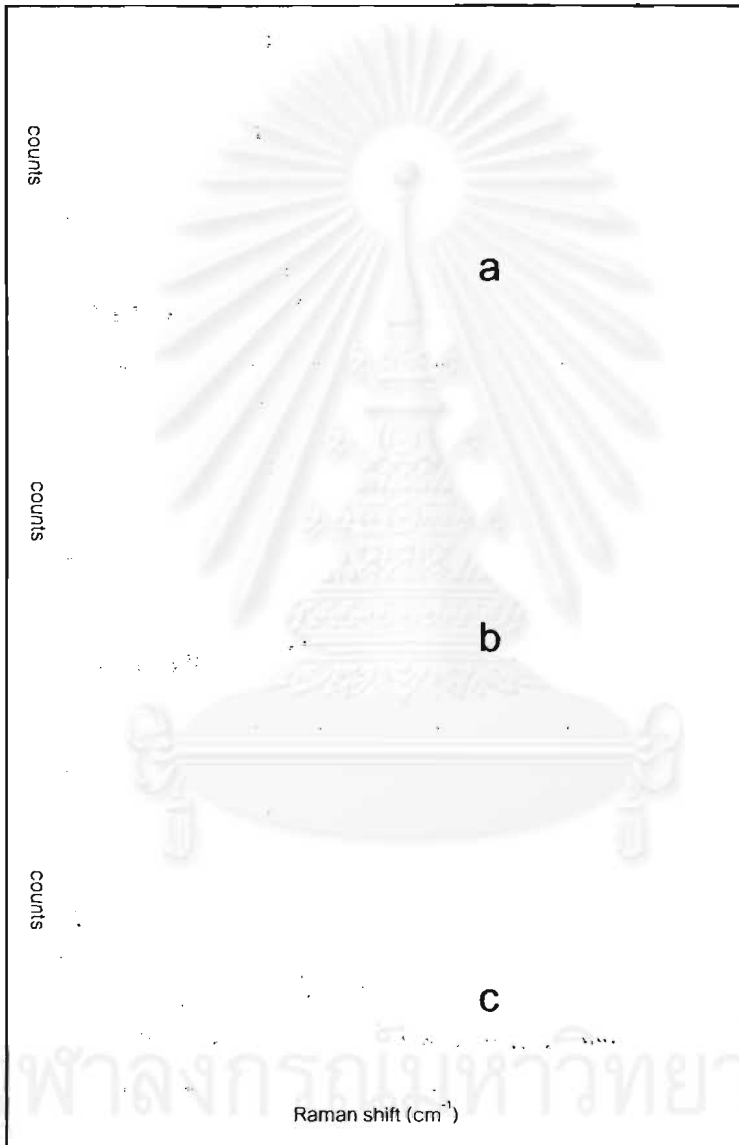


Figure 4.4    Three  raman spectra obtained from the same sample (no. PD02; Fo $_{88.9}$)
with different grain size: a) 10 mm , b) 200 microns, c) 40 microns.
It clearly shows decreasing of intensity and broadening of some peaks
are directly  relied on grain size reduction.

*4.3    Shift of Raman Spectrum*

McMillan and Hofmeister (1988) mentioned about  3 main factors that   may cause shift of Raman spectrum; they are change of  temperature, pressure   and chemical composition. From Chapter 3, it is clearly to conclude that the shift of Raman spectra is related directly to change of magnesium and iron content in samples. This informative result is  also confirmed by many works which have reported the same effect. The  downshift of Raman peak position of the same mode can be observed when the iron content of sample is increasing (decreasing of Fo content). However, slopes of each peak vary from case to case; high slope peaks are found in region belonging to $SiO_4$ internal mode ( 1000 – 450 cm$^{-1}$), while  many peaks belonging to lattice mode usually show very small variation.
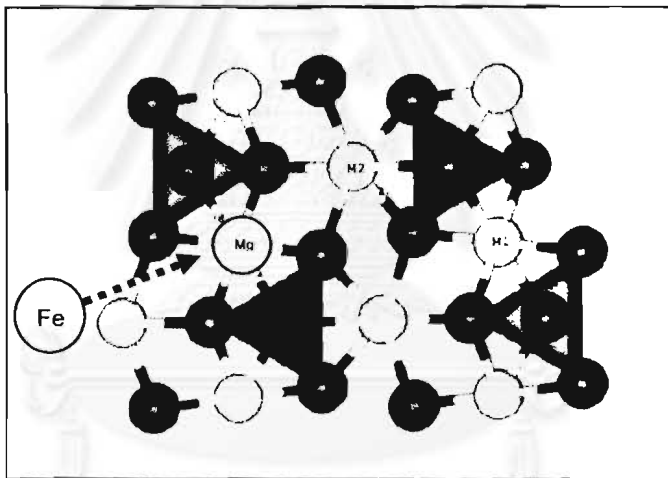


Figure 4.5  Atomic configuration of olivine showing replacement of large Fe cation to

the site of  smaller Mg cation (white balls are cations and black balls are

oxygens) (modified from de Leeuw et al. 2000)

The explanation of this effect is the change of bond strength of whole crystal structure during the change of  end-member content. Iron with bigger size will replace into the site of smaller magnesium (Figure 4.5) and the consequences can be seen with increment of volume and shortening  of Si-O bond length. It is well known that *M1* octahedra in olivine are quite regular but *M2* octrahedra are not. Therefore *M1* sites are more advantage  for iron atom to replace than *M2*  because the maximal overlapping of *d*(Fe)-*p*(oxygen) wave functions is desirable (Kolesov et al., 1995).  Lin (2000) studied

the Raman spectroscopy of the system  alpha-$Co_2SiO_4$ – alpha-$Ni_2SiO_4$. The conclusion was stated that the substitution between  cobalt  and nickel cations  yields slightly shift of internal mode with little variation. This is  because sizes of Co and Ni are nearly the same. Hence, it is clearly that the  different size of cation is the main cause of shift in Raman vibration mode. The downshift of Raman spectra will happen when larger cation replace into small one. If the cations are very different in size, the shift of spectra among the end-members are more significant, particularly in the vibration mode belonging to $SiO_4$ internal mode. Lattice modes are seem to be less affect in all cases.

## 4.4    Linear regression equations

Four main peak positions (p1, p2, p4 and p5) (Figure 4.6)  belong to internal mode (1000-450 cm$^{-1}$) revealed  high intensity, significant  shift and always present in both coarse-grained and fine-grained samples. Thus,  these peaks suitable to apply for the end-member content estimation. The regression equations of their relationship are summarized in Table 4.5.
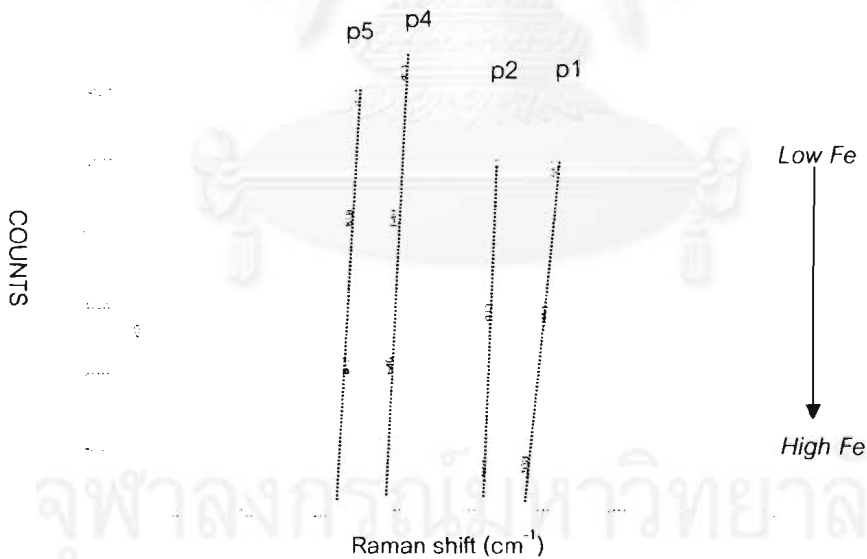


Figure 4.6   Four main peaks which are  suggested to be the most suitable peak

positions for end-member estimation (top: Fo $_{91.5}$, middle: Fo $_{70.6,}$ bottom:

Fo $_{50.5}$) and dash lines  are linked between each peak position showing

downshift continuously of lower Fo content.

Table 4.5 Linear regression equations and chi-square values of 4 suggested peak positions  which are belong to $SiO_4$ internal vibration modes.
(Y =  Frequency in $cm^{-1}$, X= end-member content )

| Peak position | Linear  regression equation |
|---------------|-----------------------------|
| p1 | $Y = 0.5388X + 910.79$ ,  $R^2 = 0.9439$ |
| p2 | $Y = 0.2030X + 899.21$ ,  $R^2 = 0.7957$ |
| p4 | $Y = 0.2124X + 834.72$ ,  $R^2 = 0.7953$ |
| p5 | $Y = 0.1485X + 808.84$ ,  $R^2 = 0.6515$ |

The  end-member  calculation of studied samples from selected Raman peak positions have been performed to find out the accuracy of  each equation by putting the value of each peak  position for X value in equations of peaks p1, p2, p4 and  p5, respectively. In comparison, the calculation results reveal the maximum deviation are upto  about 10%  from EPMA results. However, they usually fall between $\pm$ 2% - $\pm$ 5%. The end-member calculation results are summarized in Table 4.6.

### 4.5    Conclusions

The aims of this study are to  find out the possibility to apply Raman spectroscopy  for  the end-member  estimation of some natural Mg-Fe olivines.  All informations obtained from this project can be concluded as below

1. Non-polarized raman spectra within range of 1000-250 $cm^{-1}$ of 27 natural olivine  samples  were  studied  by  using  Renishaw  1000  Raman spectroscopy with 514.5 nm Ar-laser.

Table 4.6  End-member calculations from equations  of peak  positions  p1, p2, p4
and p5 respectively and their averages of  Fo contents and deviation
in comparison  with Fo contents analyzed using EPMA.

| Sample No. | Fo content by EPMA | Fo content of p1 | Fo content of p2 | Fo content of p4 | Fo content of p5 | Average | Deviation |
|---|---|---|---|---|---|---|---|
| PD16 | 91.5 | 87.6 | 87.6 | 86.1 | 81.9 | 85.8 | -5.7 |
| PD17 | 91.5 | 91.3 | 87.6 | 90.8 | 88.6 | 89.6 | -1.9 |
| PD18 | 91.5 | 91.3 | 77.8 | 86.1 | 81.9 | 84.3 | -7.2 |
| PD11 | 91.4 | 87.6 | 87.6 | 86.1 | 88.6 | 87.5 | -3.9 |
| PD15 | 91.4 | 89.5 | 87.6 | 86.1 | 81.9 | 86.3 | -5.1 |
| PD14 | 91.2 | 91.3 | 92.6 | 90.8 | 88.6 | 90.8 | -0.4 |
| PD20 | 91.1 | 85.8 | 82.7 | 86.1 | 81.9 | 84.1 | -7.0 |
| PD12 | 91.0 | 89.5 | 82.7 | 86.1 | 81.9 | 85.0 | -6.0 |
| PD10 | 90.6 | 85.8 | 82.7 | 81.4 | 81.9 | 82.9 | -7.7 |
| PD19 | 90.5 | 85.8 | 82.7 | 86.1 | 81.9 | 84.1 | -6.4 |
| PD13 | 90.0 | 89.5 | 87.6 | 86.1 | 88.6 | 87.9 | -2.1 |
| PD3 | 89.5 | 87.6 | 97.5 | 100.2 | 102.1 | 96.8 | 7.3 |
| PD9 | 89.5 | 91.3 | 92.6 | 90.8 | 95.4 | 92.5 | 3.0 |
| PD6 | 89.4 | 87.6 | 92.6 | 95.5 | 95.4 | 92.8 | 3.4 |
| PD2 | 89.0 | 91.3 | 97.5 | 95.5 | 102.1 | 96.6 | 7.6 |
| PD8 | 88.8 | 93.2 | 97.5 | 100.2 | 102.1 | 98.2 | 9.4 |
| PD4 | 88.7 | 93.2 | 92.6 | 90.8 | 88.6 | 91.3 | 2.6 |
| PD7 | 88.7 | 89.5 | 97.5 | 100.2 | 108.8 | 99.0 | 10.3 |
| PD5 | 84.8 | 91.3 | 97.5 | 95.5 | 95.4 | 94.9 | 10.1 |
| PD1 | 83.9 | 85.8 | 97.5 | 90.8 | 95.4 | 92.3 | 8.4 |
| PD735 | 73.5 | 74.6 | 67.9 | 67.2 | 61.7 | 67.9 | -5.6 |
| PD706 | 70.6 | 74.6 | 63.0 | 62.5 | 61.7 | 65.5 | -5.1 |
| PD678 | 67.8 | 72.8 | 67.9 | 71.9 | 68.4 | 70.3 | 2.5 |
| PD617 | 61.7 | 61.6 | 63.0 | 62.5 | 68.4 | 63.9 | 2.2 |
| PD605 | 60.5 | 54.2 | 63.0 | 57.8 | 54.9 | 57.5 | -3.0 |
| PD588 | 58.8 | 56.1 | 53.2 | 57.8 | 54.9 | 55.5 | -3.3 |
| PD505 | 50.5 | 50.5 | 53.2 | 53.1 | 54.9 | 52.9 | 2.4 |

2. EPMA analyses of 20 coarse-grained olivine samples revealed Fo contents ranging from 91.5 – 89.5 %.

3. Twenty coarse-grained samples show good quality of spectra. On the other hand, Raman spectra collected from seven fine-grained samples show lower quality, particularly in lattice mode (less than 500 $cm^{-1}$) region. The grain size effect has been proved as the main cause of the phenomena.

4. The relationship between the peak position shift of same mode and end-member content shows linear relationship that can be fitted with linear regression equations.

5. Four main peak positions (p1, p2, p4 and p5) mostly belonging to internal mode (1000-800 $cm^{-1}$) yield high intensity, significant shift and always present in both coarse-grained and fine-grained samples. Thus, these peaks are suitable for estimation of the end-member content.

6. Fo contents which are calculated with regression equations falling in range of about ± 2% - ± 10% deviation from the EPMA analyses.

7. For further research and related field, the wider range of Fo content of natural olivine sample are required for better correlation. Subsequently, the linear regression equations of peak positions should be more accurate and the deviation would be reduced to less than ±10%. In addition, other minerals that contain complex solid-solutions (e.g. garnet, pyroxene, amphibole etc.) are possible targets for further study.

# REFERENCES

Bonilla, I. R. 1982. Raman spectra of forsterite. J. Quant. Spectrosc. Radiat.
Transfer, 28. 6:527 - 529.

Calas, G.,and Hawthorne,F. C.1988. Introduction to spectroscopic methods.
Reviews in Mineralogy, (*Spectroscopic Methods in Mineralogy
and Geology*), 18: 1-9.

Chopelas, A. 1991. Single crystal Raman spectra of forsterite, fayalite, and
monticellite. American Mineralogist. 76:1101 - 1109.

de Leeuw, N. H., Parker, S. C., Catlow, R. A., and Price, G. D. 2000. Proton
containing defects at forsterite{101} tilt grain boundaries and stepped
surfaces. American Mineralogist. 85: 1143-1154.

Ferraro, J. R., Nakamoto, K., and Brown, C. W. 2003. Introductory raman
spectroscopy, 2nd ed. USA: Elsevier Science

Deers,W. A., Howies,R. A., and. Zussman, J.1992. An Introduction to the Rock-
Forming Minerals . Longman Sci. and Tech., Essex,   687 p.

Gaines, R. V., Catherine, H., Skinner, W., Foord, E. E., and Mason, B. 1997.
Dana' new mineralogy, 8th ed. John Wiley & Sons: 1024 – 1028.

Griffen,T.D., 1992. Silicate Crystal Chemistry. Oxford University press, p.247-269

Hawthorne, F. C., and Waychunas, G. A.,1988.  Spectrum- fitting methods.
Reviews in Mineralogy, (*Spectroscopic Methods in Mineralogy
and Geology*).18: 63 - 96.

Hofmeister, A. M., and Mao,H.-k , 2002. Redefinition of the mode Gruneisen
parameter of polyatomic substances and thermo dynamic implications.
PNAS. 99. 2: 559 – 564.

Klein C., and Hurlbut,C. S. Jr., 1999. Manual of Mineralogy. 21st ed. revised,
John Wiley & Sons:449 – 451.

Kolesov, B. A., and Tanskaya, J. V., 1996. Raman spectra and cation distribution
in the lattice of olivines. Materials Research Bulletin. 31. 8: 1035 –1044.

Kolesov, B. A., and Geiger, C. A., 2004. A Raman spectroscopic study of Fe-Mg
Olivines. Phys Chem Minerals. 31:142 – 154.

Lin, C. C., 2001. Vibrational spectroscopic study of the system

$Co_2SiO_4$ –$Ni_2SiO_4$. J. Solid State Chemistry. 157: 102-109.

McMillan, P. F., and Hess, A. C.,1988. Symmetry, group theory and quantum

mechanics. Reviews in Mineralogy, (*Spectroscopic Methods in Mineralogy and Geology*). 18 : 11 - 60.

McMillan, P. F.,and Hofmeister, A. M.,1988. Infrared and raman spectroscopy.

Reviews in Mineralogy, (*Spectroscopic Methods in Mineralogy and Geology*).18: 99 - 150.

Smith, E. and Dent, G. 2005. Modern raman spectroscopy, A practical approach.

UK:John Wiley & Sons.

Wang A., 1999. Some grain size effects on Raman scattering intensity for in situ

measurements on rocks and soils- experimental test and modeling. Thirty Lunar and Planetary Science Conference, Huston, Texas, USA.

Williams, Q., 1995. Infrared, Raman and Optical Spectroscopy of Earth Materials.

Mineral Physics and Crystallography, A handbook of Physical Constants, AGU Reference shelf 2. American Geophysical Union :291 - 301

# APPENDICES

# Appendix 1

Chemical analyses of 20  coarse-grained samples

obtained from Electron Probe Micro-Analysis (EPMA)

| | PD01-1 | PD01-2 | PD01-3 | PD01-4 | PD01-5 | PD02-1 | PD02-2 | PD02-3 | PD02-4 | PD02-5 |
|---|---|---|---|---|---|---|---|---|---|---|
| MgO | 45.39 | 45.52 | 45.60 | 45.89 | 45.22 | 48.67 | 48.92 | 48.89 | 48.87 | 47.78 |
| $Al_2O_3$ | 0.02 | 0.02 | 0.02 | 0.03 | 0.02 | 0.01 | 0.02 | 0.02 | 0.00 | 0.03 |
| $SiO_2$ | 40.70 | 40.25 | 40.30 | 40.55 | 40.15 | 40.25 | 39.97 | 39.83 | 39.85 | 39.22 |
| CaO | 0.12 | 0.14 | 0.13 | 0.14 | 0.13 | 0.13 | 0.12 | 0.13 | 0.12 | 0.13 |
| MnO | 0.14 | 0.15 | 0.21 | 0.18 | 0.15 | 0.17 | 0.14 | 0.13 | 0.15 | 0.16 |
| FeO | 15.46 | 15.41 | 15.36 | 15.45 | 15.31 | 10.69 | 10.44 | 10.88 | 10.92 | 10.34 |
| NiO | 0.28 | 0.28 | 0.28 | 0.28 | 0.31 | 0.35 | 0.36 | 0.35 | 0.33 | 0.37 |
| $Cr_2O_3$ | 0.03 | 0.02 | 0.02 | 0.00 | 0.02 | 0.03 | 0.02 | 0.04 | 0.05 | 0.02 |
| Total | 102.14 | 101.79 | 101.92 | 102.50 | 101.31 | 100.30 | 99.98 | 100.27 | 100.29 | 98.04 |
| Formula 4(O) | | | | | | | | | | |
| Mg | 1.665 | 1.677 | 1.678 | 1.679 | 1.674 | 1.785 | 1.799 | 1.797 | 1.796 | 1.793 |
| Al | 0.001 | 0.001 | 0.001 | 0.001 | 0.000 | 0.000 | 0.001 | 0.001 | 0.000 | 0.001 |
| Si | 1.002 | 0.995 | 0.995 | 0.995 | 0.997 | 0.990 | 0.986 | 0.982 | 0.982 | 0.987 |
| Ca | 0.003 | 0.004 | 0.003 | 0.004 | 0.003 | 0.003 | 0.003 | 0.003 | 0.003 | 0.004 |
| Mn | 0.003 | 0.003 | 0.004 | 0.004 | 0.003 | 0.003 | 0.003 | 0.003 | 0.003 | 0.003 |
| Fe | 0.318 | 0.319 | 0.317 | 0.317 | 0.318 | 0.220 | 0.215 | 0.224 | 0.225 | 0.218 |
| Ni | 0.006 | 0.006 | 0.006 | 0.006 | 0.006 | 0.007 | 0.007 | 0.007 | 0.007 | 0.008 |
| Cr | 0.001 | 0.000 | 0.000 | 0.000 | 0.000 | 0.001 | 0.000 | 0.001 | 0.001 | 0.000 |
| Total | 2.998 | 3.004 | 3.005 | 3.005 | 3.003 | 3.009 | 3.014 | 3.017 | 3.017 | 3.013 |
| %Fo | 83.8 | 83.9 | 83.9 | 84.0 | 83.9 | 88.9 | 89.2 | 88.8 | 88.7 | 89.0 |
| %Fa | 16.2 | 16.1 | 16.1 | 16.0 | 16.1 | 11.1 | 10.8 | 11.2 | 11.3 | 11.0 |

| | PD03-1 | PD03-2 | PD03-3 | PD03-4 | PD03-5 | PD04-1 | PD04-2 | PD04-3 | PD04-4 | PD04-5 |
|---|---|---|---|---|---|---|---|---|---|---|
| MgO | 48.89 | 50.45 | 49.59 | 49.32 | 49.12 | 49.26 | 48.52 | 49.60 | 48.32 | 49.07 |
| $Al_2O_3$ | 0.04 | 0.02 | 0.01 | 0.01 | 0.01 | 0.03 | 0.01 | 0.02 | 0.03 | 0.00 |
| $SiO_2$ | 40.38 | 41.31 | 40.04 | 40.29 | 40.41 | 40.42 | 40.88 | 41.94 | 40.47 | 41.78 |
| CaO | 0.10 | 0.10 | 0.12 | 0.11 | 0.11 | 0.13 | 0.13 | 0.14 | 0.13 | 0.12 |
| MnO | 0.14 | 0.16 | 0.14 | 0.17 | 0.13 | 0.15 | 0.13 | 0.17 | 0.18 | 0.13 |
| FeO | 10.39 | 10.39 | 10.25 | 10.38 | 10.18 | 10.83 | 11.04 | 11.17 | 10.76 | 11.02 |
| NiO | 0.35 | 0.32 | 0.34 | 0.35 | 0.33 | 0.37 | 0.35 | 0.37 | 0.38 | 0.35 |
| $Cr_2O_3$ | 0.02 | 0.04 | 0.04 | 0.02 | 0.05 | 0.02 | 0.03 | 0.03 | 0.04 | 0.04 |
| Total | 100.30 | 102.79 | 100.53 | 100.66 | 100.33 | 101.20 | 101.08 | 103.44 | 100.31 | 102.51 |
| Formula 4(O) | | | | | | | | | | |
| Mg | 1.789 | 1.800 | 1.812 | 1.800 | 1.796 | 1.792 | 1.765 | 1.763 | 1.771 | 1.757 |
| Al | 0.001 | 0.000 | 0.000 | 0.000 | 0.000 | 0.001 | 0.000 | 0.001 | 0.001 | 0.000 |
| Si | 0.991 | 0.989 | 0.982 | 0.986 | 0.991 | 0.986 | 0.998 | 1.000 | 0.995 | 1.004 |
| Ca | 0.002 | 0.003 | 0.003 | 0.003 | 0.003 | 0.003 | 0.003 | 0.003 | 0.004 | 0.003 |
| Mn | 0.003 | 0.003 | 0.003 | 0.004 | 0.003 | 0.003 | 0.003 | 0.003 | 0.004 | 0.003 |
| Fe | 0.213 | 0.208 | 0.210 | 0.212 | 0.209 | 0.221 | 0.225 | 0.223 | 0.221 | 0.221 |
| Ni | 0.007 | 0.006 | 0.007 | 0.007 | 0.007 | 0.007 | 0.007 | 0.007 | 0.008 | 0.007 |
| Cr | 0.000 | 0.001 | 0.001 | 0.000 | 0.001 | 0.000 | 0.001 | 0.001 | 0.001 | 0.001 |
| Total | 3.008 | 3.010 | 3.018 | 3.013 | 3.008 | 3.013 | 3.002 | 3.000 | 3.004 | 2.996 |
| %Fo | 89.2 | 89.5 | 89.5 | 89.3 | 89.5 | 88.9 | 88.6 | 88.6 | 88.7 | 88.7 |
| %Fa | 10.8 | 10.5 | 10.5 | 10.7 | 10.5 | 11.1 | 11.4 | 11.4 | 11.3 | 11.3 |

| | PD05-1 | PD05-2 | PD05-3 | PD05-4 | PD05-5 | PD06-1 | PD06-2 | PD06-3 | PD06-4 | PD06-5 |
|---|---|---|---|---|---|---|---|---|---|---|
| MgO | 48.26 | 49.19 | 49.26 | 49.06 | 48.85 | 46.14 | 45.53 | 45.80 | 45.74 | 45.49 |
| $Al_2O_3$ | 0.02 | 0.01 | 0.03 | 0.02 | 0.03 | 0.01 | 0.03 | 0.02 | 0.01 | 0.02 |
| $SiO_2$ | 38.87 | 39.45 | 39.45 | 38.80 | 39.03 | 40.92 | 38.93 | 38.73 | 39.29 | 38.72 |
| CaO | 0.13 | 0.13 | 0.12 | 0.14 | 0.12 | 0.11 | 0.09 | 0.09 | 0.08 | 0.10 |
| MnO | 0.16 | 0.15 | 0.15 | 0.16 | 0.16 | 0.16 | 0.20 | 0.17 | 0.17 | 0.18 |
| FeO | 10.28 | 10.34 | 10.32 | 10.26 | 10.31 | 14.58 | 14.38 | 14.55 | 14.39 | 14.26 |
| NiO | 0.34 | 0.36 | 0.32 | 0.31 | 0.35 | 0.35 | 0.30 | 0.28 | 0.32 | 0.31 |
| $Cr_2O_3$ | 0.04 | 0.03 | 0.04 | 0.02 | 0.04 | 0.02 | 0.02 | 0.03 | 0.06 | 0.03 |
| Total | 98.09 | 99.65 | 99.68 | 98.76 | 98.87 | 102.29 | 99.48 | 99.67 | 100.06 | 99.11 |
| Formula 4(O) | | | | | | | | | | |
| Mg | 1.811 | 1.817 | 1.818 | 1.829 | 1.819 | 1.684 | 1.715 | 1.724 | 1.711 | 1.720 |
| Al | 0.000 | 0.000 | 0.001 | 0.001 | 0.001 | 0.000 | 0.001 | 0.001 | 0.000 | 0.001 |
| Si | 0.978 | 0.977 | 0.977 | 0.971 | 0.975 | 1.002 | 0.983 | 0.978 | 0.986 | 0.982 |
| Ca | 0.004 | 0.003 | 0.003 | 0.004 | 0.003 | 0.003 | 0.002 | 0.003 | 0.002 | 0.003 |
| Mn | 0.003 | 0.003 | 0.003 | 0.003 | 0.003 | 0.003 | 0.004 | 0.004 | 0.004 | 0.004 |
| Fe | 0.216 | 0.214 | 0.214 | 0.215 | 0.215 | 0.298 | 0.304 | 0.307 | 0.302 | 0.302 |
| Ni | 0.007 | 0.007 | 0.006 | 0.006 | 0.007 | 0.007 | 0.006 | 0.006 | 0.006 | 0.006 |
| Cr | 0.001 | 0.001 | 0.001 | 0.000 | 0.001 | 0.000 | 0.000 | 0.001 | 0.001 | 0.001 |
| Total | 3.021 | 3.022 | 3.023 | 3.029 | 3.024 | 2.998 | 3.016 | 3.022 | 3.013 | 3.018 |
| %Fo | 89.2 | 89.3 | 89.4 | 89.4 | 89.3 | 84.8 | 84.8 | 84.7 | 84.8 | 84.9 |
| %Fa | 10.8 | 10.7 | 10.6 | 10.6 | 10.7 | 15.2 | 15.2 | 15.3 | 15.2 | 15.1 |

| | PD07-1 | PD07-2 | PD07-3 | PD07-4 | PD07-5 | PD08-1 | PD08-2 | PD08-3 | PD08-4 | PD08-5 |
|---|---|---|---|---|---|---|---|---|---|---|
| MgO | 48.71 | 49.18 | 48.83 | 48.84 | 48.64 | 49.02 | 48.99 | 49.16 | 48.66 | 48.50 |
| $Al_2O_3$ | 0.01 | 0.02 | 0.02 | 0.01 | 0.02 | 0.03 | 0.01 | 0.03 | 0.02 | 0.02 |
| $SiO_2$ | 39.60 | 39.94 | 39.04 | 39.95 | 39.28 | 39.07 | 39.99 | 40.27 | 40.47 | 40.18 |
| CaO | 0.13 | 0.14 | 0.13 | 0.15 | 0.13 | 0.11 | 0.14 | 0.14 | 0.13 | 0.12 |
| MnO | 0.15 | 0.13 | 0.12 | 0.14 | 0.19 | 0.14 | 0.18 | 0.17 | 0.16 | 0.14 |
| FeO | 10.86 | 11.03 | 10.69 | 10.82 | 10.89 | 10.86 | 10.58 | 11.11 | 10.70 | 10.81 |
| NiO | 0.33 | 0.35 | 0.34 | 0.35 | 0.38 | 0.36 | 0.38 | 0.36 | 0.35 | 0.33 |
| $Cr_2O_3$ | 0.02 | 0.03 | 0.02 | 0.04 | 0.03 | 0.04 | 0.02 | 0.04 | 0.03 | 0.04 |
| Total | 99.81 | 100.81 | 99.19 | 100.28 | 99.55 | 99.62 | 100.29 | 101.27 | 100.52 | 100.13 |
| Formula 4(O) | | | | | | | | | | |
| Mg | 1.799 | 1.799 | 1.815 | 1.794 | 1.803 | 1.816 | 1.798 | 1.790 | 1.780 | 1.782 |
| Al | 0.000 | 0.000 | 0.001 | 0.000 | 0.001 | 0.001 | 0.000 | 0.001 | 0.001 | 0.001 |
| Si | 0.981 | 0.980 | 0.974 | 0.984 | 0.977 | 0.971 | 0.984 | 0.984 | 0.993 | 0.990 |
| Ca | 0.003 | 0.004 | 0.004 | 0.004 | 0.003 | 0.003 | 0.004 | 0.004 | 0.004 | 0.003 |
| Mn | 0.003 | 0.003 | 0.003 | 0.003 | 0.004 | 0.003 | 0.004 | 0.004 | 0.003 | 0.003 |
| Fe | 0.225 | 0.226 | 0.223 | 0.223 | 0.227 | 0.226 | 0.218 | 0.227 | 0.219 | 0.223 |
| Ni | 0.007 | 0.007 | 0.007 | 0.007 | 0.008 | 0.007 | 0.008 | 0.007 | 0.007 | 0.006 |
| Cr | 0.000 | 0.001 | 0.000 | 0.001 | 0.001 | 0.001 | 0.000 | 0.001 | 0.001 | 0.001 |
| Total | 3.019 | 3.020 | 3.026 | 3.015 | 3.023 | 3.028 | 3.015 | 3.016 | 3.007 | 3.009 |
| %Fo | 88.7 | 88.7 | 89.0 | 88.8 | 88.7 | 88.8 | 89.0 | 88.6 | 88.9 | 88.8 |
| %Fa | 11.3 | 11.3 | 11.0 | 11.2 | 11.3 | 11.2 | 11.0 | 11.4 | 11.1 | 11.2 |

| | PD09-1 | PD09-2 | PD09-3 | PD09-4 | PD09-5 | PD10-1 | PD10-2 | PD10-3 | PD10-4 | PD10-5 |
|---|---|---|---|---|---|---|---|---|---|---|
| MgO | 49.61 | 49.45 | 48.99 | 49.07 | 49.61 | 50.09 | 50.25 | 50.69 | 50.85 | 50.26 |
| $Al_2O_3$ | 0.01 | 0.01 | 0.02 | 0.02 | 0.01 | 0.03 | 0.02 | 0.04 | 0.02 | 0.01 |
| $SiO_2$ | 40.26 | 38.98 | 39.19 | 39.00 | 39.57 | 39.25 | 38.27 | 38.96 | 39.63 | 38.14 |
| CaO | 0.07 | 0.08 | 0.07 | 0.07 | 0.06 | 0.11 | 0.09 | 0.10 | 0.10 | 0.08 |
| MnO | 0.15 | 0.13 | 0.18 | 0.15 | 0.15 | 0.10 | 0.08 | 0.11 | 0.11 | 0.12 |
| FeO | 10.20 | 10.45 | 10.07 | 10.06 | 10.36 | 9.11 | 9.29 | 9.22 | 9.35 | 9.21 |
| NiO | 0.37 | 0.41 | 0.39 | 0.39 | 0.36 | 0.40 | 0.37 | 0.40 | 0.39 | 0.40 |
| $Cr_2O_3$ | 0.02 | 0.05 | 0.04 | 0.07 | 0.07 | 0.03 | 0.07 | 0.08 | 0.06 | 0.07 |
| Total | 100.67 | 99.56 | 98.95 | 98.82 | 100.19 | 99.12 | 98.42 | 99.60 | 100.50 | 98.28 |
| Formula 4(O) | | | | | | | | | | |
| Mg | 1.809 | 1.831 | 1.821 | 1.827 | 1.822 | 1.851 | 1.875 | 1.867 | 1.855 | 1.879 |
| Al | 0.000 | 0.000 | 0.001 | 0.001 | 0.000 | 0.001 | 0.000 | 0.001 | 0.001 | 0.000 |
| Si | 0.985 | 0.968 | 0.977 | 0.974 | 0.975 | 0.973 | 0.958 | 0.963 | 0.970 | 0.956 |
| Ca | 0.002 | 0.002 | 0.002 | 0.002 | 0.002 | 0.003 | 0.003 | 0.003 | 0.002 | 0.002 |
| Mn | 0.003 | 0.003 | 0.004 | 0.003 | 0.003 | 0.002 | 0.002 | 0.002 | 0.002 | 0.003 |
| Fe | 0.209 | 0.217 | 0.210 | 0.210 | 0.213 | 0.189 | 0.194 | 0.190 | 0.191 | 0.193 |
| Ni | 0.007 | 0.008 | 0.008 | 0.008 | 0.007 | 0.008 | 0.007 | 0.008 | 0.008 | 0.008 |
| Cr | 0.000 | 0.001 | 0.001 | 0.001 | 0.001 | 0.001 | 0.001 | 0.002 | 0.001 | 0.001 |
| Total | 3.015 | 3.031 | 3.022 | 3.025 | 3.024 | 3.027 | 3.041 | 3.036 | 3.030 | 3.043 |
| %Fo | 89.5 | 89.3 | 89.5 | 89.5 | 89.4 | 90.6 | 90.5 | 90.6 | 90.6 | 90.6 |
| %Fa | 10.5 | 10.7 | 10.5 | 10.5 | 10.6 | 9.4 | 9.5 | 9.4 | 9.4 | 9.4 |

| | PD11-1 | PD11-2 | PD11-3 | PD11-4 | PD11-5 | PD12-1 | PD12-2 | PD12-3 | PD12-4 | PD12-5 |
|---|---|---|---|---|---|---|---|---|---|---|
| MgO | 50.69 | 51.08 | 50.46 | 50.51 | 51.37 | 50.69 | 50.73 | 50.62 | 51.28 | 50.53 |
| $Al_2O_3$ | 0.02 | 0.03 | 0.05 | 0.04 | 0.04 | 0.05 | 0.03 | 0.04 | 0.05 | 0.03 |
| $SiO_2$ | 37.92 | 38.57 | 38.86 | 38.44 | 38.67 | 37.70 | 37.46 | 38.36 | 38.66 | 37.08 |
| CaO | 0.09 | 0.10 | 0.09 | 0.10 | 0.09 | 0.10 | 0.10 | 0.10 | 0.09 | 0.10 |
| MnO | 0.09 | 0.10 | 0.10 | 0.08 | 0.08 | 0.12 | 0.11 | 0.14 | 0.18 | 0.11 |
| FeO | 8.47 | 8.68 | 8.52 | 8.27 | 8.41 | 8.82 | 8.93 | 8.80 | 8.99 | 8.78 |
| NiO | 0.40 | 0.42 | 0.37 | 0.38 | 0.37 | 0.37 | 0.38 | 0.41 | 0.38 | 0.41 |
| $Cr_2O_3$ | 0.04 | 0.08 | 0.07 | 0.05 | 0.06 | 0.06 | 0.04 | 0.05 | 0.06 | 0.06 |
| Total | 97.73 | 99.07 | 98.51 | 97.86 | 99.08 | 97.92 | 97.78 | 98.50 | 99.69 | 97.09 |
| Formula 4(O) | | | | | | | | | | |
| Mg | 1.900 | 1.889 | 1.872 | 1.886 | 1.896 | 1.901 | 1.907 | 1.884 | 1.888 | 1.913 |
| Al | 0.001 | 0.001 | 0.001 | 0.001 | 0.001 | 0.002 | 0.001 | 0.001 | 0.001 | 0.001 |
| Si | 0.954 | 0.957 | 0.967 | 0.963 | 0.957 | 0.948 | 0.945 | 0.958 | 0.955 | 0.942 |
| Ca | 0.002 | 0.003 | 0.002 | 0.003 | 0.002 | 0.003 | 0.003 | 0.003 | 0.002 | 0.003 |
| Mn | 0.002 | 0.002 | 0.002 | 0.002 | 0.002 | 0.003 | 0.002 | 0.003 | 0.004 | 0.002 |
| Fe | 0.178 | 0.180 | 0.177 | 0.173 | 0.174 | 0.186 | 0.188 | 0.184 | 0.186 | 0.186 |
| Ni | 0.008 | 0.008 | 0.007 | 0.008 | 0.007 | 0.008 | 0.008 | 0.008 | 0.008 | 0.008 |
| Cr | 0.001 | 0.002 | 0.001 | 0.001 | 0.001 | 0.001 | 0.001 | 0.001 | 0.001 | 0.001 |
| Total | 3.046 | 3.042 | 3.031 | 3.036 | 3.041 | 3.050 | 3.055 | 3.041 | 3.044 | 3.057 |
| %Fo | 91.3 | 91.2 | 91.3 | 91.5 | 91.5 | 91.0 | 90.9 | 91.0 | 90.9 | 91.0 |
| %Fa | 8.7 | 8.8 | 8.7 | 8.5 | 8.5 | 9.0 | 9.1 | 9.0 | 9.1 | 9.0 |

| | PD13-1 | PD13-2 | PD13-3 | PD13-4 | PD13-5 | PD14-1 | PD14-2 | PD14-3 | PD14-4 | PD14-5 |
|---|---|---|---|---|---|---|---|---|---|---|
| MgO | 50.31 | 50.01 | 50.11 | 50.58 | 50.27 | 50.90 | 51.74 | 51.34 | 51.06 | 51.18 |
| $Al_2O_3$ | 0.00 | 0.02 | 0.03 | 0.03 | 0.02 | 0.03 | 0.02 | 0.04 | 0.03 | 0.04 |
| $SiO_2$ | 37.91 | 37.92 | 38.13 | 38.78 | 38.04 | 37.93 | 39.26 | 38.50 | 38.15 | 37.13 |
| CaO | 0.09 | 0.07 | 0.09 | 0.06 | 0.07 | 0.10 | 0.10 | 0.09 | 0.10 | 0.10 |
| MnO | 0.14 | 0.12 | 0.16 | 0.13 | 0.19 | 0.11 | 0.12 | 0.09 | 0.11 | 0.14 |
| FeO | 9.85 | 9.99 | 9.62 | 9.65 | 9.72 | 8.72 | 8.81 | 8.66 | 8.69 | 8.57 |
| NiO | 0.32 | 0.34 | 0.30 | 0.31 | 0.35 | 0.36 | 0.40 | 0.39 | 0.37 | 0.40 |
| $Cr_2O_3$ | 0.07 | 0.06 | 0.06 | 0.09 | 0.03 | 0.05 | 0.04 | 0.05 | 0.04 | 0.04 |
| Total | 98.69 | 98.54 | 98.49 | 99.64 | 98.69 | 98.19 | 100.49 | 99.16 | 98.56 | 97.61 |
| Formula 4(O) | | | | | | | | | | |
| Mg | 1.880 | 1.872 | 1.872 | 1.866 | 1.877 | 1.901 | 1.886 | 1.897 | 1.900 | 1.927 |
| Al | 0.000 | 0.001 | 0.001 | 0.001 | 0.001 | 0.001 | 0.001 | 0.001 | 0.001 | 0.001 |
| Si | 0.950 | 0.952 | 0.956 | 0.960 | 0.952 | 0.951 | 0.960 | 0.954 | 0.952 | 0.938 |
| Ca | 0.002 | 0.002 | 0.002 | 0.002 | 0.002 | 0.003 | 0.003 | 0.002 | 0.003 | 0.003 |
| Mn | 0.003 | 0.003 | 0.003 | 0.003 | 0.004 | 0.002 | 0.002 | 0.002 | 0.002 | 0.003 |
| Fe | 0.206 | 0.210 | 0.202 | 0.200 | 0.204 | 0.183 | 0.180 | 0.179 | 0.181 | 0.181 |
| Ni | 0.006 | 0.007 | 0.006 | 0.006 | 0.007 | 0.007 | 0.008 | 0.008 | 0.008 | 0.008 |
| Cr | 0.001 | 0.001 | 0.001 | 0.002 | 0.001 | 0.001 | 0.001 | 0.001 | 0.001 | 0.001 |
| Total | 3.049 | 3.047 | 3.043 | 3.039 | 3.047 | 3.049 | 3.040 | 3.045 | 3.047 | 3.061 |
| %Fo | 90.0 | 89.8 | 90.1 | 90.2 | 90.0 | 91.1 | 91.2 | 91.3 | 91.2 | 91.3 |
| %Fa | 10.0 | 10.2 | 9.9 | 9.8 | 10.0 | 8.9 | 8.8 | 8.7 | 8.8 | 8.7 |

| | PD15-1 | PD15-2 | PD15-3 | PD15-4 | PD15-5 | PD16-1 | PD16-2 | PD16-3 | PD16-4 | PD16-5 |
|---|---|---|---|---|---|---|---|---|---|---|
| MgO | 51.69 | 51.66 | 50.97 | 51.75 | 51.82 | 51.60 | 51.46 | 51.53 | 51.46 | 51.49 |
| $Al_2O_3$ | 0.04 | 0.03 | 0.03 | 0.03 | 0.01 | 0.00 | 0.03 | 0.02 | 0.03 | 0.03 |
| $SiO_2$ | 37.62 | 38.12 | 37.82 | 38.10 | 38.08 | 38.32 | 37.79 | 38.60 | 38.79 | 37.68 |
| CaO | 0.11 | 0.08 | 0.10 | 0.11 | 0.10 | 0.08 | 0.07 | 0.06 | 0.07 | 0.07 |
| MnO | 0.14 | 0.13 | 0.10 | 0.16 | 0.12 | 0.12 | 0.15 | 0.16 | 0.12 | 0.14 |
| FeO | 8.60 | 8.54 | 8.46 | 8.51 | 8.65 | 8.38 | 8.26 | 8.35 | 8.44 | 8.42 |
| NiO | 0.38 | 0.35 | 0.41 | 0.36 | 0.40 | 0.40 | 0.36 | 0.39 | 0.36 | 0.37 |
| $Cr_2O_3$ | 0.05 | 0.02 | 0.04 | 0.04 | 0.06 | 0.06 | 0.05 | 0.05 | 0.03 | 0.04 |
| Total | 98.66 | 98.93 | 97.93 | 99.02 | 99.25 | 98.94 | 98.17 | 99.17 | 99.30 | 98.25 |
| Formula 4(O) | | | | | | | | | | |
| Mg | 1.924 | 1.914 | 1.908 | 1.916 | 1.916 | 1.910 | 1.920 | 1.901 | 1.895 | 1.922 |
| Al | 0.001 | 0.001 | 0.001 | 0.001 | 0.000 | 0.000 | 0.001 | 0.001 | 0.001 | 0.001 |
| Si | 0.939 | 0.947 | 0.950 | 0.945 | 0.944 | 0.951 | 0.946 | 0.955 | 0.958 | 0.944 |
| Ca | 0.003 | 0.002 | 0.003 | 0.003 | 0.003 | 0.002 | 0.002 | 0.002 | 0.002 | 0.002 |
| Mn | 0.003 | 0.003 | 0.002 | 0.003 | 0.002 | 0.002 | 0.003 | 0.003 | 0.003 | 0.003 |
| Fe | 0.180 | 0.177 | 0.178 | 0.177 | 0.179 | 0.174 | 0.173 | 0.173 | 0.174 | 0.176 |
| Ni | 0.008 | 0.007 | 0.008 | 0.007 | 0.008 | 0.008 | 0.007 | 0.008 | 0.007 | 0.007 |
| Cr | 0.001 | 0.000 | 0.001 | 0.001 | 0.001 | 0.001 | 0.001 | 0.001 | 0.001 | 0.001 |
| Total | 3.059 | 3.052 | 3.050 | 3.054 | 3.055 | 3.048 | 3.053 | 3.044 | 3.041 | 3.056 |
| %Fo | 91.3 | 91.4 | 91.4 | 91.4 | 91.3 | 91.5 | 91.6 | 91.5 | 91.5 | 91.5 |
| %Fa | 8.7 | 8.6 | 8.6 | 8.6 | 8.7 | 8.5 | 8.4 | 8.5 | 8.5 | 8.5 |

| | PD17-1 | PD17-2 | PD17-3 | PD17-4 | PD17-5 | PD18-1 | PD18-2 | PD18-3 | PD18-4 | PD18-5 |
|---|---|---|---|---|---|---|---|---|---|---|
| MgO | 52.62 | 52.34 | 51.94 | 52.02 | 52.87 | 52.18 | 51.77 | 51.21 | 51.97 | 51.12 |
| $Al_2O_3$ | 0.00 | 0.02 | 0.03 | 0.02 | 0.02 | 0.00 | 0.02 | 0.02 | 0.01 | 0.03 |
| $SiO_2$ | 38.83 | 38.36 | 38.63 | 38.84 | 38.91 | 38.77 | 38.32 | 37.83 | 39.08 | 37.06 |
| CaO | 0.07 | 0.06 | 0.07 | 0.07 | 0.07 | 0.07 | 0.07 | 0.08 | 0.06 | 0.06 |
| MnO | 0.13 | 0.14 | 0.11 | 0.13 | 0.10 | 0.12 | 0.12 | 0.14 | 0.14 | 0.11 |
| FeO | 8.39 | 8.64 | 8.32 | 8.53 | 8.61 | 8.65 | 8.60 | 8.58 | 8.45 | 8.45 |
| NiO | 0.38 | 0.37 | 0.34 | 0.40 | 0.34 | 0.36 | 0.37 | 0.35 | 0.33 | 0.37 |
| $Cr_2O_3$ | 0.05 | 0.06 | 0.04 | 0.03 | 0.04 | 0.04 | 0.01 | 0.06 | 0.05 | 0.03 |
| Total | 100.46 | 99.98 | 99.49 | 100.03 | 100.96 | 100.18 | 99.27 | 98.26 | 100.08 | 97.23 |
| Formula 4(O) | | | | | | | | | | |
| Mg | 1.917 | 1.920 | 1.910 | 1.904 | 1.918 | 1.908 | 1.911 | 1.911 | 1.899 | 1.930 |
| Al | 0.000 | 0.000 | 0.001 | 0.001 | 0.001 | 0.000 | 0.001 | 0.000 | 0.000 | 0.001 |
| Si | 0.949 | 0.944 | 0.953 | 0.953 | 0.947 | 0.951 | 0.949 | 0.947 | 0.958 | 0.939 |
| Ca | 0.002 | 0.002 | 0.002 | 0.002 | 0.002 | 0.002 | 0.002 | 0.002 | 0.002 | 0.001 |
| Mn | 0.003 | 0.003 | 0.002 | 0.003 | 0.002 | 0.002 | 0.003 | 0.003 | 0.003 | 0.002 |
| Fe | 0.171 | 0.178 | 0.172 | 0.175 | 0.175 | 0.177 | 0.178 | 0.180 | 0.173 | 0.179 |
| Ni | 0.007 | 0.007 | 0.007 | 0.008 | 0.007 | 0.007 | 0.007 | 0.007 | 0.007 | 0.008 |
| Cr | 0.001 | 0.001 | 0.001 | 0.001 | 0.001 | 0.001 | 0.000 | 0.001 | 0.001 | 0.001 |
| Total | 3.051 | 3.055 | 3.047 | 3.046 | 3.052 | 3.049 | 3.051 | 3.052 | 3.042 | 3.061 |
| %Fo | 91.7 | 91.4 | 91.6 | 91.5 | 91.5 | 91.4 | 91.4 | 91.3 | 91.5 | 91.4 |
| %Fa | 8.3 | 8.6 | 8.4 | 8.5 | 8.5 | 8.6 | 8.6 | 8.7 | 8.5 | 8.6 |

| | PD19-1 | PD19-2 | PD19-3 | PD19-4 | PD19-5 | PD20-1 | PD20-2 | PD20-3 | PD20-4 | PD20-5 |
|---|---|---|---|---|---|---|---|---|---|---|
| MgO | 50.35 | 50.64 | 50.17 | 50.59 | 51.07 | 51.74 | 50.98 | 51.33 | 51.81 | 52.21 |
| $Al_2O_3$ | 0.01 | 0.01 | 0.01 | 0.02 | 0.02 | 0.02 | 0.03 | 0.04 | 0.02 | 0.02 |
| $SiO_2$ | 36.93 | 37.78 | 38.05 | 37.13 | 37.99 | 39.08 | 38.34 | 38.84 | 38.65 | 39.12 |
| CaO | 0.08 | 0.10 | 0.09 | 0.07 | 0.09 | 0.11 | 0.12 | 0.11 | 0.10 | 0.11 |
| MnO | 0.13 | 0.11 | 0.13 | 0.15 | 0.09 | 0.11 | 0.12 | 0.12 | 0.10 | 0.11 |
| FeO | 9.02 | 9.50 | 9.20 | 9.24 | 9.21 | 8.94 | 8.78 | 8.94 | 8.93 | 8.75 |
| NiO | 0.35 | 0.37 | 0.33 | 0.35 | 0.38 | 0.36 | 0.35 | 0.42 | 0.39 | 0.35 |
| $Cr_2O_3$ | 0.04 | 0.06 | 0.02 | 0.02 | 0.06 | 0.03 | 0.04 | 0.05 | 0.06 | 0.05 |
| Total | 96.92 | 98.57 | 98.00 | 97.57 | 98.92 | 100.40 | 98.77 | 99.85 | 100.06 | 100.72 |
| Formula 4(O) | | | | | | | | | | |
| Mg | 1.912 | 1.892 | 1.880 | 1.910 | 1.899 | 1.889 | 1.892 | 1.885 | 1.900 | 1.899 |
| Al | 0.000 | 0.000 | 0.000 | 0.001 | 0.001 | 0.001 | 0.001 | 0.001 | 0.001 | 0.001 |
| Si | 0.941 | 0.947 | 0.957 | 0.940 | 0.947 | 0.957 | 0.955 | 0.957 | 0.951 | 0.954 |
| Ca | 0.002 | 0.003 | 0.002 | 0.002 | 0.002 | 0.003 | 0.003 | 0.003 | 0.003 | 0.003 |
| Mn | 0.003 | 0.002 | 0.003 | 0.003 | 0.002 | 0.002 | 0.003 | 0.002 | 0.002 | 0.002 |
| Fe | 0.192 | 0.199 | 0.193 | 0.196 | 0.192 | 0.183 | 0.183 | 0.184 | 0.184 | 0.178 |
| Ni | 0.007 | 0.007 | 0.007 | 0.007 | 0.008 | 0.007 | 0.007 | 0.008 | 0.008 | 0.007 |
| Cr | 0.001 | 0.001 | 0.000 | 0.000 | 0.001 | 0.001 | 0.001 | 0.001 | 0.001 | 0.001 |
| Total | 3.059 | 3.052 | 3.043 | 3.059 | 3.052 | 3.042 | 3.044 | 3.042 | 3.049 | 3.045 |
| %Fo | 90.7 | 90.4 | 90.6 | 90.6 | 90.7 | 91.1 | 91.1 | 91.0 | 91.1 | 91.3 |
| %Fa | 9.3 | 9.6 | 9.4 | 9.4 | 9.3 | 8.9 | 8.9 | 9.0 | 8.9 | 8.7 |

# Appendix 2

Raman spectra of 27 studied samples which consist of 20 coarse-grained samples and 7 fine-grained samples;

three spectra of each sample were collected.
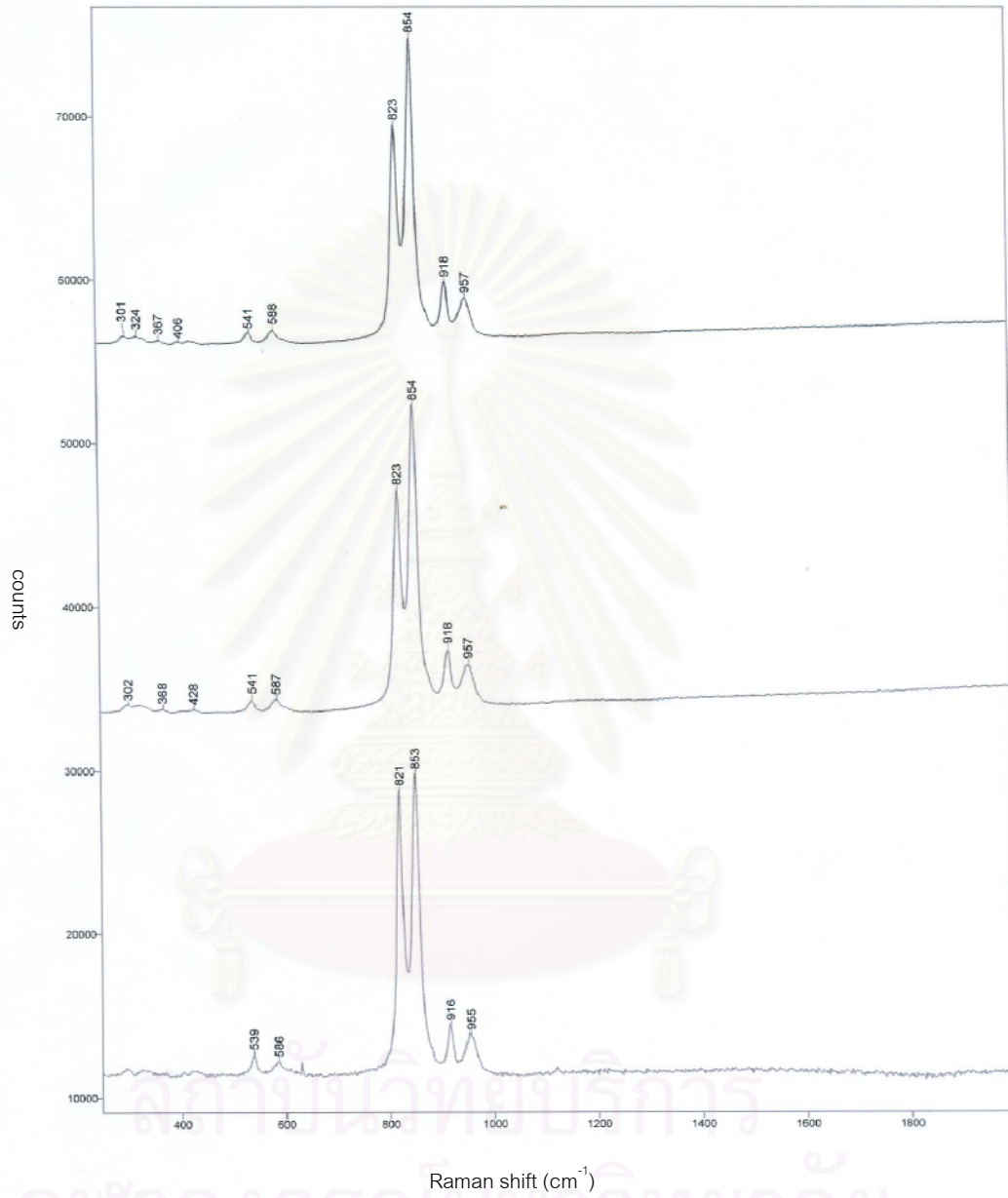
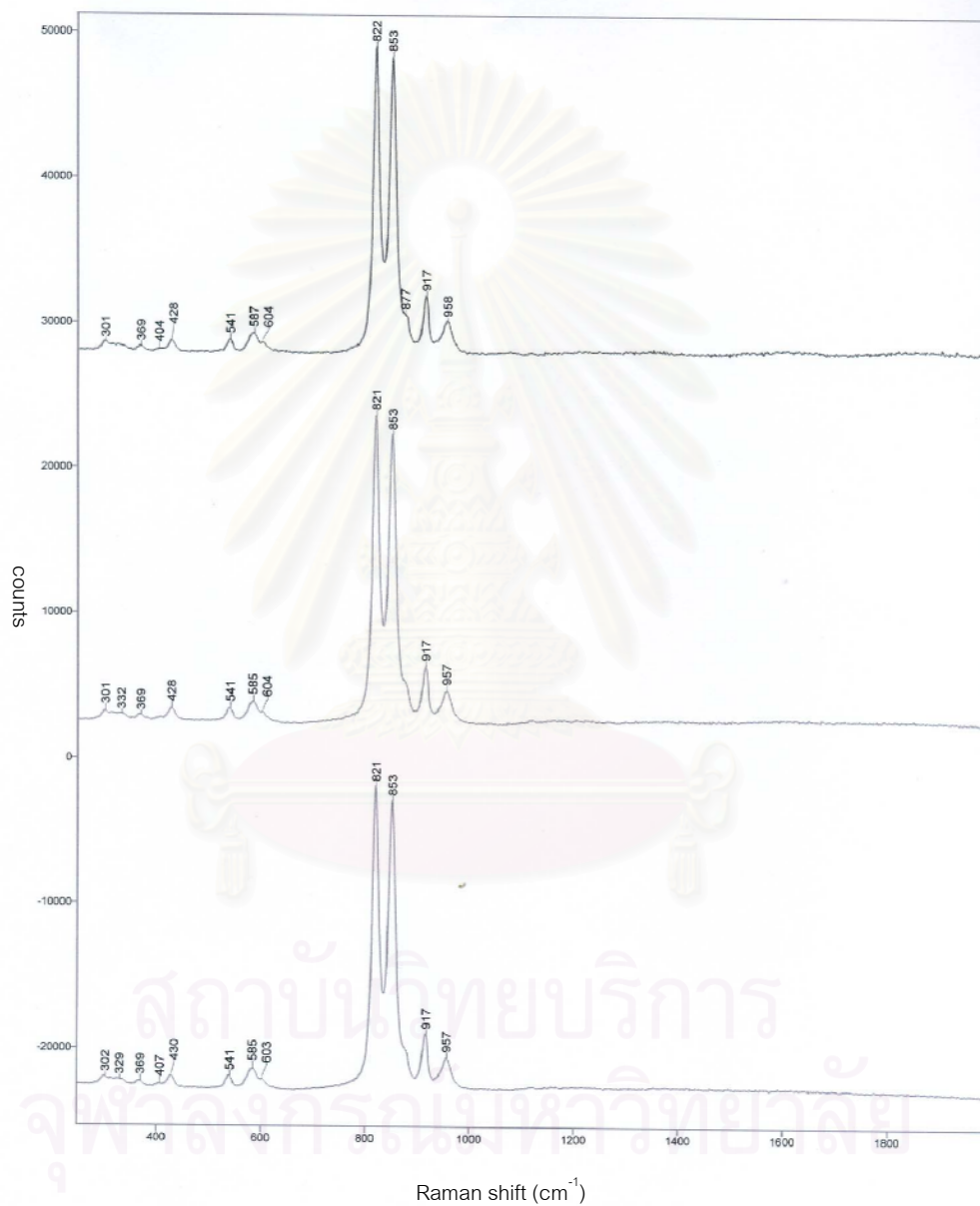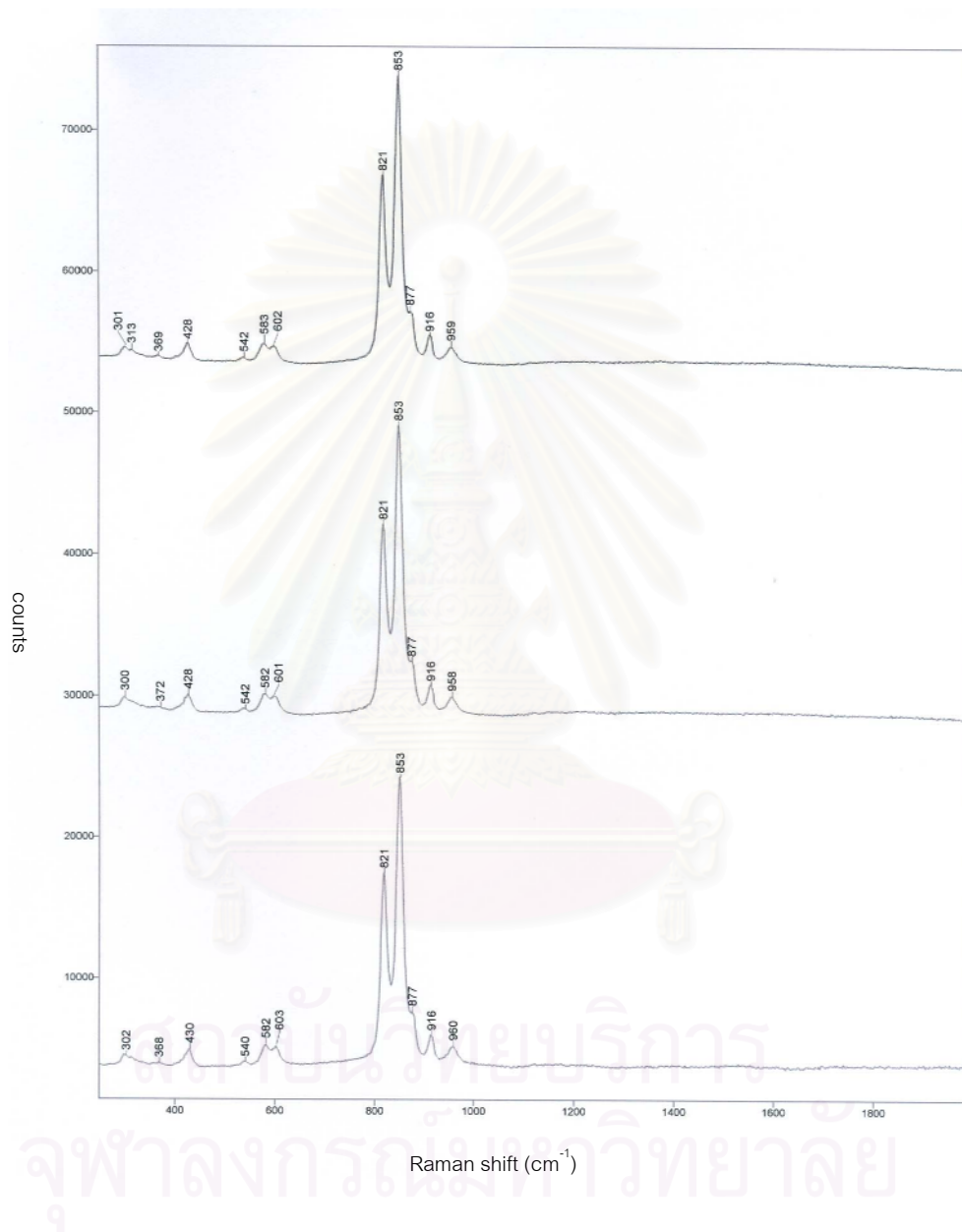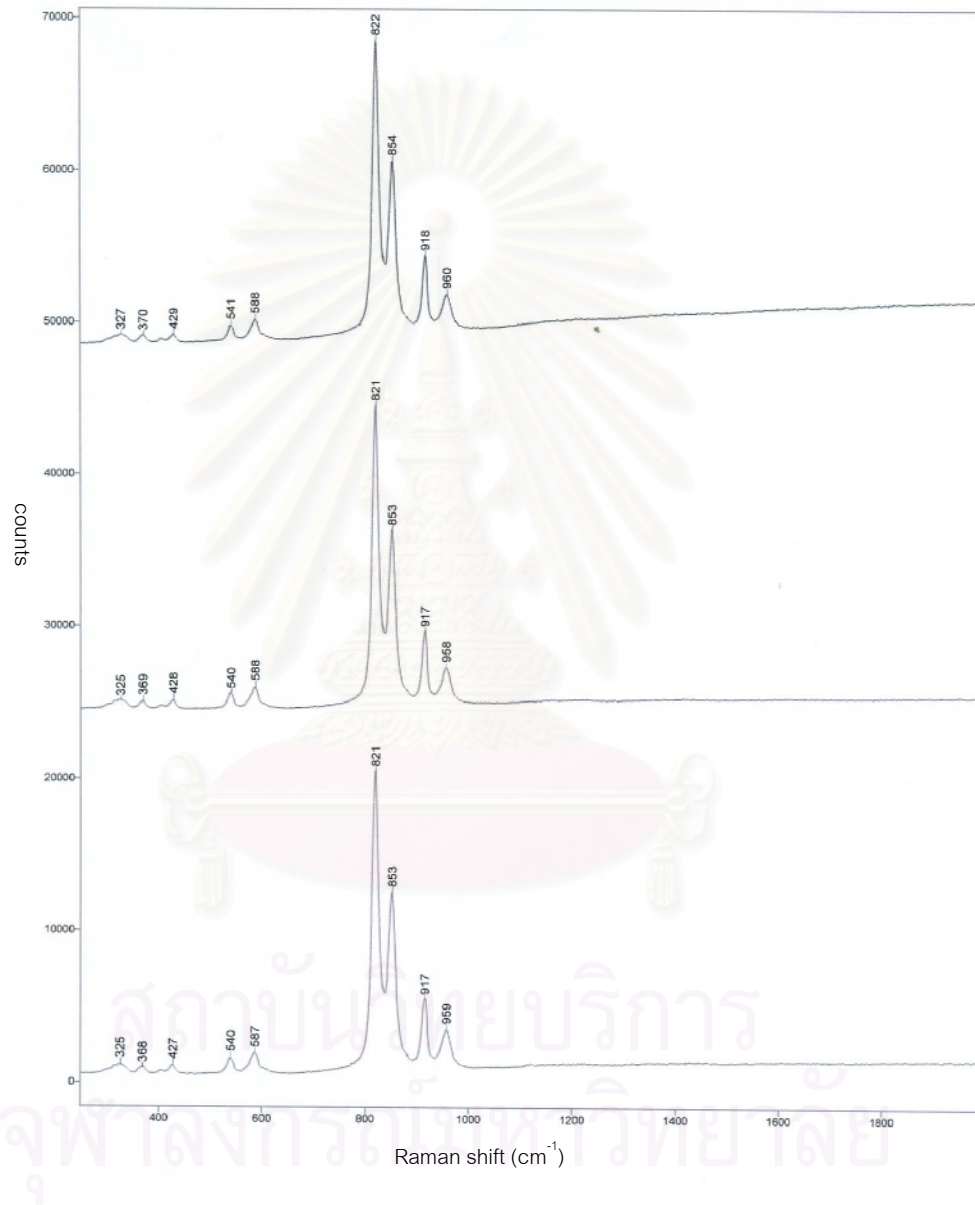Figure A2.1    Three raman spectra of sample no.PD01  which has 83.9%Fo.
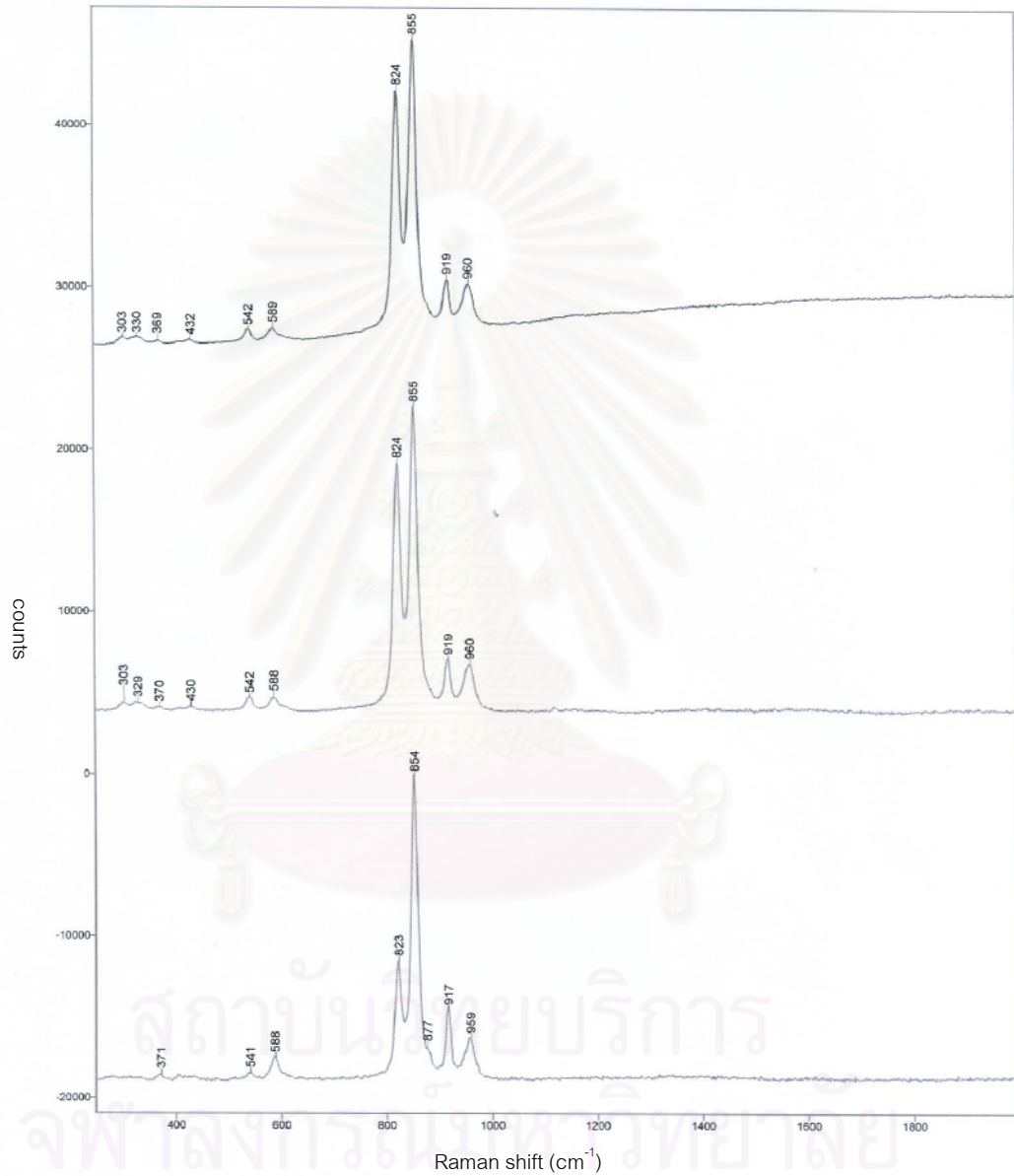
Figure A2.2    Three raman spectra of sample no. PD02 which has 88.9% Fo
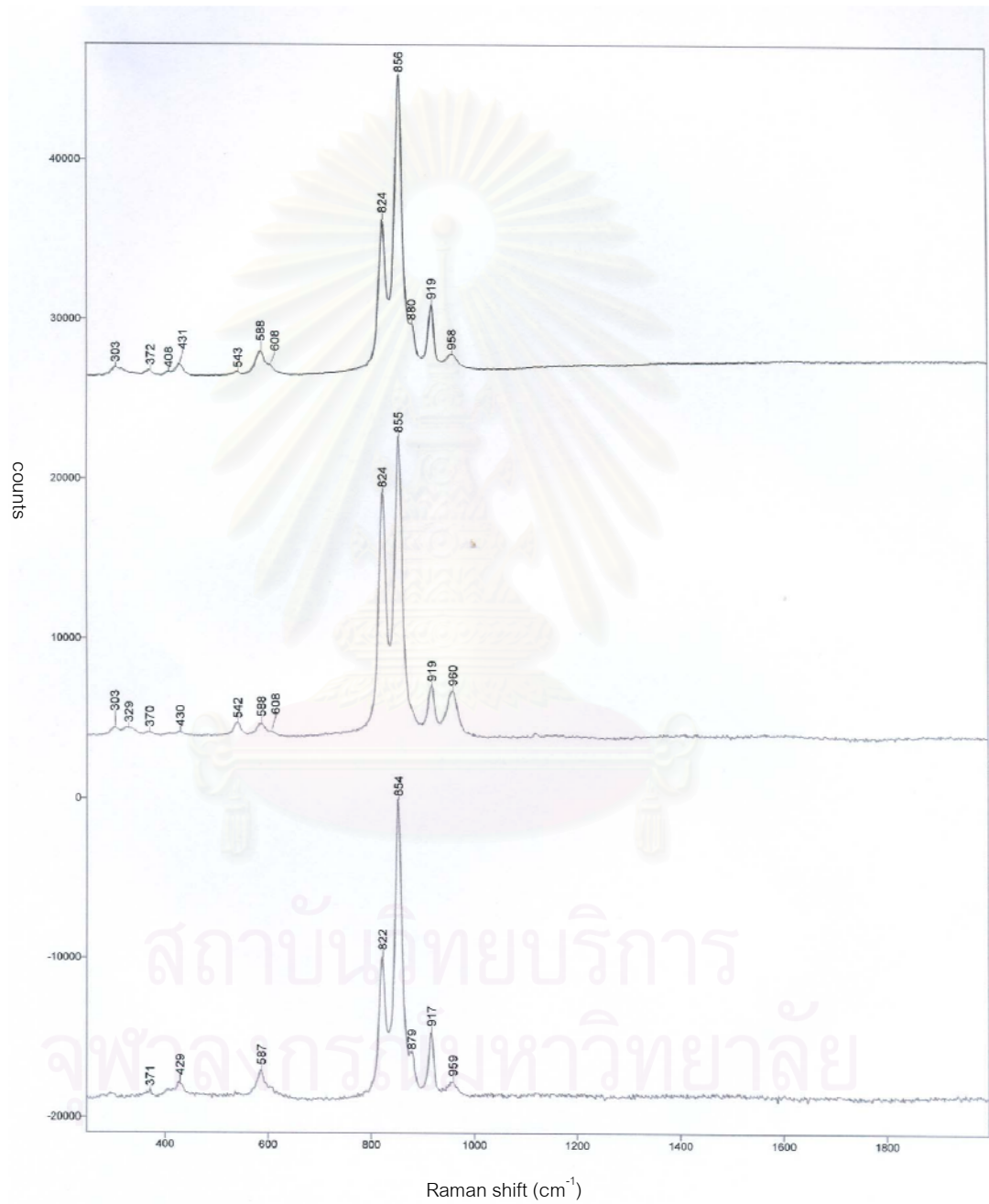
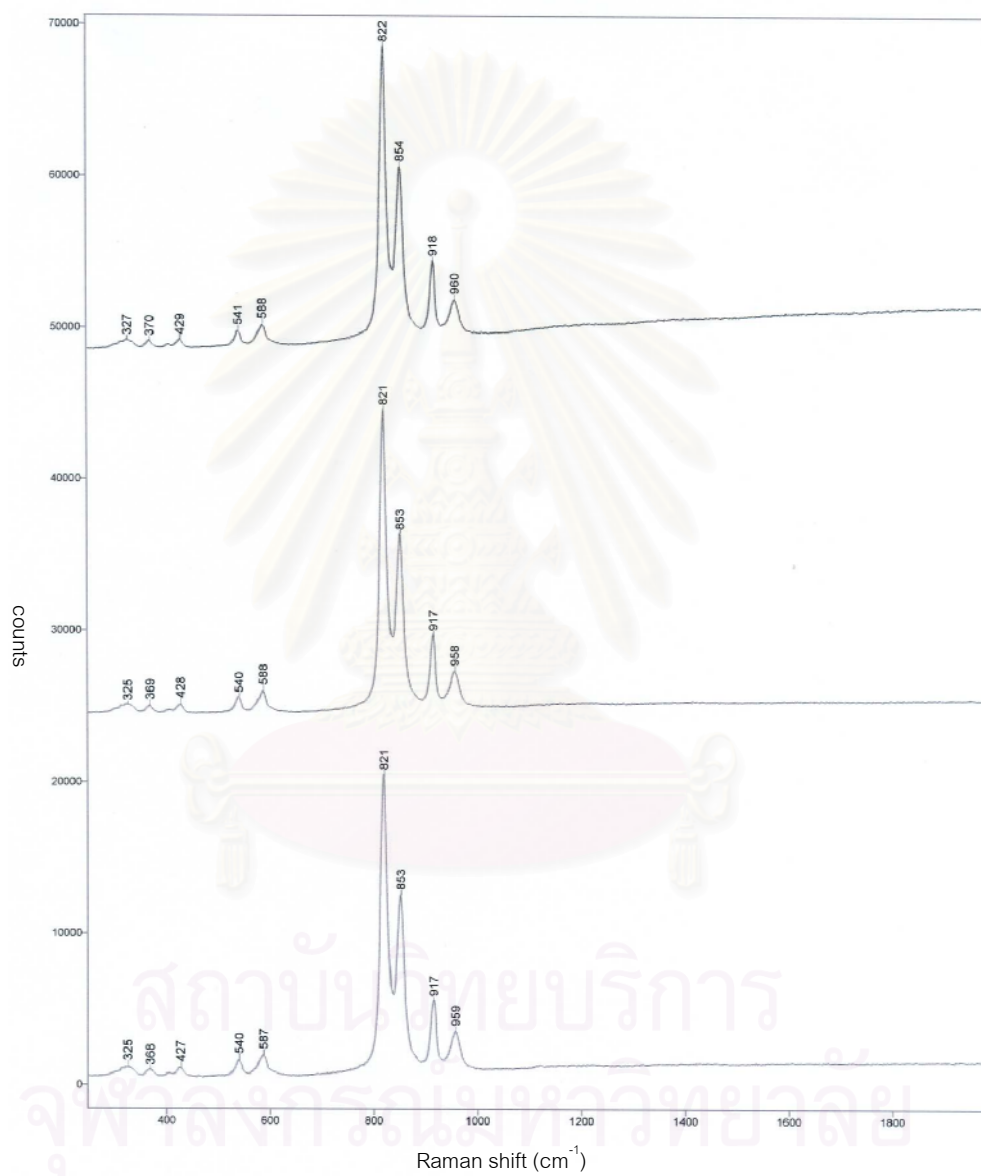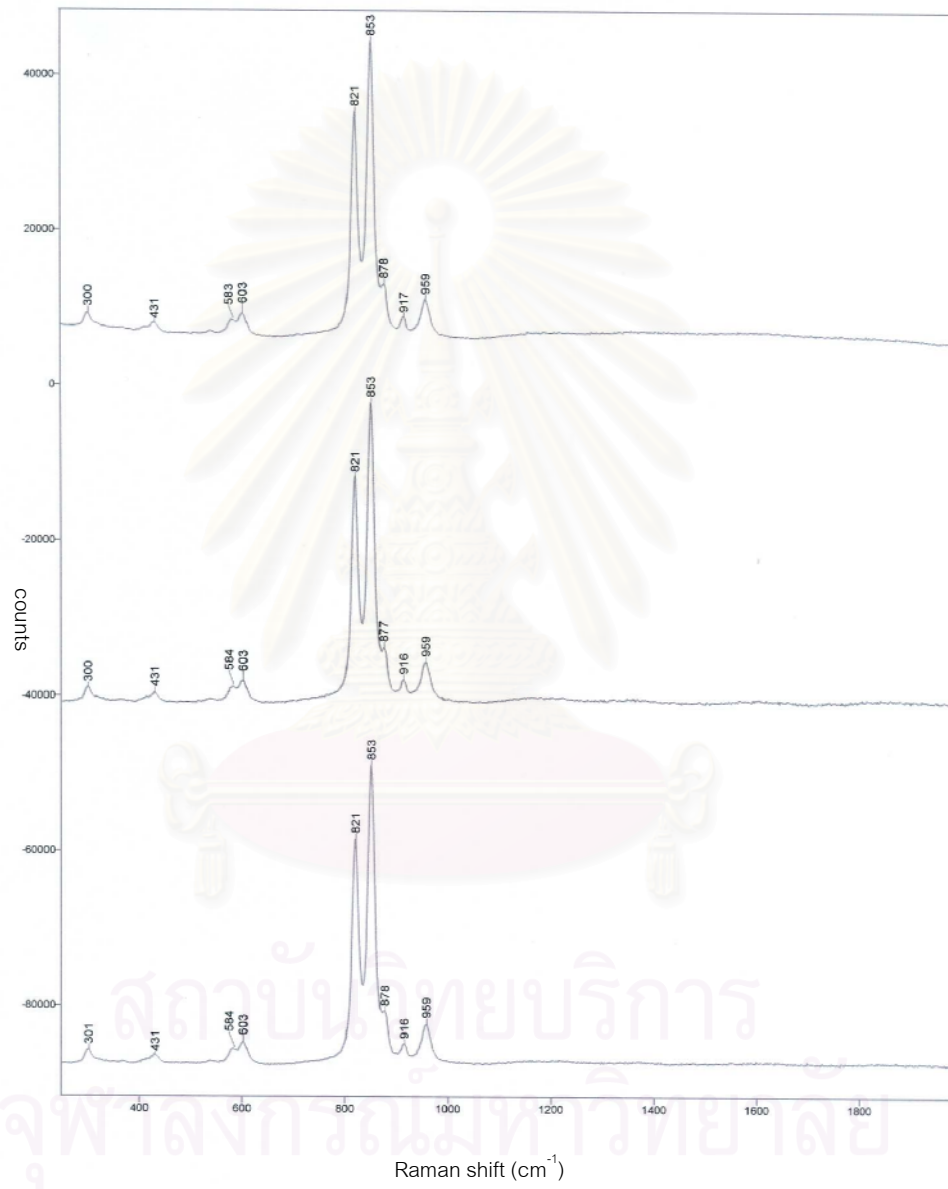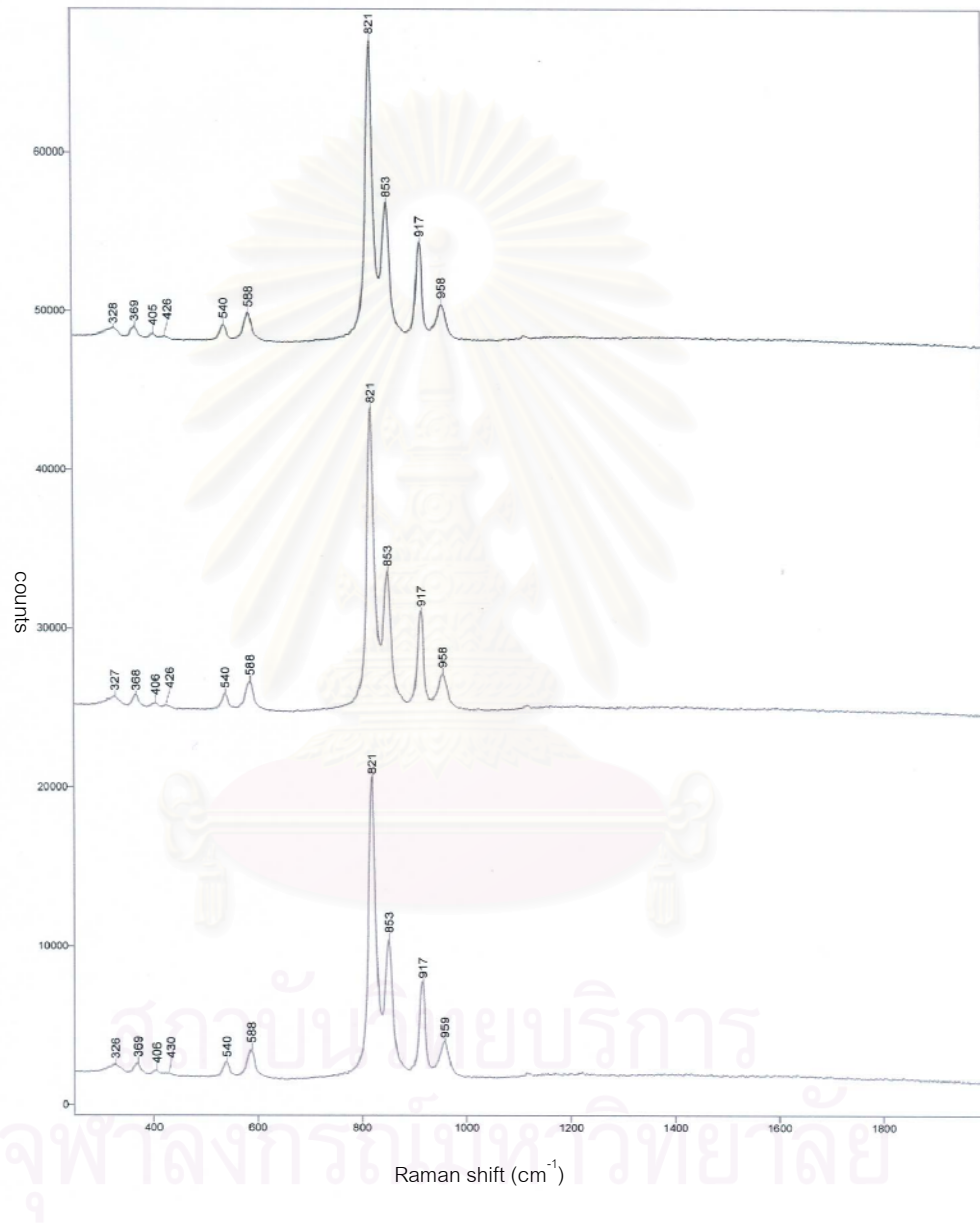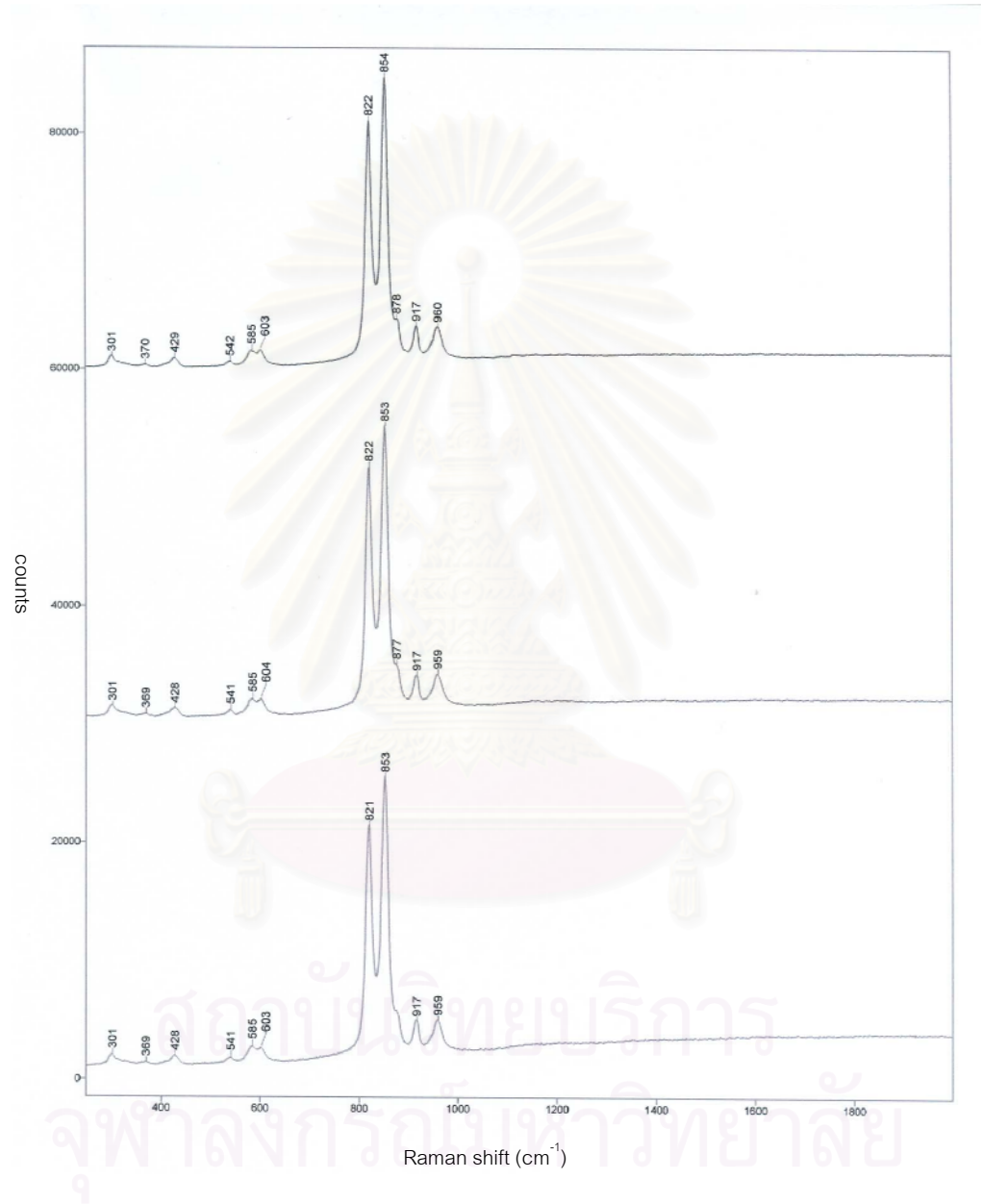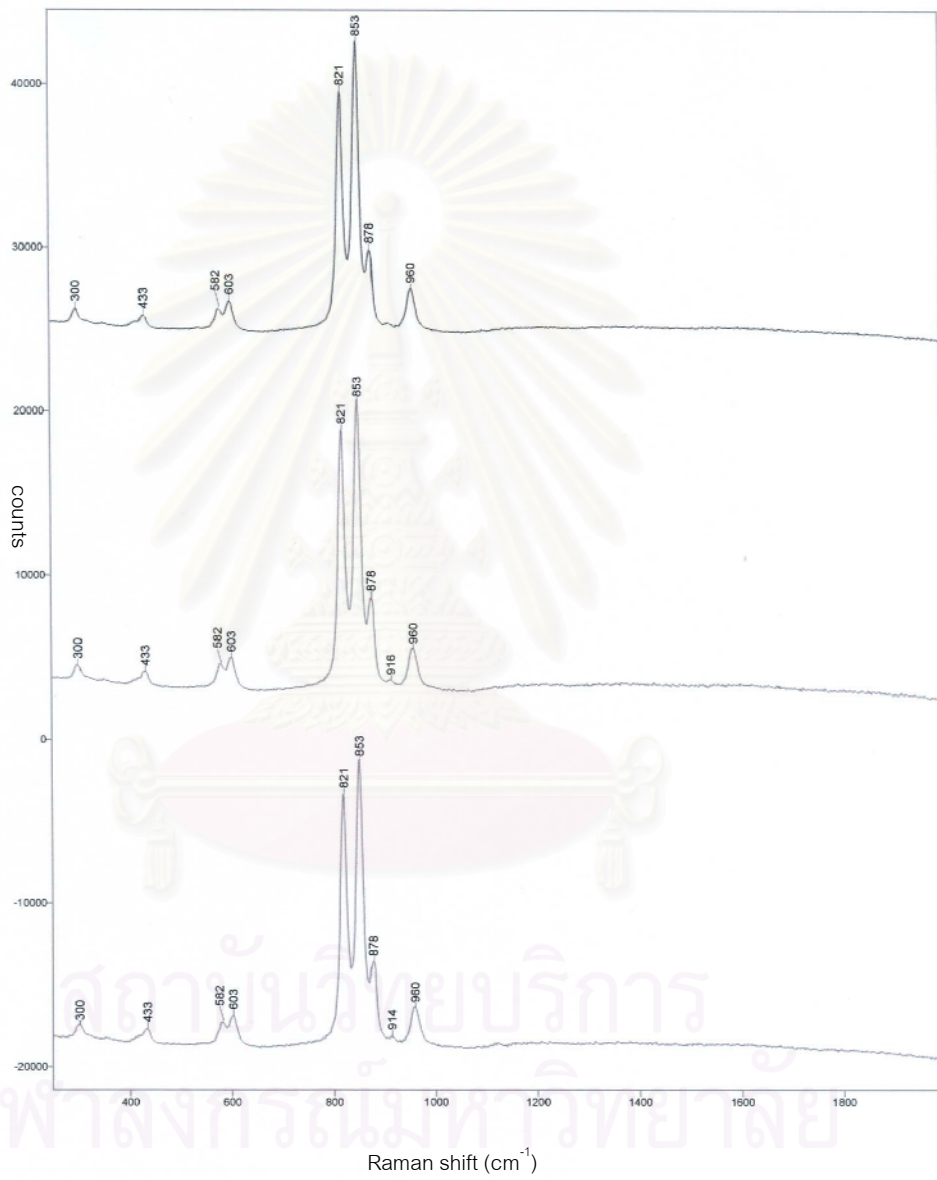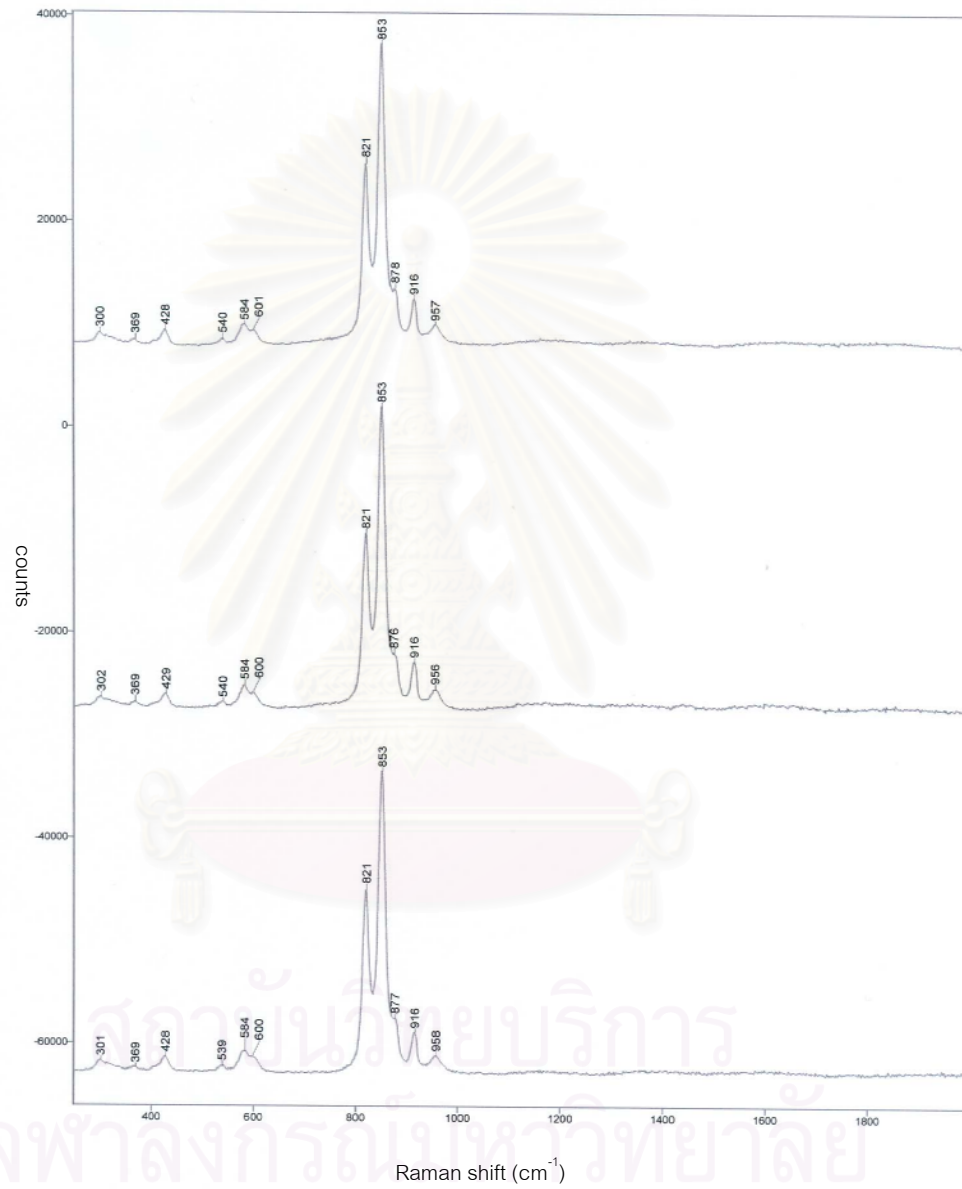Figure A2.3    Three raman spectra of sample no. PD03 which has 89.4%Fo
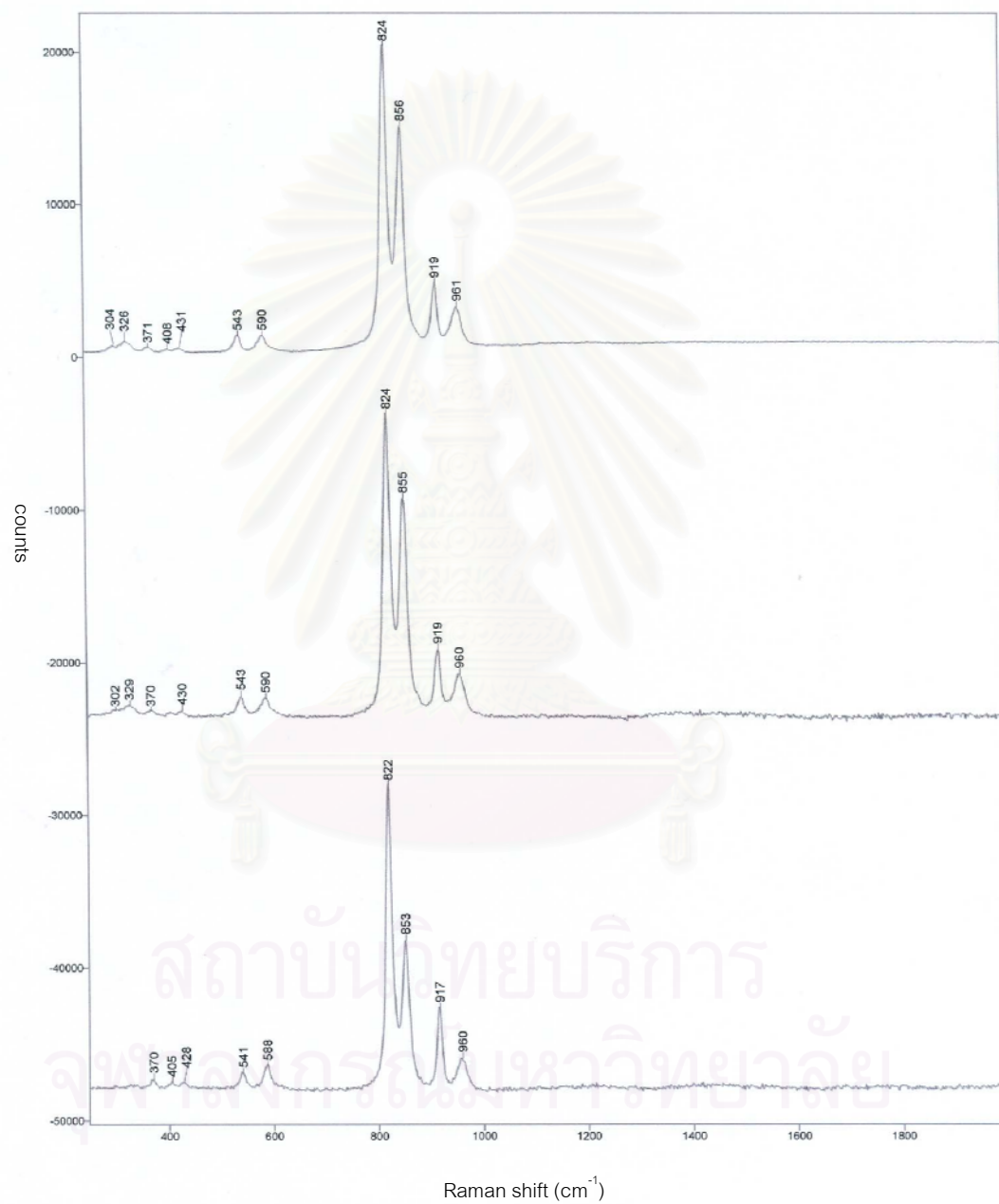
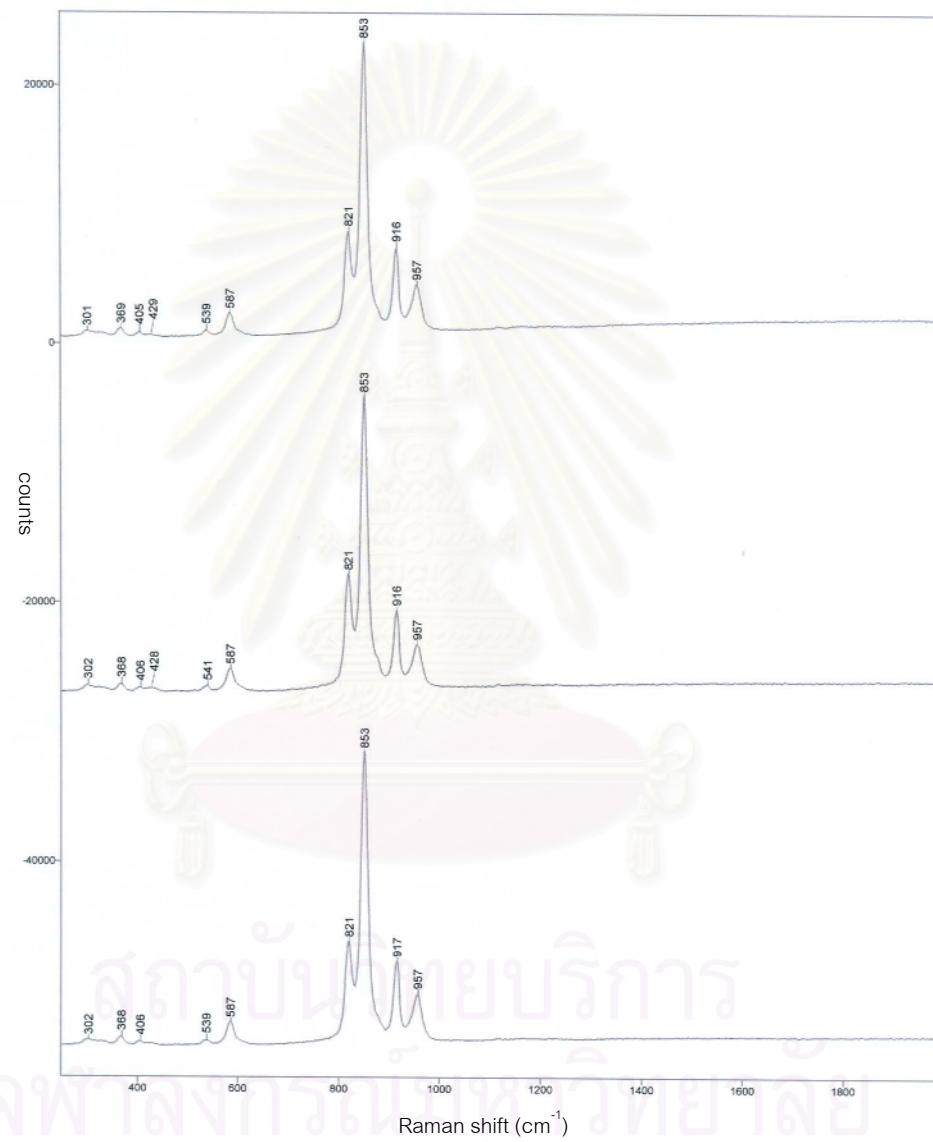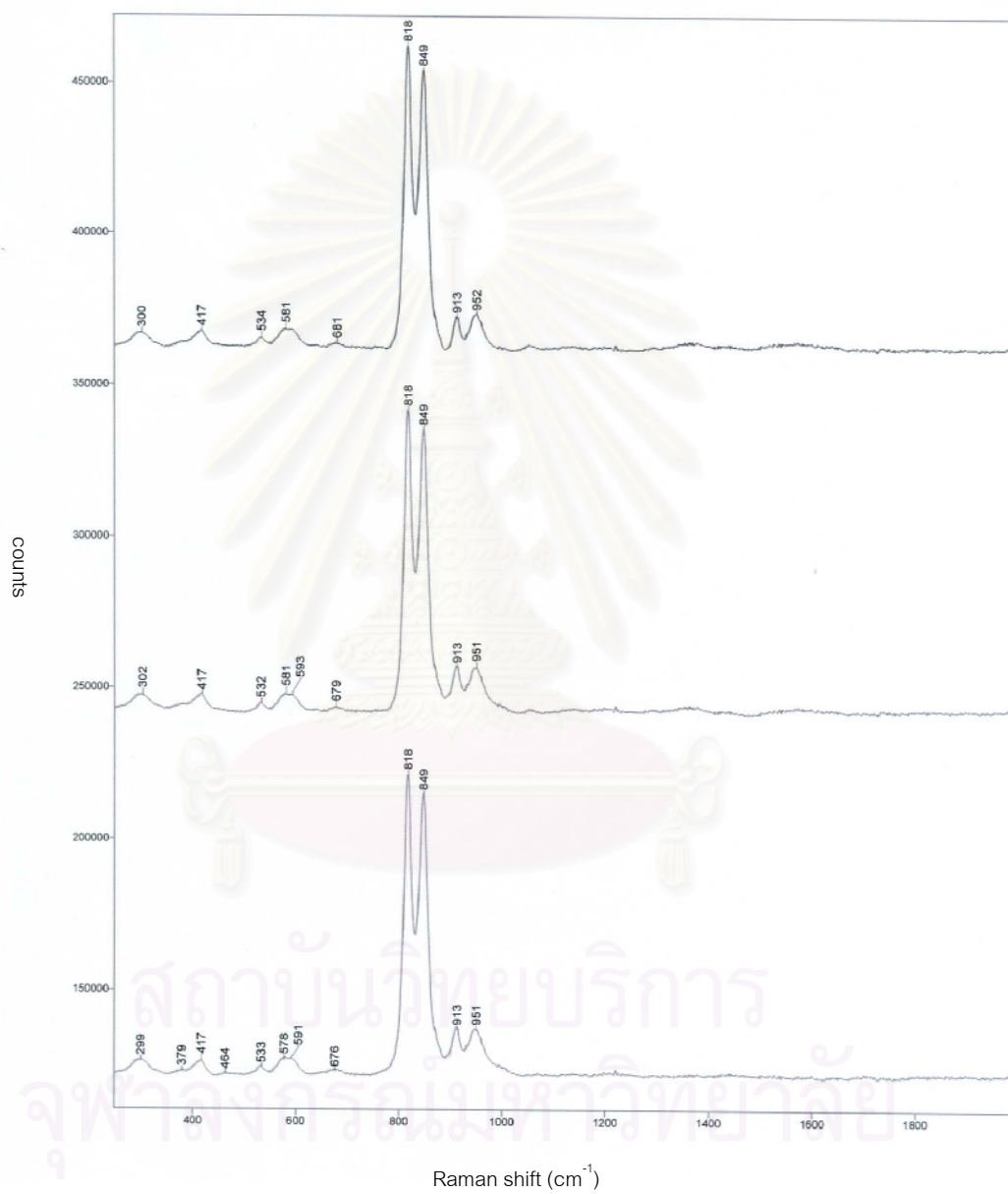Figure A2.4     Three raman spectra of sample no. PD04 which has 88.7% Fo
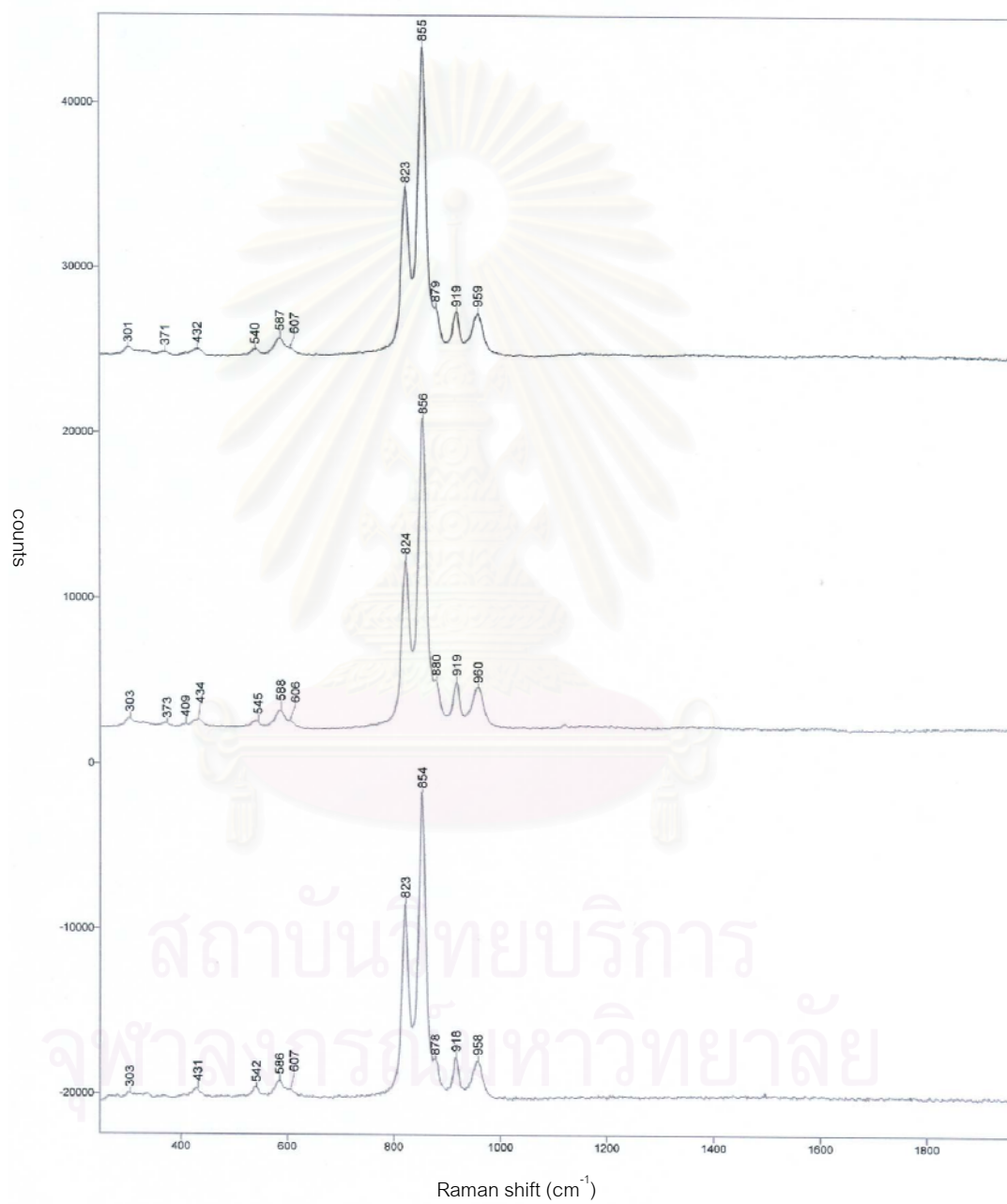
Figure A2.5    Three raman spectra of sample no. PD05 which has 89.3 % Fo
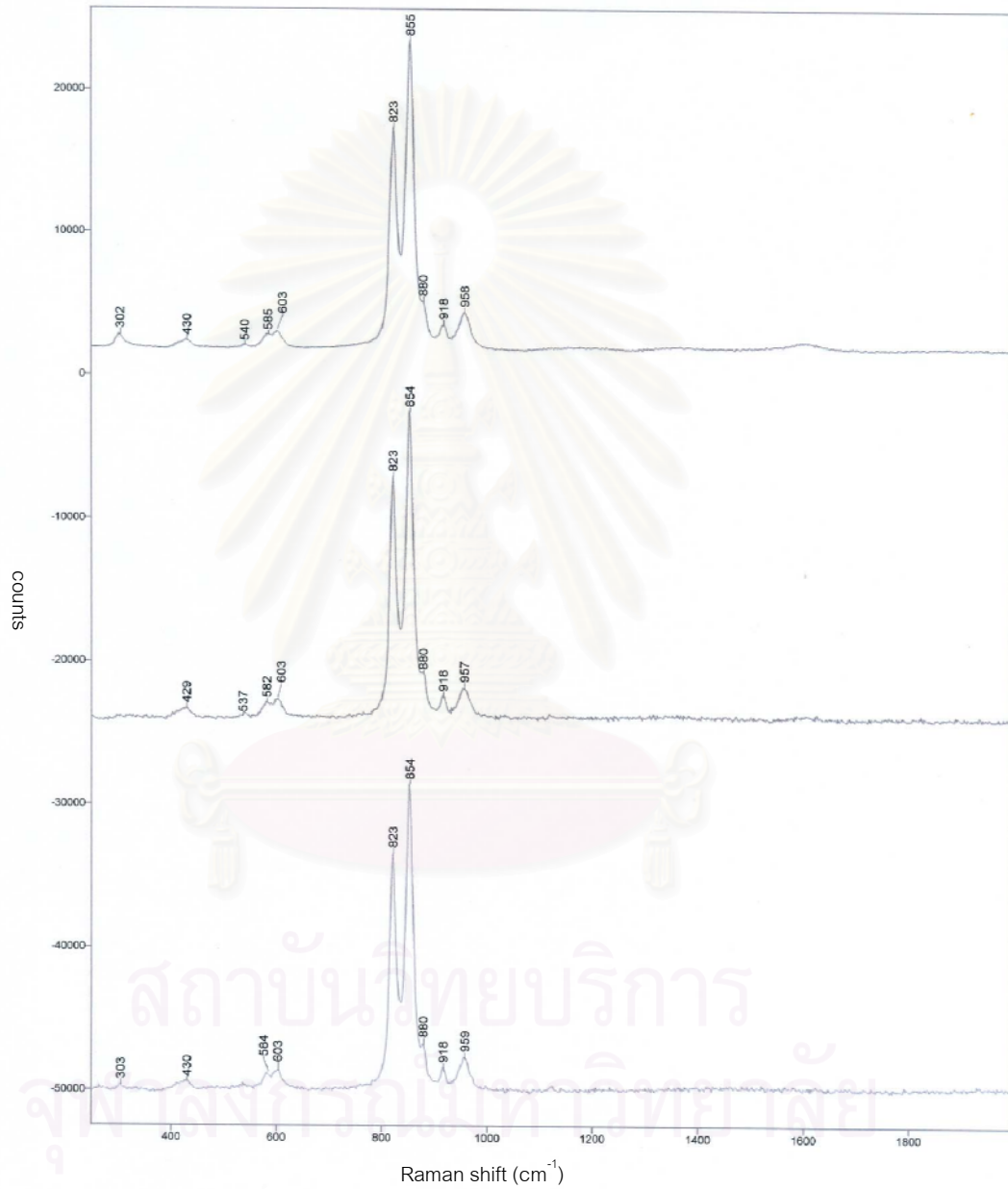
Figure A2.6    Three raman spectra of sample no. PD06 which has 84.8% Fo
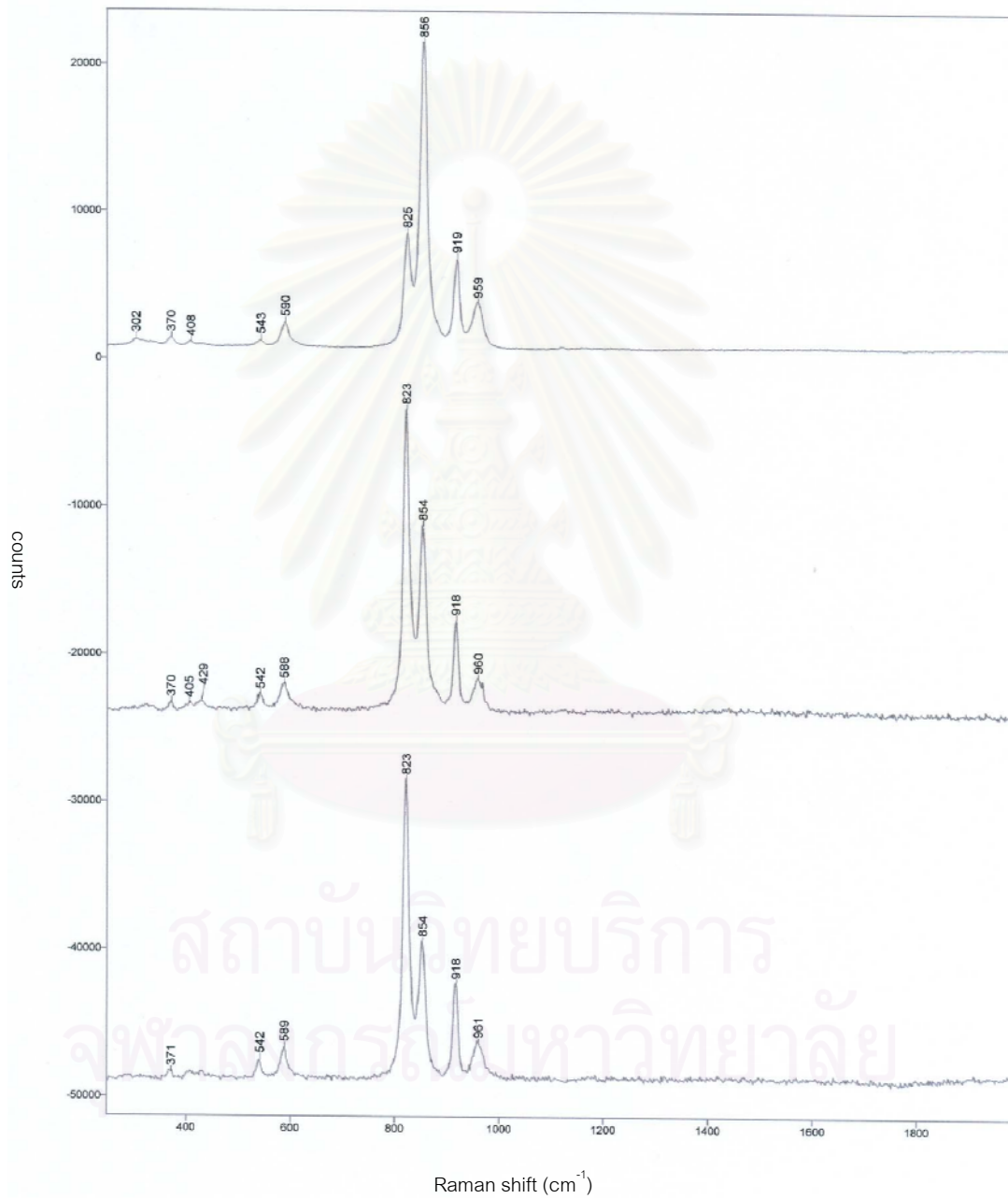
Figure A2.7    Three raman spectra of sample no. PD07 which has 88.8% Fo
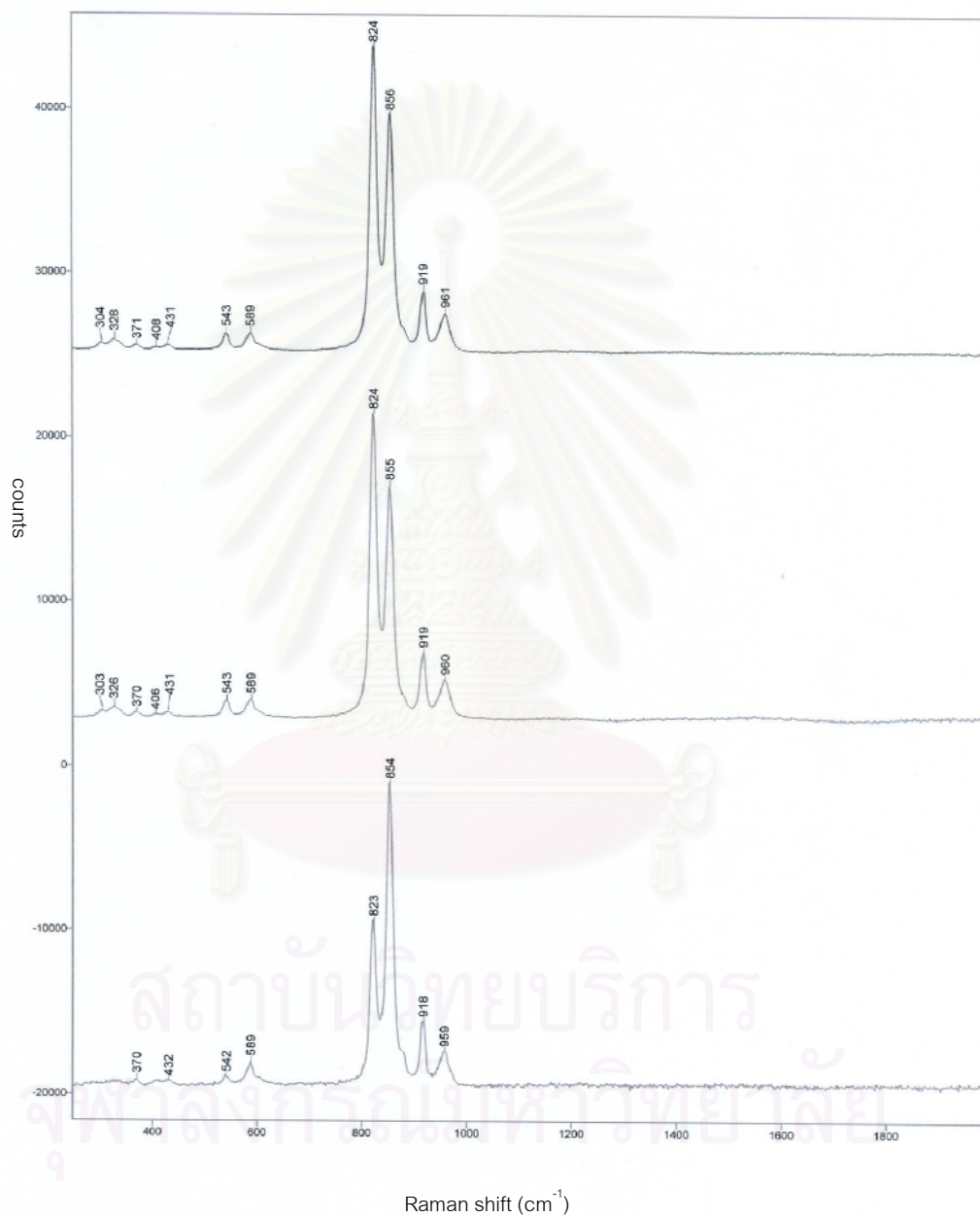
Figure A2.8    Three raman spectra of sample no.PD08 which has 88.8% Fo
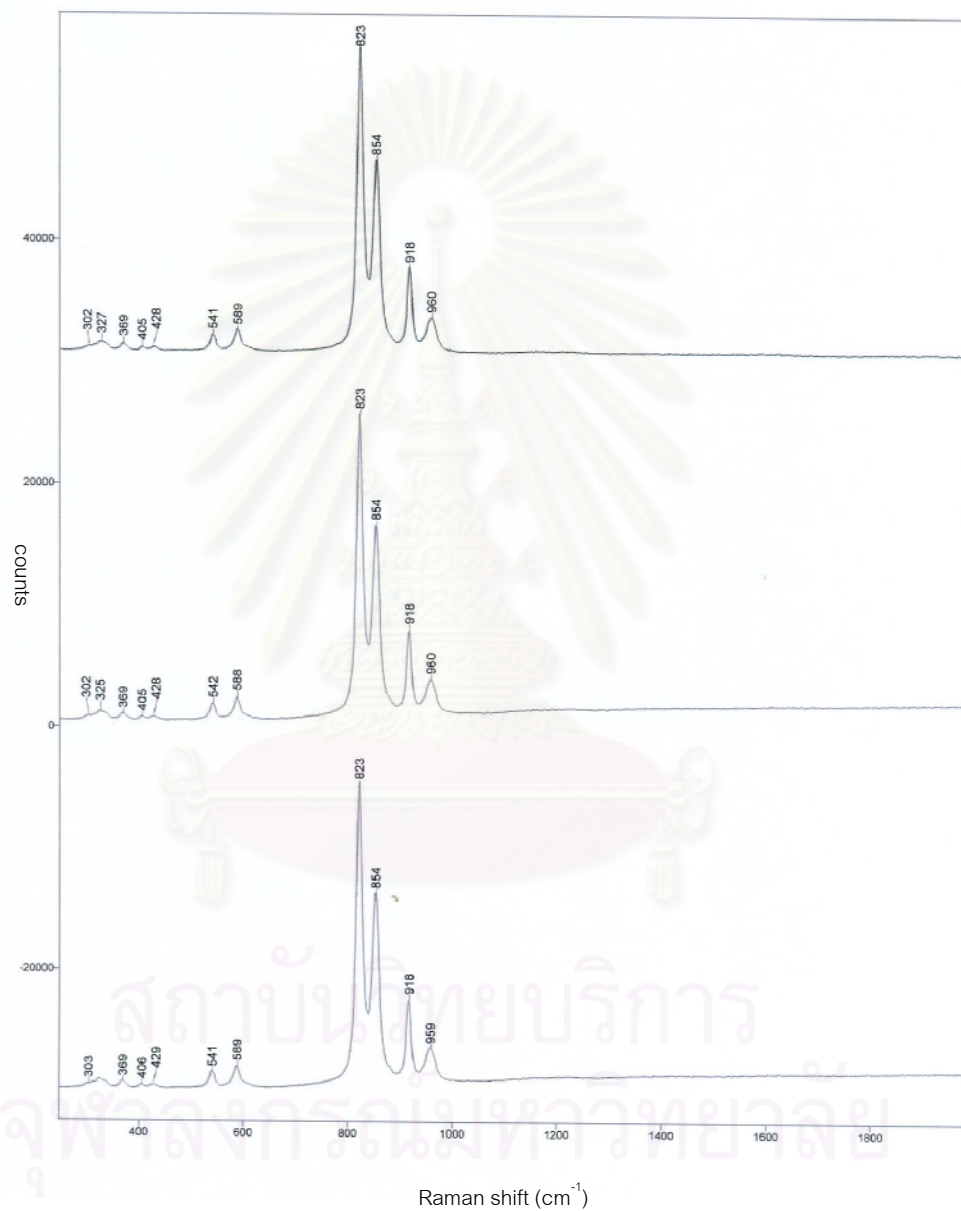
Figure A2.9   Three raman spectra of sample no. PD09 which has 89.4% Fo
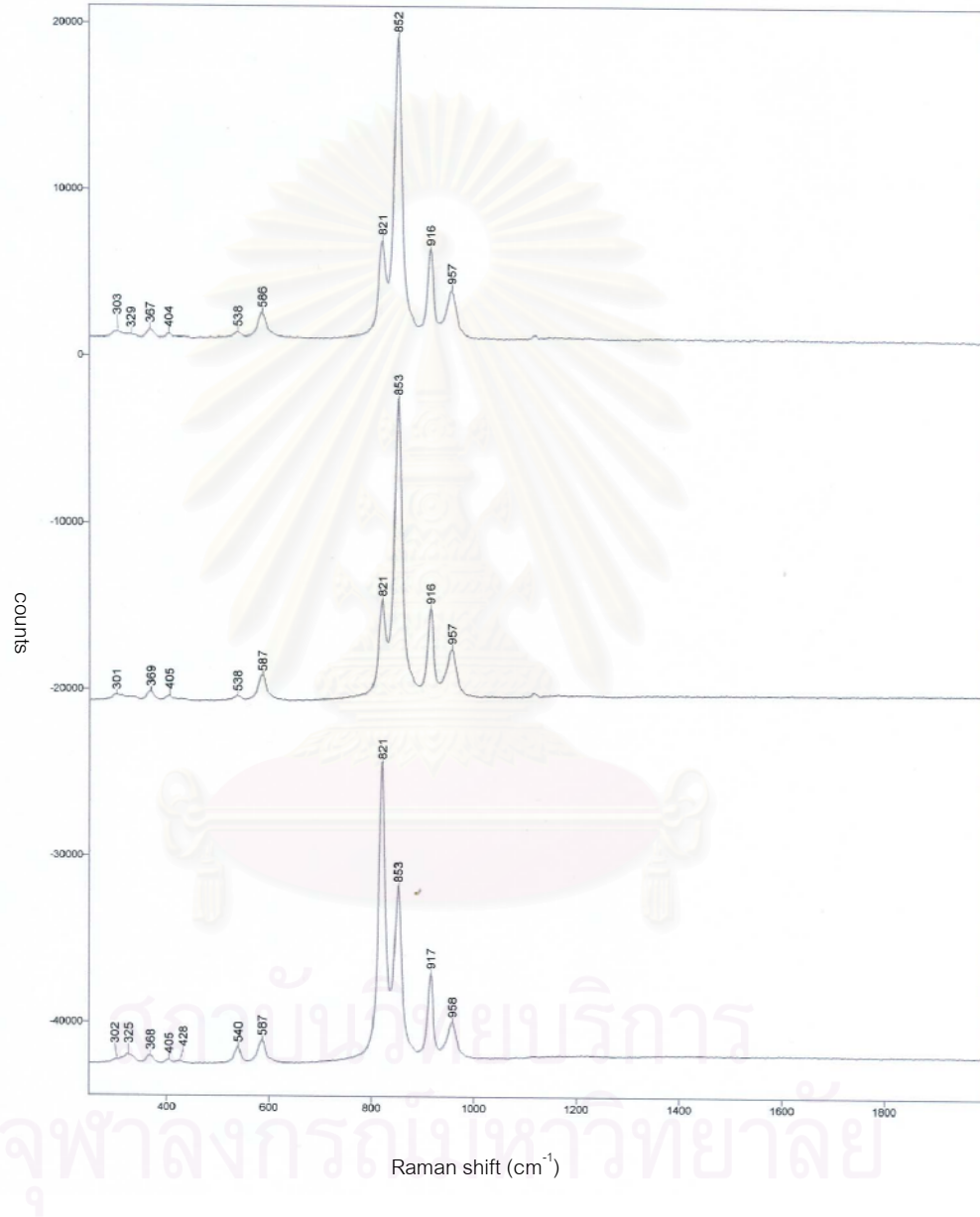
Figure A2.10    Three raman spectra of sample no. PD10 which has 90.6% Fo

Figure A2.11     Three raman spectra of sample no. PD11 which has 91.4% Fo

Figure A2.12   Three raman spectra of sample no. PD12 which has 91.0% Fo

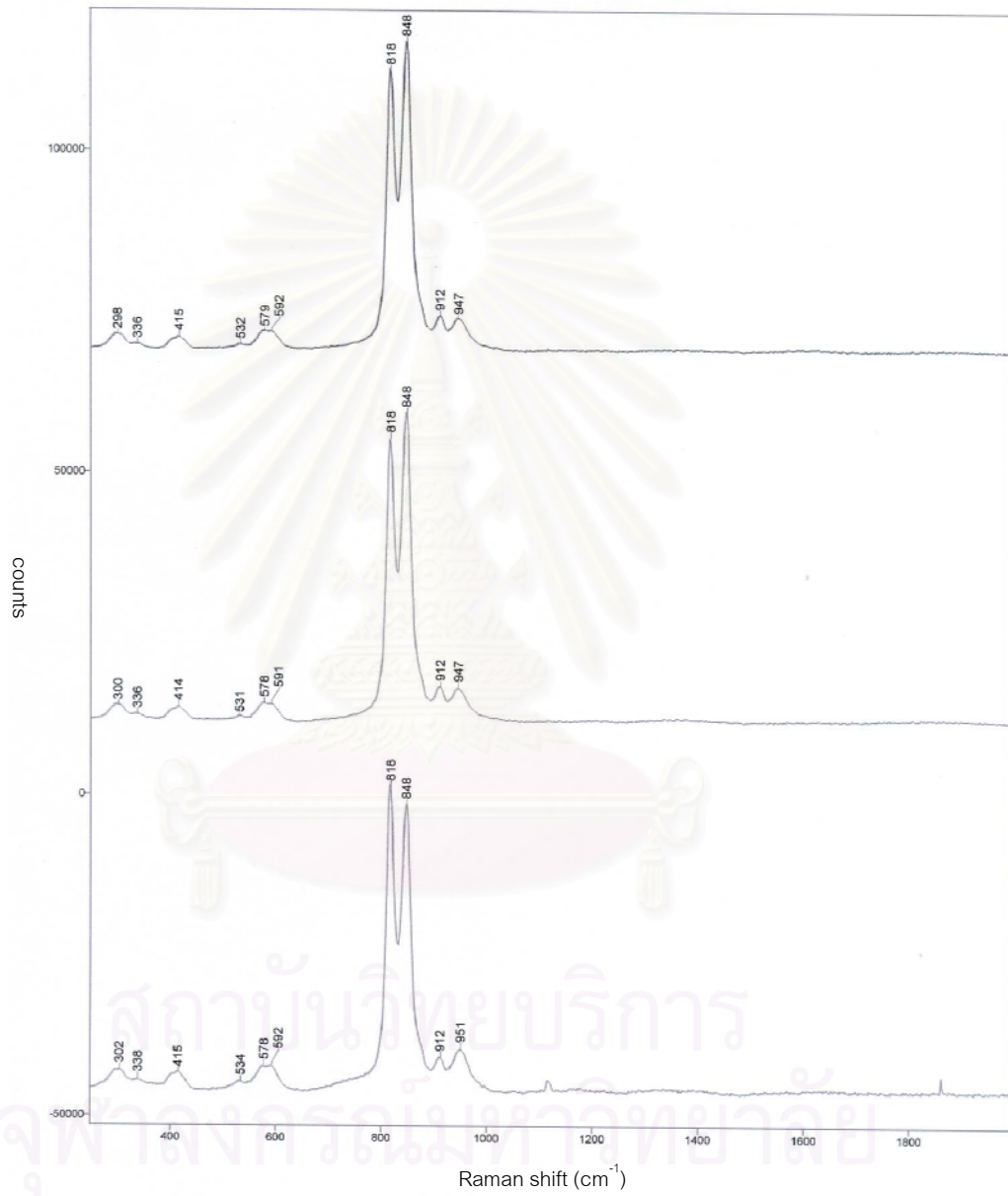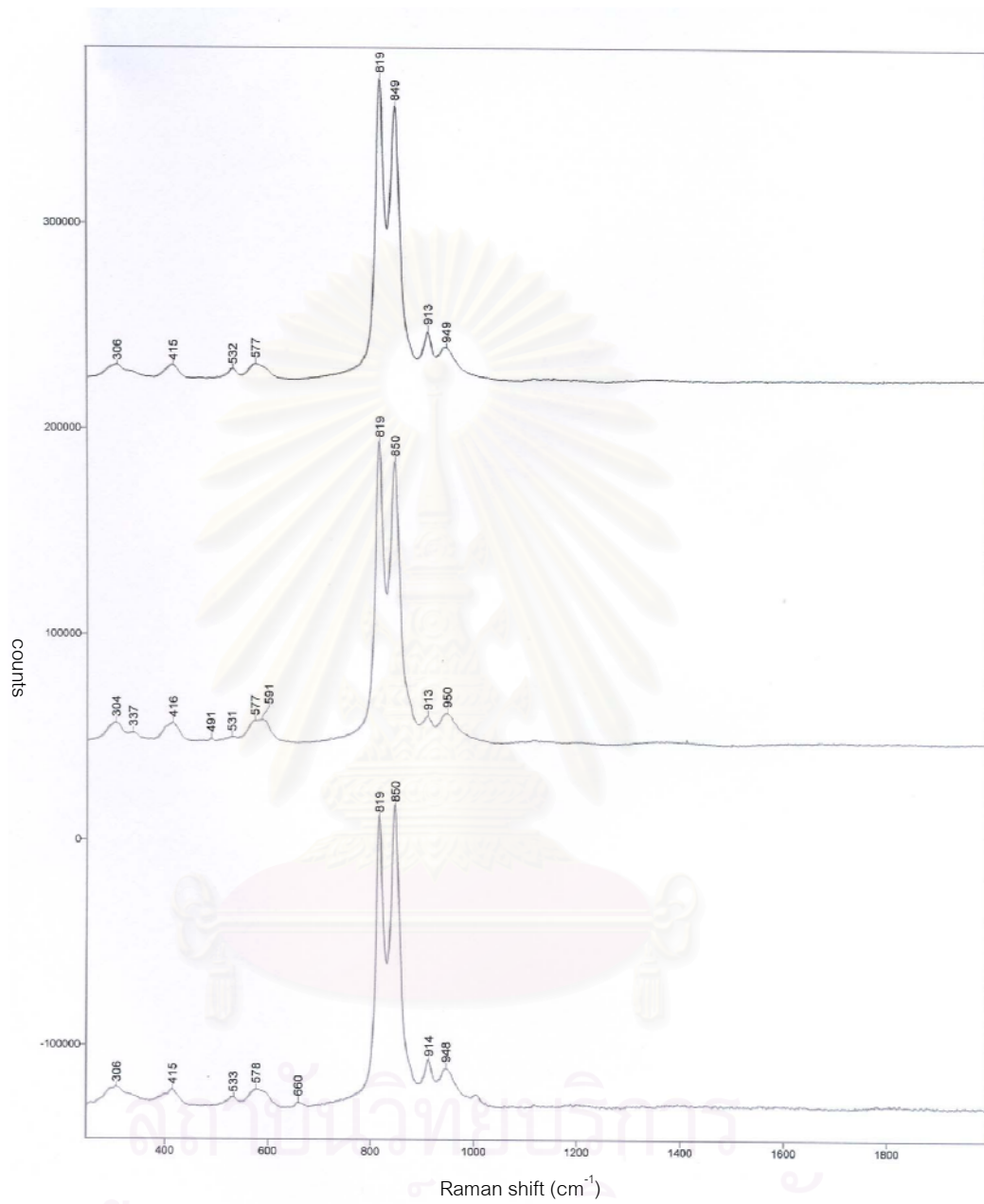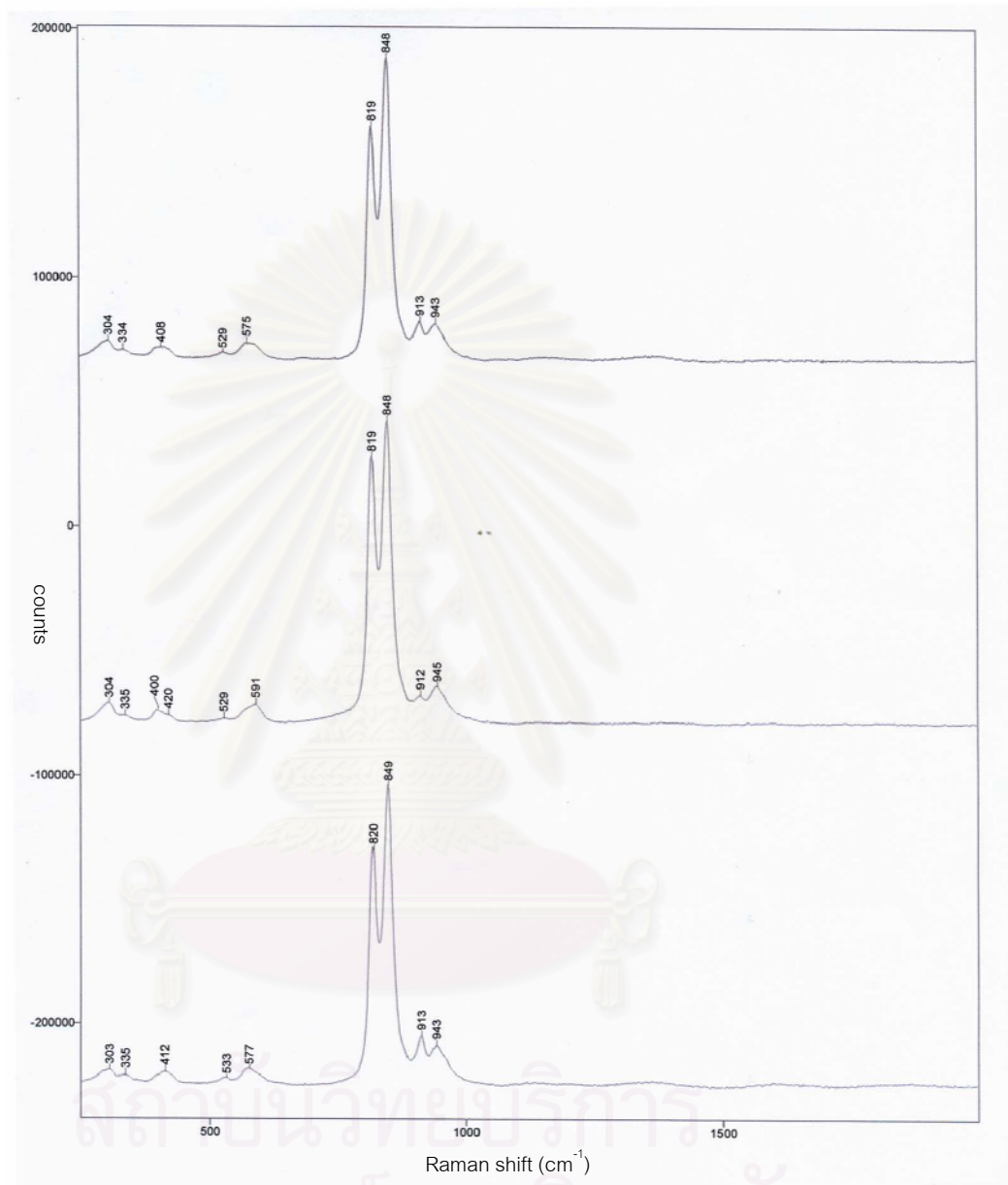Figure A2.13    Three raman spectra of sample no. PD13 which has 90.0% Fo

Figure A2.14      Three raman spectra of sample no.PD14 which has 91.2% Fo

Figure A2.15   Three raman spectra of sample no. PD15  which has 91.4% Fo

Figure A2.16    Three raman spectra of sample no. PD16 which has 91.5% Fo

Figure A2.17  Three raman spectra of sample no. PD17 which has 91.5% Fo

Figure A2.18    Three raman spectra of sample no. PD18 which has 91.4% Fo

Figure A2.19    Three raman spectra of sample no. PD19 which has 90.6% Fo

Figure A2.20    Three raman spectra of sample no. PD20 which has 91.1% Fo

Figure A2.21     Three raman spectra of sample no. PD735 which has 73.5% Fo

Figure A2.22    Three raman spectra of sample no. PD706 which has 70.6% Fo

Figure A2.23    Three raman spectra of sample no. PD678 which has 67.8% Fo

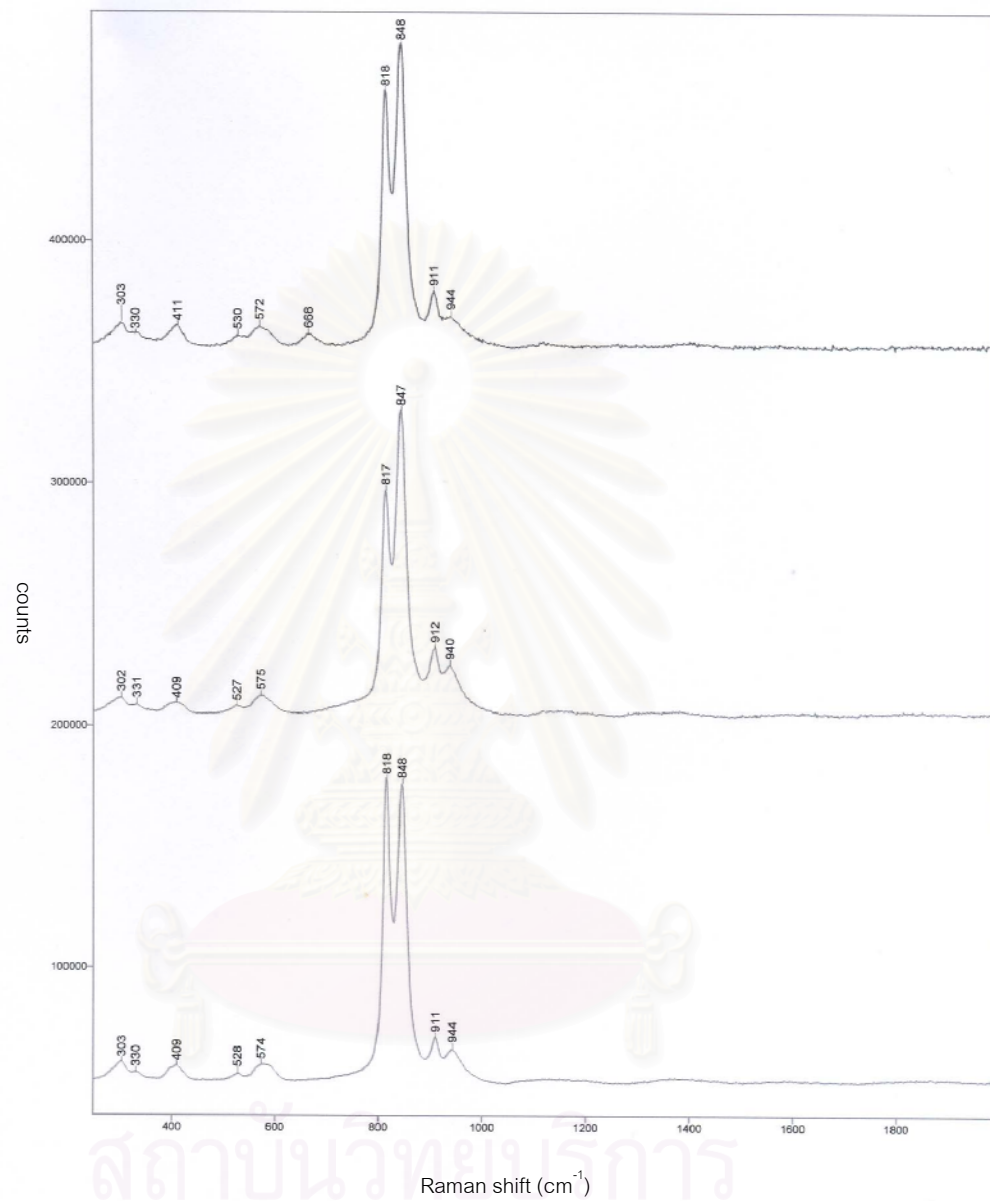Figure A2.24     Three raman spectra of sample no. PD617 which has 61.7% Fo

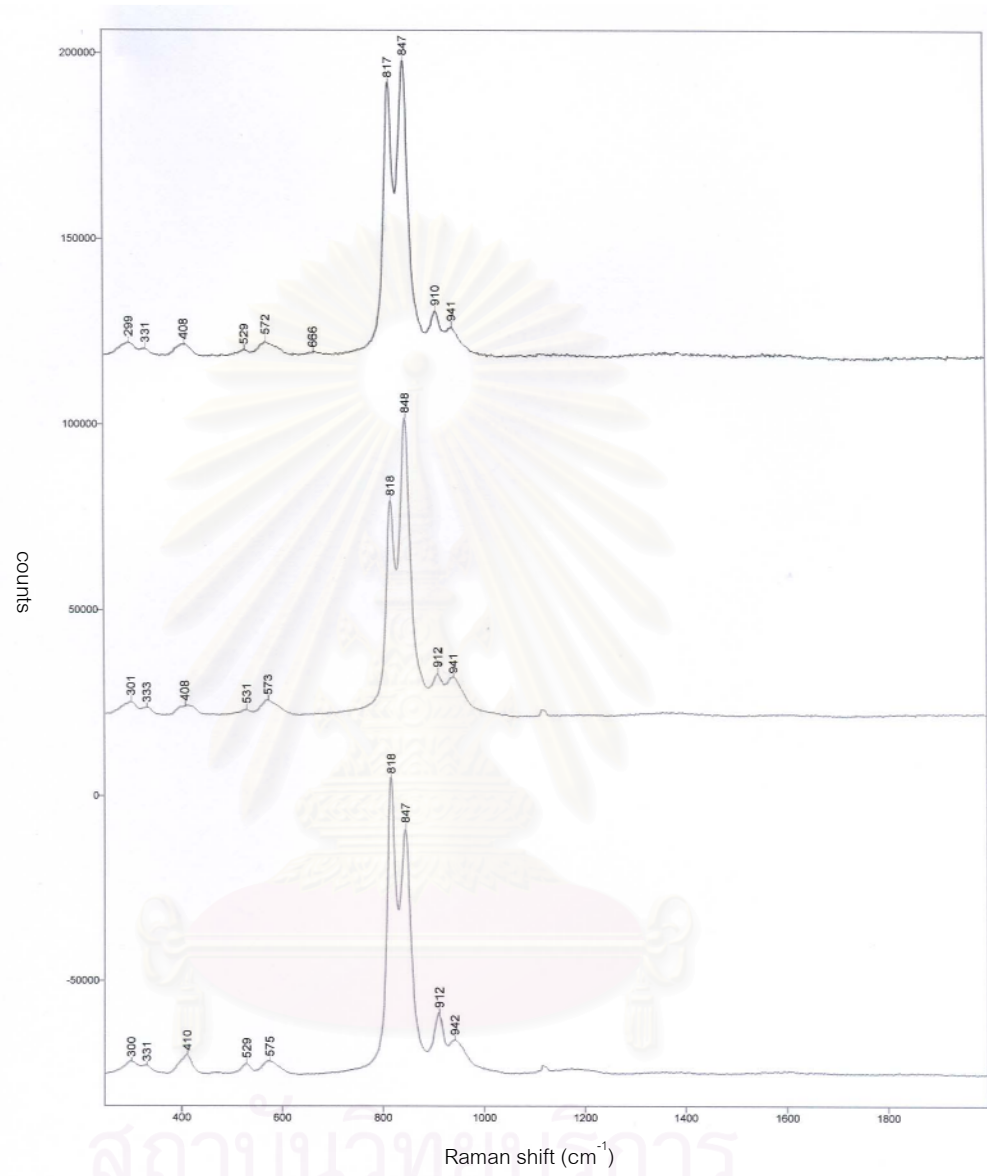Figure A2.25     Three raman spectra of sample no. PD605 which has 60.5% Fo

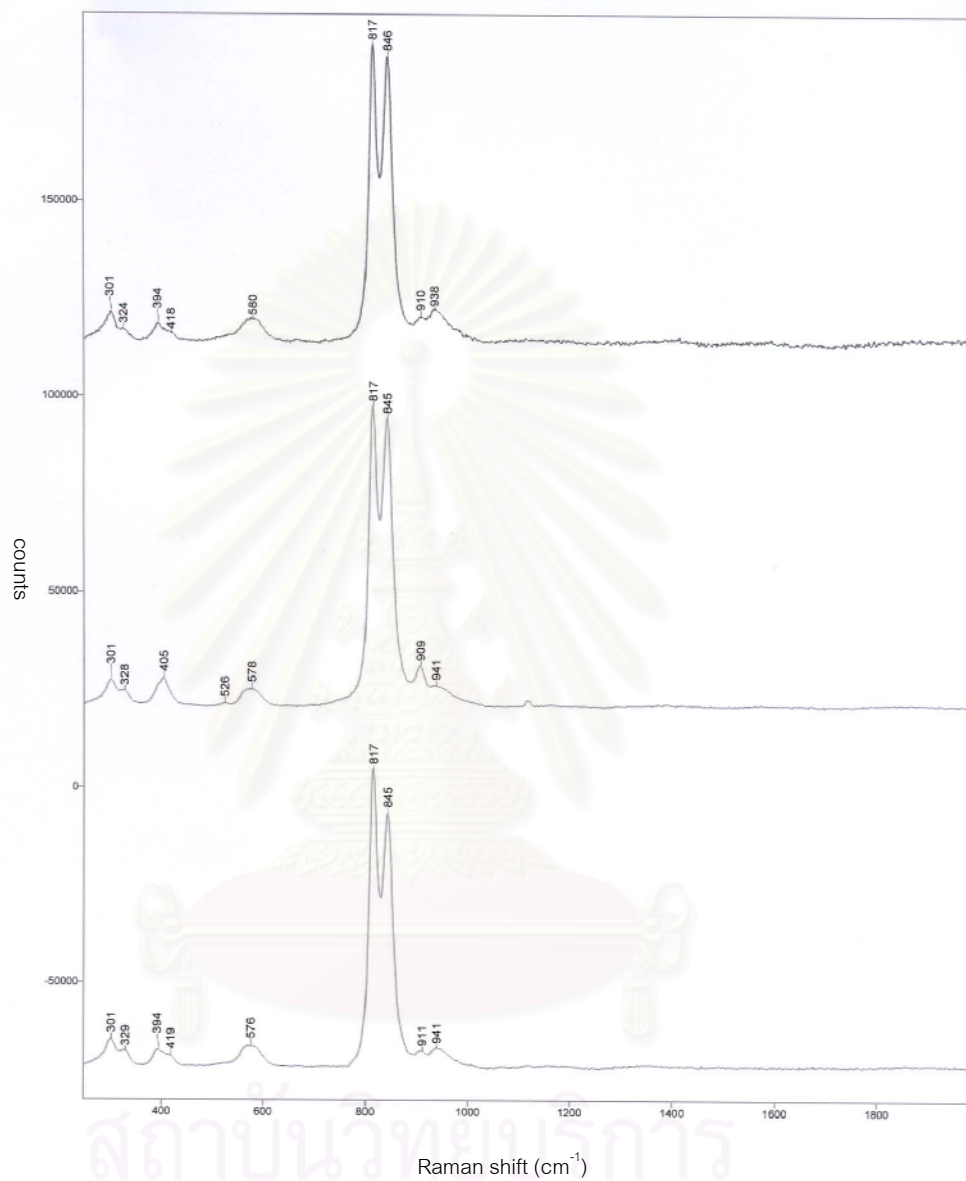Figure A2.26    Three raman spectra of sample no. PD588 which has 58.8% Fo

Figure A2.27    Three raman spectra of sample no. PD505 which has 50.5% Fo

# BIOGRAPHY

Mr. Thanong Leelawatanasuk was born on January 16, 1978 in Bangkok, Thailand. He graduated with bachelor degree in Geology from the Department of Geology, Faculty of science, Chulalongkorn University in 1998. Recently, he works at the Gem and Jewelry Institute of Thailand(Public Organizatin) and also studies in a Master program in Geology at Chulalongkorn University.